HHS Public Access

Author manuscript

J Med Chem. Author manuscript; available in PMC 2022 April 22.

Published in final edited form as:

J Med Chem. 2021 April 22; 64(8): 5099–5122. doi:10.1021/acs.jmedchem.1c00164.

Structure–Activity Relationship of Heterocyclic $P2Y_{14}$ Receptor Antagonists: Removal of the Zwitterionic Character with Piperidine Bioisosteres

Young-Hwan Jung[#],
Molecular Recognition Section, Laboratory of Bioorganic Chemistry, National Institute of Diabetes and Digestive and Kidney Diseases, National Institutes of Health, Bethesda, Maryland 20892, United States

Veronica Salmaso[#],
Molecular Recognition Section, Laboratory of Bioorganic Chemistry, National Institute of Diabetes and Digestive and Kidney Diseases, National Institutes of Health, Bethesda, Maryland 20892, United States

Zhiwei Wen,
Molecular Recognition Section, Laboratory of Bioorganic Chemistry, National Institute of Diabetes and Digestive and Kidney Diseases, National Institutes of Health, Bethesda, Maryland 20892, United States

John M. Bennett,
Molecular Recognition Section, Laboratory of Bioorganic Chemistry, National Institute of Diabetes and Digestive and Kidney Diseases, National Institutes of Health, Bethesda, Maryland 20892, United States

Ngan B. Phung,
Molecular Recognition Section, Laboratory of Bioorganic Chemistry, National Institute of Diabetes and Digestive and Kidney Diseases, National Institutes of Health, Bethesda, Maryland 20892, United States

David I. Lieberman,

Corresponding Author Kenneth A. Jacobson – Molecular Recognition Section, Laboratory of Bioorganic Chemistry, National Institute of Diabetes and Digestive and Kidney Diseases, National Institutes of Health, Bethesda, Maryland 20892, United States; Phone: 301-496-9024; kennethj@niddk.nih.gov; Fax: 301-480-8422.
[ll]Jagiellonian University Medical College, 30-688Kraków, Poland 31-007, Poland (T.P.K.).

Supporting Information

The Supporting Information is available free of charge at https://pubs.acs.org/doi/10.1021/acs.jmedchem.1c00164.

Synthesis (Schemes S1 and S2), pain model data, esterase cleavage curves, off-target binding inhibition curves, pharmacological data, and molecular modeling data including tables reporting analysis of MD simulations, plots of ligand RMSD, ligand–receptor interaction energy and number of contacts during MD simulations, last frame complex structure for compounds **29**, **32**, and **33**, ADME tox procedures and results, predicted LogD and LogS, patch clamp hERG assay, and NMR and mass spectra of triazole derivatives (PDF)

3D coordinates of $hP2Y_{14}R$ in complex with **29**, obtained through molecular docking (PDB)

3D coordinates of $hP2Y_{14}R$ in complex with **32**, obtained through molecular docking (PDB)

Video S1, 30 ns MD simulations of $hP2Y_{14}R$ in complex with compound **29** (AVI)

Video S2, 30 ns MD simulations of $hP2Y_{14}R$ in complex with compound **32** (AVI)

Molecular formula strings of compounds **1a–1d**, **3a**, **3b**, **4–36**, and **37a–37c** (CSV)

The authors declare no competing financial interest.

Molecular Recognition Section, Laboratory of Bioorganic Chemistry, National Institute of Diabetes and Digestive and Kidney Diseases, National Institutes of Health, Bethesda, Maryland 20892, United States

Varun Gopinatth,
Molecular Recognition Section, Laboratory of Bioorganic Chemistry, National Institute of Diabetes and Digestive and Kidney Diseases, National Institutes of Health, Bethesda, Maryland 20892, United States

John C. R. Randle,
Random Walk Ventures, LLC, Boston, Massachusetts 02111, United States

Zhoumou Chen,
Department of Pharmacology and Physiology and the Henry and Amelia Nasrallah Center for Neuroscience, Saint Louis University School of Medicine, St. Louis, Missouri 63104, United States

Daniela Salvemini,
Department of Pharmacology and Physiology and the Henry and Amelia Nasrallah Center for Neuroscience, Saint Louis University School of Medicine, St. Louis, Missouri 63104, United States

Tadeusz P. Karcz,
Immunity, Inflammation and Disease Laboratory, National Institute of Environmental Health Sciences, National Institutes of Health, Durham, North Carolina 27709, United States

Donald N. Cook,
Immunity, Inflammation and Disease Laboratory, National Institute of Environmental Health Sciences, National Institutes of Health, Durham, North Carolina 27709, United States

Kenneth A. Jacobson
Molecular Recognition Section, Laboratory of Bioorganic Chemistry, National Institute of Diabetes and Digestive and Kidney Diseases, National Institutes of Health, Bethesda, Maryland 20892, United States

[#] These authors contributed equally to this work.

Abstract

A known zwitterionic, heterocyclic $P2Y_{14}R$ antagonist **3a** was substituted with diverse groups on the central phenyl and terminal piperidine moieties, following a computational selection process. The most potent analogues contained an uncharged piperidine bioisostere, prescreened in silico, while an aza-scan (central phenyl ring) reduced $P2Y_{14}R$ affinity. Piperidine amide **11**, 3-aminopropynyl **19**, and 5-(hydroxymethyl)isoxazol-3-yl) **29** congeners in the triazole series maintained moderate receptor affinity. Adaption of 5-(hydroxymethyl)isoxazol-3-yl gave the most potent naphthalene-containing (**32**; MRS4654; IC_{50}, 15 nM) and less active phenylamide-containing (**33**) scaffolds. Thus, a zwitterion was nonessential for receptor binding, and molecular docking and dynamics probed the hydroxymethylisoxazole interaction with extracellular loops. Also, amidomethyl ester prodrugs were explored to reversibly block the conserved carboxylate group to provide neutral analogues, which were cleavable by liver esterase, and in vivo efficacy

demonstrated. We have, in stages, converted zwitterionic antagonists into neutral molecules designed to produce potent $P2Y_{14}R$ antagonists for in vivo application.

Graphical Abstract

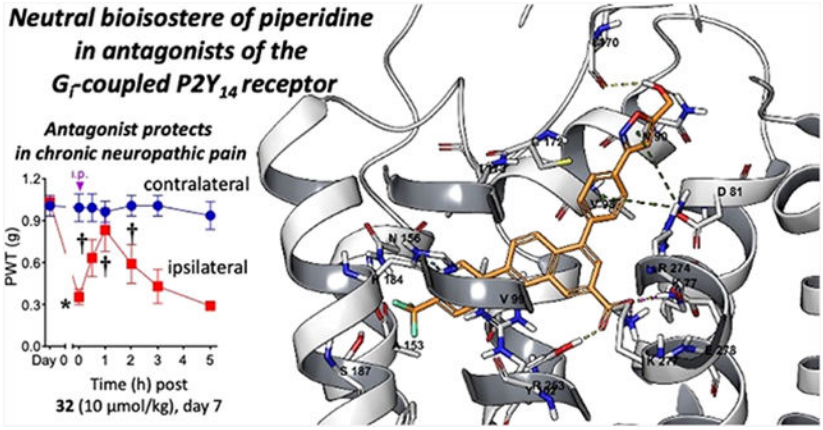

INTRODUCTION

The $P2Y_{14}$ receptor ($P2Y_{14}R$) is a target for the treatment of inflammatory diseases, including pulmonary and renal conditions, and selective $P2Y_{14}R$ antagonists have demonstrated efficacy in animal models of asthma, pain, diabetes, and acute kidney injury.[1-8] Its endogenous agonists are uridine-5′-diphosphoglucose (UDPG) and other UDP-sugars, and UDP itself acts as a partial agonist. This G_i protein-coupled receptor is one of three $P2Y_{12}R$-like receptors in purinergic signaling pathways.[9] UDPG acts as damage-associated molecular pattern (DAMP), and thus, competitive $P2Y_{14}R$ antagonists have antiinflammatory effects.[3] $P2Y_{14}R$ antagonists are considered for the development of new treatments of asthma and peripheral inflammation, although antagonist effects in the CNS are not well characterized and might be detrimental. For example, tonic $P2Y_{14}R$ activation helps to maintain astrocytes by preventing the secretion of matrix metalloproteinase-9.[10]

Various $P2Y_{14}R$ antagonists have been reported, and the most well explored class is derived from 7-phenyl-2-naphthalenecarboxylic acid.[1,2,11-14]. Although there is no report yet of a $P2Y_{14}R$ X-ray crystallographic structure, we have applied a structure-guided approach using homology modeling and molecular dynamics (MD) simulation to the design of new antagonist ligands.[1,2,14] The nucleotide agonist-bound $P2Y_{12}R$ structure[15] serves as a suitable protein template for $P2Y_{14}R$ homology, with 44% sequence identity between $P2Y_{12}R$ and $P2Y_{14}R$.[1,2,14] Previous studies have analyzed the structure–activity relationship (SAR) of high affinity antagonist 4-[4-(4-piperidinyl)phenyl]-7-[4-(trifluoromethyl)phenyl]-2-naphthalene-carboxylic acid (PPTN, **1a**, Chart 1) and its analogues, e.g., potent *N*-acetyl derivative **1b** and triazole derivatives **3a**, **4**, and **5**.[1,2,7,11,14,16] Compound **1a** is a highly selective antagonist for the $P2Y_{14}R$ among the family of eight P2YRs; this chemical series has no evidence of an interaction with other P2YRs or of residual receptor agonism.[16,17] Therefore, we consider this to be a viable, high affinity scaffold for the design of new $P2Y_{14}R$ antagonists. As a screening tool, we

previously introduced a high affinity fluorescent antagonist **2**, which shows a functional K_i of 80 pM and serves as a versatile screening tool in a flow cytometry assay using Chinese hamster ovary (CHO) cells overexpressing the human (h) $P2Y_{14}R$ and human embryonic kidney (HEK)293 cells overexpressing the mouse (m) $P2Y_{14}R$.[2,7,16] Consistently reproducible IC_{50} values can be obtained for newly synthesized antagonists, although these inhibitory constants underestimate the compounds' affinity by at least one order of magnitude.[2]

However, the prototypical antagonist **1a** is not optimal for in vivo administration as it shows a high cLogP and low oral bioavailability (5%, mouse).[18] Its hydrophobicity precluded the use of [^{3}H]**1a** as a radioligand for $P2Y_{14}R$ assays due to high nonspecific binding.[2] Furthermore, **1a** is a zwitterionic ligand, which affects assessment of its drug-likeness, lipophilicity and absorption in vivo, although various zwitterionic drugs are used therapeutically.[19] Previously, we introduced alternative scaffolds to replace the phenyl-naphthalene moiety and substituted the phenyl-piperidine moiety with extended polar chains that reduced the cLogP but did not increase the receptor affinity of **1a** and in some cases introduced other liabilities, such as human ether-a-go-go-related gene (hERG) inhibition.[1,2,14] One possible solution to overcome the deficiencies of **1a** is described in a report on its prodrug derivative in which the essential benzoic acid group was protected as a neutral ester moiety.[18] Here, we applied the same prodrug approach that was reported for the prodrug of **1a**, by introducing a *N,N*-dimethylamidomethyl ester at the essential aryl carboxylate group in three high affinity $P2Y_{14}R$ antagonists. We demonstrated that the parent, active drug in each case could be recovered upon treatment of the prodrug form with purified liver esterase in vitro. Furthermore, several prodrug derivatives showed efficacy in a mouse asthma model that surpassed the efficacy of the parent drugs.

Another structural modification of **1a** found to lower its hydrophobicity was the bioisosteric replacement of the hydrophobic naphthalene moiety of **1a** in the form of a triazolyl-phenyl group, which was the starting point of our SAR study.[14] This biaryl moiety is predicted to maintain a similar conformation to the naphthalene when receptor-bound, as we showed previously for moderately potent $P2Y_{14}R$ antagonists **3a**, **4**, and **5**. A further impediment to attaining drug-like properties in this chemical series is the secondary amine in the piperidine moiety. Finding an alternative terminal group in place of piperidine, especially one that lacks a positively charged group, would be desirable and has been attempted in previous SAR reports.[1,2] For example, compound **5** provides moderate affinity and enhanced aqueous solubility with a simple 4-carboxamido group in place of piperidine. However, this compound shows rapid clearance in vivo and unacceptable hERG inhibition.[2] In this study, we have modified the piperidine moiety and the central phenyl ring of the triazole derivatives to search for alternatives that might be more druglike than reference zwitterionic compounds **1a** and **3a**. Piperidine bioisosteres were screened by modeling the proposed analogues' interaction with a $P2Y_{14}R$ model, and the most affinity enhancing group (5-(hydroxymethyl)isoxazol-3-yl) was predicted as a high scoring hit. Subsequently, we combined this neutral bioisostere of piperidine with the naphthalene core. Thus, both structure-based and empirical approaches were followed to probe the $P2Y_{14}R$ SAR.

RESULTS

Computational Selection of Substituent Groups and Initial Chemical Synthesis.

A previously reported hP2Y$_{14}$R homology model was used to guide scaffold and functional group modification in this antagonist series, featuring a conserved aryl carboxylate on the central ring of the scaffold interacting with three polar side chains in TMs (transmembrane helices) 2, 3, and 7, specifically Lys77$^{2.60}$, Tyr102$^{3.33}$, and Lys277$^{7.35}$, respectively.[1,14] These interactions were found to be maintained during MD simulation of receptor–antagonist complexes.[1,14]

Following our earlier SAR studies of heterocyclic P2Y$_{14}$R antagonists,[1,2,14] we turned our attention to the replacement of the piperidine moiety of **3a** initially and subsequently of **1a**, with diverse groups, including cyclic and acyclic and charged and uncharged moieties. The selection of groups was based both on the commercial availability of functionalized *p*-substituted phenyl starting materials for the Suzuki coupling (Schemes 1-3) and on computational predictions. We initiated this study with a computational selection of favored *p*-substituted phenyl derivatives to enable high affinity receptor binding, by varying group "R" in the triazole series related to **3a** (Scheme 1). A hP2Y$_{14}$R homology model,[14] based on a nucleotide-bound hP2Y$_{12}$R[15] structure (sequence identity, 44%) and refined with induced fit docking of high affinity antagonist **1a** followed by MD simulations, was used for the computational work. A computational screening based on docking and MD simulation of analogues containing the proposed R groups was employed to prioritize the candidate synthesis.

The R groups were selected from a manually assembled list of 20 commercially available bromo-aryl precursors for the Suzuki reaction with intermediate **38** (Scheme 1), together with five compounds that could be easily synthesized using commercial precursors (compounds **8**, **9**, **11**, **14**, and **19**). The list of 24 screened compounds is reported in Figure S1 (Supporting Information). The azido R group in **93** was discarded and not included in computation and subsequent synthesis because of lack of MD parameters for this substituent. The R groups were incorporated on the antagonist scaffold computationally, the resulting compounds were docked to the receptor structure, and the stability of the receptor-bound complexes was assessed using MD. Three 30 ns MD replicates were run for each complex, and the average results over the three replicates were compared to reference compounds **1a** and **3a**. With the objective being to account for both enduring geometric and energetic stabilities of the complexes, we employed the weighted dynamic scoring function[20] (wDSF) method to evaluate the outcome of the simulations. This method computes the cumulative ligand–receptor energy during the MD simulation (here the sum of electrostatic and van der Waals contributions), which is frame-by-frame weighted by the RMSD of the ligand heavy atoms (eq 1)

$$\mathrm{wDSF} = \frac{\sum_{t=0}^{n} \mathrm{IE}_{L-R}}{\mathrm{RMSD}} \quad (1)$$

The slope of the line fitting the wDSF values versus the number of frames was used to compare the complexes. This scoring system evaluates the enduring strength of the interaction, as previously reported,[20] and a lower slope value (higher absolute value) identifies a more stable ligand pose. We used the average slope of **3a** over the three MD replicates as cutoff to prioritize the synthesis of our dataset of compounds. In the case of compound **31**, whose tetrazole moiety might exist as two possible tautomers, both tautomers were simulated, and the 1*H*-tetrazole was selected as the one minimizing the wDSF/time slope. Thus, compounds **8**, **11**, **14**, **18**, **19**, **22**, **23**, **25**, **27**, **29**, and **31**, showing a lower wDSF/time slope as compared to **3a** (Table S1, Supporting Information), were selected as best candidates of the series and consequently prioritized for synthesis and testing, followed then by all the other compounds of the series (Table 1). Compound **6** with a piperazine substituent, already synthesized and whose binding affinity was reported to be 233 nM,[2] showed a wDSF/time slope lower than **3a**. Two compounds reported in Figure S1 have not been synthesized: the synthesis of the hydroxy-oxadiazole-bearing compound **91** was not successful, while compound **92** with the 4-hydroxy-piperidine substituent, selected for its low wDSF/time slope value, was not synthesized because this moiety combined with the naphthoic acid scaffold was previously reported to provide high affinity.[58]

The synthetic routes for R group substitution, either according to modeling predictions for bioisosteres or with other substitution, are shown in Schemes 1-Scheme 5 Among the synthesized analogues in the triazole series, the terminal group contained an aryl–CO or aryl–NH linker (**7**–**14**), a halogen (**15**), a carbon-linked acyclic moiety (**16**–**21**), or a carbon-linked cyclic moiety (**22**–**31**). Scheme 1 shows the synthetic route to triazole analogues containing an aryl–CO or aryl–NH linker (**7**–**14**). The Suzuki reaction of **38** with *N*-(*tert*-butoxycarbonyl)-4-bromoaniline, 4-bromobenzoic acid, or *tert*-butyl (3-(4-bromobenzamido)propyl)carbamate yielded **39**, **44**, and **45**, respectively, followed by deprotection reactions (removal of methyl ester and *N*-Boc protecting groups) to provide **7**, **10**, **13**, and **14**. The primary amine of compound **40** was *N*-acetylated (**41**), *N*-benzoylated (**42**), or coupled with the piperidinyl group (**43**), and the products were then deprotected to yield **8**, **9**, **11**, and **12**. Since the *N*-acetyl derivative **1b** was particularly potent in binding and in vivo efficacy,[2,7] we prepared the corresponding *N*-formyl derivative **1c** using reported formylation conditions using acetic formic anhydride[21] and *N*-trifluoroacetyl derivative **1d**.

The triazole series containing a halogen (**15**), a carbon-linked acyclic moiety (**16**–**21**), or a carbon-linked cyclic moiety (**22**–**31**) was synthesized, as shown in Schemes 2 and 3, to provide **15**–**31**. The Suzuki reaction of **38** with various aryl groups containing a halogen (**47**), a carbon-linked acyclic moiety (**17** and **48**–**51**), or a carbon-linked cyclic moiety (**55**-**63**) followed by deprotection reactions provided **15**, **16**, **18**-**21**, and **22**-**31**.

Combination of Favored Groups: Extended SAR and Modeling.

The main success of the computational screening and of the consequent synthetic effort in the triazole series was the identification of a piperidine bioisostere in compound **29**, where the removal of the zwitterionic character was compatible with relatively high $P2Y_{14}R$ affinity (IC_{50}, 296 nM). For this reason, we focused on this compound and we report here its hypothetical binding mode. The docking pose of compound **29** (Figure 1) resembles the one

previously reported for its piperidine-bearing analogue **3a**.[1,14] The carboxylate moiety is involved in electrostatic and H bond interactions with Lys77$^{2.60}$, Lys277$^{7.35}$, and Tyr102$^{3.33}$. Arg274$^{7.32}$, Arg253$^{6.55}$, and His184$^{5.36}$ (using Ballesteros–Weinstein notation[22]) are compatible with π–charge and π–π interactions with the *p*-CF_3-phenyl, triazolyl, and peripheral aryl substituents of the central benzoic acid (Figure 1A). During 30 ns MD simulation, the ligand appeared stable (Figure S2A, Supporting Information), with an inter-replicate average RMSD of 2.23 Å (Table S2, Supporting Information). The interaction energy fluctuated slightly around a plateau during the simulations (Figure S2B), with an inter-replicate average value of −207 kcal mol^{-1}. The H bond interactions between the ligand carboxylate moiety and Lys77$^{2.60}$, Tyr102$^{3.33}$, and Lys277$^{7.35}$ were endured during the simulations, with an inter-replicate average persistence of about 93, 88, and 77%, respectively. Compound **29** was in contact with 15 residues for more than 95% of the time in all three replicates (Figure S2C). In addition to Lys77$^{2.60}$, Lys277$^{7.35}$, and Tyr102$^{3.33}$, the central scaffold was surrounded by Asp81$^{2.64}$, Val93$^{3.24}$, Ala98$^{3.29}$, Val99$^{3.30}$, Cys172^{EL2}, and Phe191$^{5.43}$. More externally, Gly80$^{2.63}$, Gly83$^{2.66}$, Leu84^{EL1}, Gly85^{EL1}, Asn90$^{3.21}$, and Ile170^{EL2} surrounded the 5-(hydroxymethyl)isoxazol-3-yl substituent of **29**. This particular R group appeared involved in a H bond with Asn90$^{3.21}$ in the docking pose, which was transient during the MD simulations. During the three MD replicates, the 5-(hydroxymethyl)-isoxazol-3-yl group transiently interacted with residues in EL1 and EL2 or on the extracellular tip of TMs, making H bonds especially with Gly85^{EL1}, Asn90$^{3.21}$, and Ile170^{EL2} (Figure S4A,C,E for the three replicates and Video S1, Supporting Information). The capability of the hydroxymethyl moiety to stabilize the ligand through H bonds supports the binding affinity improvement of compound **29** (5-(hydroxymethyl)isoxazole) as compared to compound **28** (plain isoxazole), which was not included in the list of prioritized compounds (wDSF/time slope lower than compound **3a**, Table S1).

The piperidine ring substitution with a 5-(hydroxymethyl)-isoxazol-3-yl moiety was thus able to contribute to ligand stabilization with the aforementioned interaction pattern. Given the success of this biososteric group in the initial triazole series, its receptor interactions were analyzed in the context of naphthalene-containing (**32**) and phenyl-amide-containing (**33**) scaffolds.[2,11] The hypothetical binding mode of compound **32** at the hP2Y_{14}R model (Figure 1B) resembles the pose previously reported for **1a**.[14] As previously discussed for compound **29**, the carboxylate of compound **32** makes H bonds with Lys77$^{2.60}$, Lys277$^{7.35}$, and Tyr102$^{3.33}$ that are maintained on average during the three MD replicates for 77, 81, and 62% of the simulation time, respectively (Table S2 and Figure S4B,D,F, Supporting Information). As compared to **29**, compound **32** appeared more geometrically stable during the simulations, with small RMSD deviations from a plateau: the inter-replicate average RMSD value was 2.07 Å, with fluctuations within a 1–3 Å range (Table S2 and Figure S3A, Supporting Information). With an inter-replicate average interaction energy of −211 kcal mol^{-1} and a wDSF/time slope of −100.70 (Table S2, Supporting Information), compound **32** seemed encouraging, and in fact, its affinity for hP2Y_{14}R turned out to be 15 nM, as will be discussed below. In addition to Lys77$^{2.60}$, Lys277$^{7.35}$, and Tyr102$^{3.33}$, compound **32** was surrounded by residues Gly80$^{2.63}$, Asp81$^{2.64}$, Gly85^{EL1}, Asn90$^{3.21}$, Val93$^{3.24}$, Cys94$^{3.25}$, Ala98$^{3.29}$, Val99$^{3.30}$, Asn156$^{4.60}$, Cys172^{EL2}, His184$^{5.36}$, Ser187$^{5.39}$, Asn188$^{5.40}$, Phe191$^{5.43}$, and Arg253$^{6.55}$ for more than 95% of the simulation time. A stable H bond was

maintained between Gly85^{EL1} and the hydroxyl group of the 5-(hydroxymethyl)isoxazol-3-yl substituent, especially in replicates 1 and 2 (Figure S4B,D,F, Supporting Information). The isoxazole oxygen and nitrogen atoms transiently interacted with Cys172^{EL2}, bridging interactions between EL1 and EL2 (Video S2, Supporting Information).

The same stability was not reached in the case of compound **33**, where the 5-(hydroxymethyl)isoxazol-3-yl substituent was combined to the phenyl-amide-containing scaffold. An average inter-replicate RMSD of 4.53 Å was experienced by the ligand, with huge deviations from the initial state especially in replicate 2 (Table S2 and Figure S5A,E, Supporting Information). The H bond with Lys277$^{7.35}$ was not conserved during the three replicates, and the interaction with Lys77$^{2.60}$ was lost in replicate 2. The average ligand–receptor interaction energy (−148 kcal mol^{-1}) significantly worsened as compared to compounds **29** and **32**, with the 5-(hydroxymethyl)isoxazol-3-yl substituent not making stable contacts with specific residues. The amido group replacing half of the naphthalene scaffold introduced higher flexibility to the molecule, which rotated to interact mainly with Arg253$^{6.55}$ in replicates 1 and 3, and with His184$^{5.36}$ in replicate 2, with a general deviation from the initial state and the binding mode of compounds **29** and **32**.

Scheme 4A shows the combination of the 5-(hydroxymethyl)isoxazol-3-yl group of potent derivative **29** with the naphthalene ring of **1a** to give compound **32**. The Suzuki reaction product of **64** with (3-(4-bromophenyl)-isoxazol-5-yl)methanol was hydrolyzed to yield **32**. A 5-(hydroxymethyl)isoxazol-3-yl analogue **33** with an amide group replacing the triazole ring was synthesized, as shown in Scheme 4B. This follows our previous report and that of Zhang et al. on amide incorporation.[2,11] For synthesis of amide analogue **33**, the carboxylic acid of **65** was converted into a methyl ester in **66**, which then coupled with 4-(trifluoromethyl)benzoic acid. Compound **67** reacted with bis(pinacolato)diboron (B_2pin_2, **68**) followed by the Suzuki reaction to yield **69**. Subsequently, **69** was hydrolyzed to afford **33**.

Subsequently, with the aim to further explore modifications of the central scaffold in this antagonist series, we empirically modified the central phenyl ring with nitrogen substitution (“aza-scan”), leading to triazole derivatives **34–36** (Scheme 5), which could be compared to **3a**. Adding a ring nitrogen or shifting its position within an aromatic ring is a known approach to modulate the activity of bioactive molecules.[23,24]

The aza-scan of the central phenyl ring of **3a** was accomplished, as shown in Scheme 5. The carboxylic groups of **69** and **70** were protected as methyl esters in **72** and **73**. The amine functionality of **71–73** was converted into an azide in **74–76** followed by the click reaction with 4-ethynyl-α,α,α-trifluorotoluene to yield **77–79**. Subsequently, a Suzuki reaction with *tert*-butyl 4-(4-(4,4,5,5-tetramethyl-1,3,2-dioxa-borolan-2-yl)phenyl)piperidine-1-carboxylate yielded **80–82**, which then were deprotected to afford **34–36**, respectively.

Since many P2YR ligands contain anionic groups, we wanted to test experimentally if a phosphate monoester could serve the same role as the essential carboxylate of **3a**.[2,16] Therefore, we synthesized phosphate ester **3b** (Scheme S1, Supporting Information) and determined its hP2Y$_{14}$R affinity. The synthetic route to phosphate derivative **3b** began with

LAH reduction of the methyl ester of compound **88** to a primary alcohol **89**, which was phosphorylated with di-*tert*-butyl *N,N*-diethylphosphoramidite to afford **90**. Subsequently, a deprotection reaction yielded **3b**.

Pharmacological Characterization.

The inhibition by the newly synthesized analogues of binding of fluorescent tracer **2** was measured in hP2Y$_{14}$R-expressing CHO cells (Table 1).[1,2] The computational screening procedure adopted enabled the discrimination of submicromolar ligands, with some false negative and false positive exceptions. In particular, 13 out of 24 compounds showed a wDSF/time slope lower than compound **3a** (−70.55), in addition to **1b**, compounds **8**, **11**, **14**, **18**, **19**, **22**, **23**, **25**, **27**, **29**, and **31** and the piperazine **6** and 4-hydroxy-piperidine **92** compounds (Table S1, Supporting Information). A threshold of 1 μM was used to define positive compounds, and according to this metric, we were able to identify 8 true positives out of the 13 selected compounds: ligands **8**, **11**, **14**, **18**, **19**, **29**, and **31** and the piperazine compound **6**[2] had submicromolar affinity. The compound bearing the 4-hydroxy-piperidine substituent **92** was not part of this study, aimed to explore chemical groups different than piperidine. However, this modification in the naphthoic acid series was associated with high affinity for the chimpanzee P2Y$_{14}$R.[58] Compounds **22**, **23**, **25**, and **27** were false positives (affinity higher than 1 μM), while ligands **13** and **30**, whose IC$_{50}$ turned out to be <1 μM, were missed (false negatives). This screening was not meant to accurately predict a precise ranking of binding affinities. Given the limitations of a structure obtained by homology modeling, we did not expect a perfect correlation between computational and experimental results, but we exploited modeling to drive the synthesis of new compounds, and we were able to identify seven new submicromolar hP2Y$_{14}$R ligands.

Compounds **1a**, **3a**, and **4–6** (Table 1) are included as archival compounds for comparison. The *N*-trifluoroacetyl derivative **1d** in the naphthalene series had 8.7-fold lower hP2Y$_{14}$R affinity than the corresponding *N*-acetyl **1b**, which was similar to the corresponding *N*-formyl analogue **1c** (IC$_{50}$ ≈ 30 nM). Four aniline and simple acylated aniline derivatives in the triazole series **7–10** had relatively weak affinity (1–3 μM). Two zwitterionic molecules, i.e., piperidine amide **11** and 3-aminopropyl **18** derivatives, and anionic isoxazole **29** were found to maintain moderate receptor affinity with IC$_{50}$ values ≤300 nM. The *N*-Boc protected forms of **11** and **18**, i.e., **12** and **20**, were >100-fold weaker in binding than the parent amines. *p*-Carboxyphenyl derivative **13** and its amino-propylamide **14** were equipotent (IC$_{50}$ ≈ 0.6 μM), with **14** having 3.5-fold lower affinity than the corresponding thienyl derivative **4**.[1] Neutral functional group substitutions of the phenyl ring, **15–17**, showed only weak to intermediate affinity. Tetrazole, a common carboxylate bioisostere,[1] in compound **31** (IC$_{50}$ ≈ 0.9 μM) maintained the intermediate affinity of the corresponding carboxylate **13**.

Homologues of potent **18** and **29** (unsaturated chain in equipotent **19** and isoxazole derivatives **28** and **30**, respectively) were compared. Hydroxybutyl derivative **21** and small cycloalkyl-amino derivatives, **22–26**, either Boc-protected or unprotected, and oxetane **27** all bound weakly. The hydroxymethylisoxazole derivative **29** showed higher affinity than its hydroxyethyl homologue **30**, and the unsubstituted isoxazole **28** was 7.5-fold weaker than

29. The 5-(hydroxymethyl)isoxazol-3-yl group was incorporated into naphthalene-containing **32** and phenyl-amide-containing **33** scaffolds. Compound **32** proved to be antagonist of the highest hP2Y$_{14}$R affinity in the present set of compounds with an IC$_{50}$ of 15 nM. Thus, the restoration of the naphthalene scaffold in **32** increased the affinity by 20-fold, but the phenyl-amide scaffold reduced affinity 25-fold compared to the triazole series.

We turned our attention to the central phenyl ring's SAR in the triazole series. An aza-scan of this ring indicated reduced P2Y$_{14}$R affinity of compounds **34–36** in relation to parent **3a**. 4-Phenylpicolinic acid derivative **34** had slightly greater affinity than 2-phenylisonicotinic **35** and 6-phenylpicolinic **36** acid derivatives, but the affinities were nevertheless in the μM range. Thus, an aza-scan at any of the three CH positions failed to enhance the affinity (≥53-fold weaker) compared to **3a**. Efforts to replace the important carboxylate group of **3a** with a different anionic group, i.e., phosphate **3b**, greatly reduced affinity. The measured affinity of **3b** was 1900-fold weaker (IC$_{50}$, 60.5 ± 6.9 μM) than **3a**. Thus, this carboxylate group that we propose to be buried deeply in the binding site remained an essential requirement for high P2Y$_{14}$R affinity.

It is important to maintain receptor affinity across species, in order to perform in vivo preclinical testing in small animals, with the mouse being the most commonly used species in initial evaluation.[3-7] Therefore, several of the new compounds (**11**, **19**, **29**, and **32**) were compared in affinity at hP2Y$_{14}$R and mP2Y$_{14}$R (Figure 2 and Table 2) using our reported fluorescence binding procedures.[2] Compound **29** had slightly enhanced affinity (IC$_{50}$, 184 nM) at the mP2Y$_{14}$R versus the human homologue, while **11**, **19**, and **32** had nearly the same affinity in the two species.

The solubility (using the pION method)[2,25,26] and lipophilicity (based on the HPLC retention time)[2,27] were determined for the 5-(hydroxymethyl)isoxazol-3-yl compounds **29** and **32**. The aqueous solubility (mean ± SEM) of **29** was 3.72 ± 0.87 μg mL^{-1} (7.34 μM) at pH 7.4 and 0.60 ± 0.09 μg mL^{-1} at pH 4.0, and the compound showed a hydrophilicity gain of −1.06 cLogP units compared to **1a**. The aqueous solubility values of **32** were 2.43 ± 0.13 μg mL^{-1} (4.96 μM, pH 7.4) and 0.14 ± 0.02 μg mL^{-1} (pH 4.0). Potent antagonist **32** showed a hydrophilicity gain of −0.80 cLogP units compared to **1a**. It is worth noting that the three prodrugs **37a–37c** (Table 3) were readily soluble in DMSO at 20 mg mL^{-1} as this solvent has been required for the in vivo testing of this chemical series. Reference compound **1a** could not dissolve at a concentration of 20 mg mL^{-1} in DMSO and required the addition of 1 N NaOH (1 equiv) in order to dissolve in DMSO at a near maximal concentration of 5 mM (2.38 mg mL^{-1}).

Off-target interactions of selected analogues (**11**, **13**, **18**, **16**, **18**, **19**, **29–32**, **37a**, and **37c**) were analyzed by radioligand binding at 46 receptors and channels by the Psychoactive Drug Screening Program (PDSP, Figure S6, Supporting Information), performed as reported previously.[28] Several compounds in this chemical series previously were found to have off-target activity at DOR (δ-opioid receptor, 2.75 μM, **1a**).[1] Weak off-target interactions were detected, but not extensively (K_i, μM, receptor): **11**, 2.33 ± 0.15 (σ_1R), 2.0 ± 0.4 (DOR); **16**, 0.931 ± 0.388 (σ_2R), 2.81 ± 0.18 (TSPO); **29**, 2.65 ± 0.74 (H$_1$R), 0.751 ± 0.101 (TSPO), 6.9 ± 1.9 (DOR); **31**, 2.26 ± 1.28 (σ_2R), 3.30 ± 1.76 (DOR); and **32**, 2.68 ± 0.21 (σ_1R), 4.78 ±

1.00 (σ_2R), 4.63 ± 0.87 (TSPO). Compounds **6**, **13**, **18**, and **19** did not show any off-target interactions in the standard PDSP screen. *N*-Formyl **1c** (% inhibition at 10 μM or K_i, μM: $5HT_{1D}$, 81%; α_{1B}, 2.65; α_{2A}, 3.97; α_{2B}, 82%; D_1, 0.52; D_5, 1.44; σ_1, 0.759; σ_2, 84%; H_4, 1.70) and previously reported[7] *N*-acetyl **1b** ($5HT_{1D}$, 1.75 ± 0.54; $5HT_{1E}$, 3.91 ± 0.35; $5HT_{5A}$, 2.34 ± 1.25; D_1, 1.39 ± 0.12; α_{1A}, 3.14 ± 0.68; α_{2C}, 4.31 ± 0.82; β_3, 0.86 ± 0.40; TSPO, 0.508 ± 0.044) analogues showed some off-target interactions. Prodrug **37a** was promiscuous in off-target binding, with 18 interactions found in the μM range, while prodrug **37c** only inhibited binding at σ_2R (0.59 μM).

Absorption, distribution, metabolism, excretion, and toxicology (ADMET) properties were determined for compound **32** (Tables 4 and 5), by the same methods as in Jung et al.[2] Moderate inhibition by **32** of CYP2C9 was observed (IC_{50}, 10 μM), but there was no inhibition of four other CYPs. The compound was stable in simulated gastric and intestinal fluids, in plasma of three species, and in human and mouse liver microsomes. However, the half-life in rat microsomes was 48 min. The rat and mouse plasma protein binding of 10 μM **32** was measured as ~100%. High plasma protein binding has been a recurrent disadvantage of this series of $P2Y_{14}$R antagonists.[1,2,23] In vivo pharmacokinetics in the rat (Table 5 and Figure S10, Supporting Information) indicated a high i.p. bioavailabilty, with a much longer half-life than the reference carboxamide **5**, and linear systemic exposure with increasing dose. We did not determine oral biovailability of **32** because of the reported low %*F* of **1a** and **5** in this chemical series.[1,18] The peak concentration of **32** (10 mg kg^{-1}, i.p., 4 h post-injection) was 786 ng mL^{-1} (1.61 μM). The clinical signs for all rat groups at all time points (up to 24 h) were normal.

Carboxamide analogue **5** was previously shown to potently inhibit hERG (Table 4). hERG inhibition was determined by two methods (fluorescence and electrophysiological)[29,30] as have been done for other $P2Y_{14}$R antagonists.[2] The fluorescence assay utilized a commercial hERG binding fluorescence polarization assay with a tetramethyl-6-carboxyrhodamine (TAMRA) fluorophore.[30] This fluorescence method indicated an IC_{50} of >30 μM for the novel antagonist **32**. Also, compounds **1a**, **1b**, and **32** were measured using a patch clamp assay with CHO cells expressing the full length hERG protein, by measuring the block of hERG outward current amplitude (Supporting Information).[29] By this electrophysiological method, compounds **1a** and **32** did not inhibit hERG (IC_{50} or EC_{50}, >30 μM), while compound **1b** showed a slight activation at high concentrations (EC_{50}, 16.0 μM). Thus, an improvement in the hERG liability was demonstrated for the bioisostere-containing compound **32**.

Prodrug Synthesis and Cleavage by Liver Esterases.

Following the lead of Robichaud et al.[18] with the report of a *N,N*-dimethylamidomethyl ester prodrug of potent zwitter-ionic antagonist **1a**, prodrug derivatives of novel, potent $P2Y_{14}$R antagonists were synthesized. Fully uncharged prodrug derivative of the 5-(hydroxymethyl)isoxazol-3-yl derivative **32**, the potent bioisostere of the piperidine moiety, was synthesized in the naphthalene series (**37b**). Also, the prodrug **37c** derived similarly from *N*-acetyl derivative **1b** is fully uncharged. For comparison, we also applied the same prodrug derivatization to reference triazole derivative **3a** to provide the cationic molecule

37a. Scheme 6 shows the preparation of prodrugs (**37a– 37c**) having a *N,N*-dimethylamidomethyl ester as a promoiety. The Boc-protected piperidine **86**, 5-(hydroxymethyl)isoxazol-3-yl derivative **32**, and *N*-acetyl derivative **1b** were utilized for esterifying the free carboxylic acid using 2-chloro-*N,N*-dimethylacetamide in the presence of K_2CO_3 or Cs_2CO_3 as the base to provide **87**, **37b**, and **37c**, respectively. Subsequently, the deprotection reaction of the Boc group of **87** yielded **37a**.

As an in vitro model system for studying the relative cleavage rates of the ester prodrugs, we used porcine liver esterase (PLE).[31] The prodrug derivatives **37a–37c** were shown to regenerate the corresponding parent drugs, **3a**, **32**, and **1b**, respectively, upon incubation with PLE (Table 3 and Figures S7-S9, Supporting Information). The triazole-containing prodrug **37a** was the most rapidly cleaved, while the naphthalene-containing prodrugs **37b** and **37c** did not reach 50% cleavage after 72 h at 37 °C. All of the prodrugs were stable for 24 h upon aqueous incubation in the absence of PLE.

In Vivo Efficacy of Novel $P2Y_{14}R$ Antagonist 32.

We first tested the potent 5-(hydroxymethyl)isoxazol-3-yl derivative **32** in a well-established mouse model of neuropathic pain caused by chronic constriction of the sciatic nerve (CCI)[32] at a dose of 10 μmol kg^{-1} (4.9 mg kg^{-1}, i.p., Figure 3). Previously, we demonstrated that **1a**, **1b**, and **3a** and other $P2Y_{14}R$ antagonists of this series were effective in reducing chronic pain in this model and reached full reversal in some cases (Table S3, Supporting Information).[2,7] A maximal 71.0 ± 17.4% reversal of CCI-induced mechano-allodynia was observed 1 h post-injection of **32**, and the degree of protection declined during the following 2 h and was not statistically significant at 3 or 5 h. No side effects were evident at this dose.

Selected compounds were examined for their ability to reduce eosinophils in the bronchoalveolar lavage fluid (BALF) in an ovalbumin/*Aspergillus* mouse asthma model.[2,17,33] Compounds **1a**, **1b**, **3a**, and **32** (10 mg kg^{-1}) were administered prior to allergen challenge at a dose of 20 μmol kg^{-1}, i.p. Airway inflammation was determined 2 days post-challenge (Figure 4). Also, the corresponding prodrug derivatives **37a–37c** of triazole **3a**, 5-(hydroxymethyl)-isoxazole **32**, and *N*-acetyl-piperidine **1b** derivatives, respectively, were administered at the same dose. Eosinophil counts in the BALF were reduced following administration of reference antagonist **1a** or several of the prodrugs. In fact, **37b** and **37c** significantly reduced eosinophils to a greater extent than the parent antagonists, which showed no significant reduction. Other immune cells showed no significant effect, except the lymphocyte count following administration of prodrug **37a** trended higher than in a vehicle control.

DISCUSSION

This study has been guided by insights from $P2Y_{14}R$ molecular modeling. The potent analogues **29** and **32** contained an uncharged piperidine bioisostere, which was among the hits selected using in silico prescreening. The hypothetical receptor interactions of the favored 5-(hydroxymethyl)isoxazol-3-yl moiety were analyzed by subsequent docking and MD simulations. Although the piperidine-amide derivative **11** in the triazole series showed

comparable affinity to **29**, it was poorly soluble in aqueous medium, and we did not prepare the corresponding naphthalene derivative.

We have sought to increase the druglikeness[34] of this chemical series of potent $P2Y_{14}R$ antagonists. Through SAR exploration, we have, in stages, removed the zwitterionic character of the widely used antagonist **1a**. We have identified the uncharged 5-(hydroxymethyl)isoxazol-3-yl substituent in compounds **29** and **32** as a piperidine bioisostere in the $P2Y_{14}R$ binding site. The discovery of potent antagonist **32** having the preferred naphthalene scaffold and active in vivo in a chronic pain model greatly improved the unacceptable hERG activity of a previously reported non-amino containing carboxamide **5**, but it showed high plasma protein binding. Another concern was that isoxazole rings have been reported to be susceptible to ring opening biotransformations, although many experimental drugs, even some approved drugs (sulfisoxazole, risperidone, and leflunomide), contain this moiety.[35,36] For example, an isoxazole moiety was found to be beneficial in a series of antinociceptive σ_1R antagonists.[37] The high microsomal stability and in vivo rat pharmacokinetics of compound **32** indicated that it is not rapidly metabolized. Nevertheless, it will be useful to further study the in vivo metabolism of **29** and **32**.

Affinity differences between two species, human and mouse, are not a major concern for this compound class.[2] In the more potent naphthalene series, compound **32** showed IC_{50} values of 15 and 19 nM at the $hP2Y_{14}R$ and $mP2Y_{14}R$, respectively, which are similar to the affinity of compound **1a**. This chemically neutral substituent allowed us to prepare a completely neutral prodrug derivative **37b**, which was shown to be cleaved with liver esterase to regenerate the active drug **32**. Although we determined the relative parent drug recovery in all three cases after ester cleavage catalyzed by liver esterase, this model system cannot be used to predict the cleavage kinetics in vivo for a given route of administration. There are multiple esterases present in the plasma, stomach, intestines, and other organs, which would also be expected to catalyze this cleavage. Interspecies differences would also apply to generalizing the in vitro results to the in vivo biotransformation.[38]

The activity of **32** in a mouse model of chronic neuropathic pain establishes the ability of this bioisosteric approach to discover $P2Y_{14}R$ antagonists with substantial in vivo efficacy. However, it is to be noted that at the dose of 10 μmol kg^{-1}, the reversal of mechano-allodynia was less prolonged or efficacious than with **1a** or **1b**.[7]

The lack of in vivo activity of the prodrug **37a** in the protease model of murine asthma might be a result of its relatively rapid enzymatic cleavage to **3a**, which itself was inactive in the same in vivo assay. Thus, the prodrug **37a** might be largely cleaved prior to reaching the site of action. The other prodrugs **37b** and **37c** were highly efficacious in the asthma assay and were more slowly cleaved to the active drugs in the model esterase system. The correlation of slower ester cleavage with the naphthalene scaffold suggests that these esters might be more sterically hindered than the triazole **37a** in the esterase active site to attenuate hydrolysis. The higher in vivo efficacy might also be related to **37b** and **37c** both being neutral molecules as the lack of a formal charge could promote their distribution/diffusion to the site of action followed by cleavage to the active parent drug. However, additional

pharmacokinetic studies of the prodrugs are needed in order to point to a mechanism for the differential activities.

CONCLUSIONS

In a structure-guided approach, we systematically replaced the piperidine and central phenyl groups of $P2Y_{14}R$ antagonist **3a** with diverse groups. A computational selection process provided a priority list for the initial synthetic foray. A suitable bioisostere for the piperidine moiety was identified as the 5-(hydroxymethyl)isoxazol-3-yl group, which was transferred from the triazole-containing scaffold of **3a** to the naphthalene series to provide **32** with high affinity at both $hP2Y_{14}R$ and $mP2Y_{14}R$. However, an empirical aza-scan of the central phenyl ring of **3a** was unsuccessful in maintaining affinity.

Thus, a zwitterion was nonessential for receptor binding, which was probed through docking and MD simulation. Also, a reported *N,N*-dimethylamidomethyl ester prodrug moiety was used to reversibly block the conserved carboxylate group to provide neutral analogues, which were proven cleavable by liver esterase. We have, in stages, converted zwitterionic antagonists into neutral molecules that are designed to produce potent $P2Y_{14}R$ antagonists for in vivo application. Among the analogues derivatized as prodrugs are the novel and potent compound **32** containing a neutral bioisostere of the piperidine group present in reference antagonist **1a**. The resulting prodrug **37b** and *N*-acetyl derivative **37c** showed substantial efficacy in a protease mouse model of allergic asthma, which surpassed the parent drugs' efficacy. Thus, by searching for piperidine bioisosteres and applying a prodrug strategy, we have, in stages, arrived at novel, tractable $P2Y_{14}R$ antagonists for in vivo studies. Thus, by using insights into the drug–receptor interaction, we have expanded this heterocyclic class of potent $P2Y_{14}R$ antagonists, which hold promise for treating a range of inflammatory diseases.

EXPERIMENTAL PROCEDURES

Molecular Modeling.

Molecular Docking.—A previously published model of $hP2Y_{14}R$[14] was employed in this study. The structure was obtained by homology modeling using an agonist-bound $hP2Y_{12}R$ X-ray structure (PDB ID: 4PXZ[15]) as a template and then refined through induced fit docking of the antagonist **1a** and MD simulations of the complex. The Schrödinger suite (Maestro 2020-1)[39] was used for general modeling operations, like protein preparation through the Protein Preparation Wizard[40] tool and drawing and minimization of the compounds using the OPLS3 force field.[41] All His residues were protonated at the N^{δ} nitrogen (designated HSD in the CHARMM nomenclature).

Docking was performed with Glide SP,[42] employing a grid centered on the previously published pose of the antagonist **1a**, with an inner box of 10 Å and an outer box of 30 Å. Maximum 20 poses were generated for each compound, and a post-docking minimization was included. One pose was selected for each compound by visual inspection, considering the presence of interactions with $Lys77^{2.60}$, $Y102^{3.33}$, and $K277^{7.35}$, similarly to the previously published **1a** binding mode.

Molecular Dynamics.—The complexes between hP2Y$_{14}$R and each compound were prepared for MD simulations using the HTMD[43] module and then inserted in a 90 Å × 90 Å 1-palmitoyl-2-oleoyl-*sn*-glycero-3-phosphocholine (POPC) lipid bilayer generated through the VMD Membrane Plugin,[44] according to the orientation provided by the Positioning of Proteins in Membrane (PPM)[45] web server. TIP3P[46] water molecules were added to the systems (with a positive and negative padding of 15 Å on the *z* axis), which were then neutralized by Na^+/Cl^- counterions at a concentration of 0.154 M.

The MD simulations were carried out with ACEMD[47] as a molecular dynamics engine. The CHARMM36[48,49] force field was employed for proteins, lipids, water, and ions and the CGenFF[50,51] force field for the ligands, with assignment of missing parameters by analogy through the ParamChem[52] web service.

The systems were minimized (5000 conjugate gradient steps) and then submitted to an equilibration stage of 40 ns MD simulation in the NPT ensemble, applying positional harmonic restraints to ligand and protein atoms (0.8 kcal mol^{-1} Å^{-2} for ligand atoms, 0.85 kcal mol^{-1} Å^{-2} for Cα carbon atoms, and 0.4 kcal mol^{-1} Å^{-2} for the other protein atoms) that were linearly reduced after 20 ns. Three 30 ns replicates of MD simulations were run in the NVT ensemble, starting from the equilibrated system. A pressure around 1 atm was maintained by a Berendsen barostat (relaxation time, 800 fs) during the equilibration, and a temperature of about 310 K was kept by a Langevin thermostat (damping constants of 1 and 0.1 ps^{-1} for equilibration and production, respectively). The time step was set to 2 fs, and the hydrogen-containing bonds were constrained by the M-SHAKE[53] algorithm. A 9 Å nonbonded interaction cutoff and a 7.5 Å switching distance were employed, and long-range electrostatic interactions beyond the cutoff were computed with the particle mesh Ewald (PME)[54] method (1 Å grid spacing). All the simulations were run on NVIDIA Tesla P100 GPUs of the NIH HPC Biowulf cluster.

Molecular Dynamics Analysis.—The MD trajectories were analyzed with an in-house script written in Tcl, employing VMD 1.9.3.[44] The complexes were aligned to their initial conformation by superposition of the protein Cα carbon atoms. H bonds were estimated using the VMD Hbonds plugin, using a donor–acceptor distance of 3.5 Å and a donor–H–acceptor angle of 30°. Ligand–protein electrostatic and van der Waals interactions were computed with NAMD.[55] The data were plotted using gnuplot[56] (version 5.0) software. The weighted dynamic scoring function (wDSF) was computed with a python3 script, employing Pandas and SciPy for the linear fitting of the points and slope computation. Frames every 100 ps were taken into account for the wDSF analysis.

Chemical Synthesis.

Reagents and Instrumentation.—All reagents and solvents were purchased from Sigma-Aldrich (St. Louis, MO), Enamine, Ltd. (Monmouth Jct., NJ; compound **69**), Alchem Pharmtech, Inc. (Monmouth Jct., NJ; compound **70**), or ChemScene, LLC (Monmouth Jct., NJ; compound **71**) unless noted. ^{1}H NMR spectra were obtained with a Bruker 400 spectrometer using $CDCl_3$, CD_3OD, and DMSO-d_6 as solvents. Chemical shifts are expressed in δ values (ppm) with tetramethylsilane (δ 0.00) for $CDCl_3$ and water (δ 3.30)

for CD_3OD. NMR spectra were collected with a Bruker AV spectrometer equipped with a z-gradient [^1H,^{13}C,^{15}N]-cryoprobe. TLC analysis was carried out on glass sheets precoated with silica gel F254 (0.2 mm) from Sigma-Aldrich. The purity of final compounds was checked using an Agilent 1260 Infinity HPLC equipped with an Agilent Eclipse 5 μm XDB-C18 analytical column (250 × 4.6 mm; Agilent Technologies Inc.; Palo Alto, CA). Mobile phase: linear gradient solvent system, 10 mM triethylammonium acetate/CH_3CN from 95:5 to 5:95 in 20 min or CH_3CN/0.1% formic acid and 5% methanol in water from 30:70 to 55:45 in 20 min; the flow rate was 1.0 mL min^{-1}. Peaks were detected by UV absorption with a diode array detector at 210, 254, and 280 nm. All derivatives tested for biological activity showed >95% purity by HPLC analysis (detection at 254 nm). Low-resolution mass spectrometry was performed with a JEOL SX102 spectrometer with 6 kV Xe atoms following desorption from a glycerol matrix or on an Agilent LC/MS 1100 MSD, with a Waters (Milford, MA) Atlantis C18 column. High-resolution mass spectroscopic (HRMS) measurements were performed on a proteomics optimized Q-TOF-2 (MicromassWaters) using external calibration with polyalanine, unless noted. Observed mass accuracies are those expected based on known instrument performance as well as trends in masses of standard compounds observed at intervals during the series of measurements. Reported masses are observed masses uncorrected for this time-dependent drift in mass accuracy. tPSA (total polar surface area) was calculated using ChemDraw Professional (PerkinElmer, Boston, MA, v. 16.0). cLogP was calculated as reported.[57] The synthesis of **1b** was recently described.[7]

General Procedures: Deprotection Reactions. Method A.—A mixture of compound (1 equiv) and potassium hydroxide (5 equiv) in methanol/water (2:1) was stirred at 50 °C. This mixture was neutralized with 1 N HCl until pH was 5–6. The slightly acidic mixture was evaporated under reduced pressure and purified by silica gel column chromatography (dichloromethane/methanol/acetic acid = 95:5:0.1) or semipreparative HPLC (10 mM triethylammonium acetate buffer/acetonitrile = 80:20 to 20:80 in 40 min) to afford the compound as a white solid.

Method B.—A solution of compound in trifluoroacetic acid/tetrahydrofuran (2:1) was stirred at room temperature. The solvent was evaporated with toluene under reduced pressure. The residue was purified by silica gel column chromatography (dichloromethane/methanol = 95:5) or semipreparative HPLC (10 mM triethylammonium acetate buffer/acetonitrile = 80:20 to 20:80 in 40 min) to afford the compound as a white solid.

General Procedures: Suzuki Reaction. Method C.—The mixture of compound **38** (1 equiv), $Pd(PPh_3)_4$ (0.06 equiv), and potassium carbonate (3 equiv) in *N,N*-dimethylformamide was purged with nitrogen gas for 15 min, and then various aryl halides (1.2 equiv) were added to the mixture. The mixture was stirred at 85 °C for 5 h and then allowed to be cooled to room temperature. This mixture was partitioned between ethyl acetate (5 mL) and water (10 mL). The aqueous layer was extracted with ethyl acetate (5 mL × 2), and then the combined organic layer was washed with brine (3 mL), dried ($MgSO_4$ or Na_2SO_4), filtered, and evaporated under reduced pressure. The residue was purified by silica gel column chromatography to afford the compound as a white solid.

Method D.—The mixture of compound **38** (1 equiv) and aryl halide (1.2 equiv) in dimethoxyethane/2 M Na_2CO_3 aqueous solution (10:1) was purged with nitrogen gas for 30 min, and then $PdCl_2$(dppf) (0.1 equiv) was added to the mixture. The mixture was stirred at 60 °C for 4 h. After cooling at room temperature, this mixture was partitioned between ethyl acetate (5 mL) and water (10 mL). The aqueous layer was extracted with ethyl acetate (5 mL × 2), and then the combined organic layer was washed with brine (3 mL), dried ($MgSO_4$ or Na_2SO_4), filtered, and evaporated under reduced pressure. The residue was purified by silica gel column chromatography to afford the compound as a white solid.

Method E.—A mixture of compound **38** (1 equiv) and aryl bromide (1.2 equiv) in DMF/H_2O (10:1; 20 mM) was purged with nitrogen gas for 30 min, and then $Pd(PPh_3)_4$ (0.05 equiv) and Na_2CO_3 (3 equiv) were added to the mixture, which was stirred for 1 h at 40–120 °C. The aqueous layer was extracted with ethyl acetate twice, and then the combined organic layer was washed with brine, dried ($MgSO_4$ or Na_2SO_4), filtered, and evaporated under reduced pressure. The residue was purified by silica gel column chromatography to afford the compound as white solids.

Method F.—The mixture of compound **38** (1 equiv), $Pd(PPh_3)_4$ (0.06 equiv), potassium carbonate (3 equiv), and various aryl halides (1.2 equiv) in *N,N*-dimethylformamide was purged with nitrogen gas for 15 min. The mixture was stirred at 100 °C for 30–90 min in microwave. After microwave irradiation, the mixture was allowed to be cooled at room temperature. This mixture was partitioned between ethyl acetate (5 mL) and water (10 mL). The aqueous layer was extracted with ethyl acetate (5 mL × 2), and then the combined organic layer was washed with brine (3 mL), dried (Na_2SO_4), filtered, and evaporated under reduced pressure. The residue was purified by silica gel column chromatography to afford the compound as a white solid.

4-(4-(1-Formylpiperidin-4-yl)phenyl)-7-(4-(trifluoromethyl)-phenyl)-2-naphthoic Acid (1c).—To a solution of acetic formic anhydride (1 mL from Ac_2O and formic acid = 2:1, v/v) was slowly added compound **1a** (10 mg, 0.019 mmol) at 0 °C. After complete addition, cooling was continued for 3 h, and the mixture was then stirred at rt for 12 h. The reaction mixture was evaporated under reduced pressure. The residue was purified by silica gel column chromatography (dichloromethane/methanol = 50:1) to afford the compound **1c** (7.0 mg, 71%) as a white solid. HPLC purity: 98% (R_t = 14.62 min). ^{1}H NMR (400 MHz, DMSO-d_6): δ 8.73 (s, 1H), 8.64 (s, 1H), 8.08–7.96 (m, 5H), 7.90–7.88 (m, 3H), 7.50–7.44 (m, 4H), 4.37–4.34 (m, 1H), 3.85–3.81 (m, 1H), 3.22–3.16 (m, 1H), 2.97–2.90 (m, 1H), 2.77–2.70 (m, 1H), 1.96–1.89 (m, 2H), 1.68–1.47 (m, 2H). MS (ESI, *m/z*): 504.2 $[M + 1]^+$. ESI-HRMS (*m/z*): calcd $[M + 1]^+$ for $C_{30}H_{25}NO_3F_3$, 503.1787; found, 504.1792.

4-(4-(1-(2,2,2-Trifluoroacetyl)piperidin-4-yl)phenyl)-7-(4-(trifluoromethyl)phenyl)-2-naphthoic Acid (1d).—To trifluoroacetic anhydride (100 μL) was slowly added compound **1a** (10 mg, 0.019 mmol) at 0 °C. After complete addition, cooling was continued for 1 h, and the mixture was then stirred at rt for 2 h. The reaction mixture was evaporated under reduced pressure. The residue was purified by silica gel column chromatography (dichloromethane/methanol = 50:1) to afford compound **1d** (10.0

mg, 92%) as a white solid. HPLC purity: 99% (R_t = 16.92 min). ^{1}H NMR (400 MHz, $CDCl_3$): δ 8.80 (s, 1H), 8.27 (s, 1H), 8.12–8.07 (m, 2H), 7.86–7.77 (m, 5H), 7.53 (d, J = 8.00 Hz, 2H), 7.39 (d, J = 8.00 Hz, 2H), 4.81–4.78 (m, 1H), 4.25–4.22 (m, 1H), 3.37–3.30 (m, 1H), 3.01–2.92 (m, 2H), 2.15–2.11 (m, 2H), 1.91–1.81 (m, 2H). MS (ESI, *m/z*): 570.1 $[M - 1]^-$. ESI-HRMS (*m/z*): $[M - 1]^-$ calcd for $C_{31}H_{22}NO_3F_6$, 570.1504; found, 570.1493.

(4′-(Piperidin-4-yl)-5-(4-(4-(trifluoromethyl)phenyl)-1H-1,2,3-triazol-1-yl)-[1,1′-biphenyl]-3-yl)methyl Dihydrogen Phosphate (3b).—Method B. Yield: 69%. HPLC purity: 96% (R_t = 8.58 min). ^{1}H NMR (400 MHz, DMSO-d_6): δ 9.20–9.19 (m, 1H), 8.05–8.03 (m, 2H), 7.96 (s, 1H), 7.85 (s, 1H), 7.79 (d, J = 8.00 Hz, 2H), 7.74 (s, 1H), 7.67 (d, J = 8.40 Hz, 2H), 7.34 (d, J = 7.60 Hz, 2H), 4.82–4.80 (m, 2H), 2.96–2.92 (m, 2H), 2.66–2.58 (m, 3H), 1.71–1.67 (m, 2H), 1.56–1.49 (m, 2H). MS (ESI, *m/z*): 559.2 $[M + 1]^+$. ESI-HRMS (*m/z*): $[M + 1]^+$ calcd for $C_{27}H_{27}N_4O_4F_3P$, 559.1722; found, 559.1716.

4′-Amino-5-(4-(4-(trifluoromethyl)phenyl)-1H-1,2,3-triazol-1-yl)-[1,1′-biphenyl]-3-carboxylic Acid (7).—Method A. Yield: 62%. HPLC purity: 97% (R_t = 8.96 min). ^{1}H NMR (400 MHz, CD_3OD): δ 9.25 (s, 1H), 8.48 (s, 1H), 8.37 (s, 2H), 8.16 (d, J = 8.00 Hz, 2H), 7.79 (d, J = 8.00 Hz, 2H), 7.73 (d, J = 8.40 Hz, 2H), 7.62 (d, J = 8.40 Hz, 2H). MS (ESI, *m/z*): 425.1 $[M + 1]^+$. ESI-HRMS (*m/z*): $[M + 1]^+$ calcd for $C_{22}H_{16}N_4O_2F_3$, 425.1225; found, 425.1221.

4′-Acetamido-5-(4-(4-(trifluoromethyl)phenyl)-1H-1,2,3-triazol-1-yl)-[1,1′-biphenyl]-3-carboxylic Acid (8).—Method A. Yield: 76%. HPLC purity: 99% (R_t = 7.95 min). ^{1}H NMR (400 MHz, CD_3OD): δ 9.21 (s, 1H), 8.46 (s, 1H), 8.34 (d, J = 7.20 Hz, 2H), 8.13 (d, J = 8.00 Hz, 2H), 7.76 (d, J = 8.40 Hz, 2H), 7.72 (s, 4H), 2.15 (s, 3H). MS (ESI, *m/z*): 467.1 $[M + 1]^+$. ESI-HRMS (*m/z*): $[M + 1]^+$ calcd for $C_{24}H_{18}N_4O_3F_3$, 467.1331; found, 467.1330.

4′-Benzamido-5-(4-(4-(trifluoromethyl)phenyl)-1H-1,2,3-triazol-1-yl)-[1,1′-biphenyl]-3-carboxylic Acid (9).—Method A. Yield: 73%. HPLC purity: 99% (R_t = 9.48 min). ^{1}H NMR (400 MHz, DMSO-d_6): δ 9.70 (s, 1H), 8.41 (s, 1H), 8.29 (broad s, 2H), 8.21 (d, J = 7.60 Hz, 2H), 8.00–7.97 (m, 4H), 7.90–7.83 (m, 4H), 7.62–7.54 (m, 3H). MS (ESI, *m/z*): 529.1 $[M + 1]^+$. ESI-HRMS (*m/z*): $[M + 1]^+$ calcd for $C_{29}H_{20}N_4O_3F_3$, 529.1488; found, 529.1489.

4′-((tert-Butoxycarbonyl)amino)-5-(4-(4-(trifluoromethyl)-phenyl)-1H-1,2,3-triazol-1-yl)-[1,1′-biphenyl]-3-carboxylic Acid (10).—Method A. Yield: 50%. HPLC purity: 99% (R_t = 10.36 min). ^{1}H NMR (400 MHz, CD_3OD): δ 9.25 (s, 1H), 8.48 (s, 1H), 8.37–8.35 (m, 2H), 8.16 (d, J = 8.40 Hz, 2H), 7.78 (d, J = 8.00 Hz, 2H), 7.71 (d, J = 8.40 Hz, 2H), 7.58 (d, J = 8.40 Hz, 2H), 1.54 (s, 9H). MS (ESI, *m/z*): 525.2 $[M + 1]^+$. ESI-HRMS (*m/z*): $[M + 1]^+$ calcd for $C_{27}H_{24}N_4O_4F_3$, 525.1750; found, 525.1755.

4′-(Piperidine-4-carboxamido)-5-(4-(4-(trifluoromethyl)phenyl)-1H-1,2,3-triazol-1-yl)-[1,1′-biphenyl]-3-carboxylic Acid (11).—Method B. Yield: 87%. HPLC purity: 99% (R_t = 21.20 min). ^{1}H NMR (400 MHz, DMSO-d_6): δ 8.03–8.01 (m, 4H), 7.83 (s, 1H), 7.68 (d, J = 8.40 Hz, 2H), 7.30–7.25 (m, 5H), 2.70–2.68 (m, 2H), 2.23–2.20 (m,

2H), 2.00–1.93 (m, 1H), 1.44–1.27 (m, 4H). MS (ESI, *m/z*): 536.2 $[M + Na]^+$. ESI-HRMS (*m/z*): $[M + 1]^+$ calcd for $C_{28}H_{25}N_5O_3F_3$, 536.1909; found, 536.1913.

4′-(1-(tert-Butoxycarbonyl)piperidine-4-carboxamido)-5-(4-(4-(trifluoromethyl)phenyl)-1H-1,2,3-triazol-1-yl)-[1,1′-biphenyl]-3-carboxylic Acid (12).—Method A. Yield: 82%. HPLC purity: 98% (R_t = 24.10 min). ^{1}H NMR (400 MHz, DMSO-d_6): δ 9.73 (s, 1H), 8.43 (s, 1H), 8.38 (s, 1H), 8.27 (s, 1H), 8.20 (d, J = 8.00 Hz, 2H), 7.90 (d, J = 8.40 Hz, 2H), 7.91–7.77 (m, 4H), 4.05–3.97 (m, 2H), 2.92–2.75 (m, 3H), 1.85–1.76 (m, 2H), 1.56–1.45 (m, 2H), 1.41 (s, 9H). MS (ESI, *m/z*): 658.2 $[M + Na]^+$. ESI-HRMS (*m/z*): $[M + Na]^+$ calcd for $C_{33}H_{32}N_5O_5F_3Na$, 658.2253; found, 658.2256.

5-(4-(4-(Trifluoromethyl)phenyl)-1H-1,2,3-triazol-1-yl)-[1,1′-bi-phenyl]-3,4′-dicarboxylic Acid (13).—Method A. Yield: 68%. HPLC purity: 99% (R_t = 13.46 min). ^{1}H NMR (400 MHz, DMSO-d_6): δ 9.77 (s, 1H), 8.56–8.53 (m, 2H), 8.36 (broad s, 1H), 8.20 (d, J = 8.00 Hz, 2H), 8.11 (d, J = 8.40 Hz, 2H), 8.00 (d, J = 8.40 Hz, 2H), 7.91 (d, J = 8.40 Hz, 2H). MS (ESI, *m/z*): 454.1 $[M + 1]^+$. ESI-HRMS (*m/z*): $[M + 1]^+$ calcd for $C_{23}H_{15}N_3O_4F_3$, 454.1015; found, 454.1017.

4′-((3-Aminopropyl)carbamoyl)-5-(4-(4-(trifluoromethyl)-phenyl)-1H-1,2,3-triazol-1-yl)-[1,1′-biphenyl]-3-carboxylic Acid (14).—Method B. Yield: 63%. HPLC purity: 97% (R_t = 12.68 min). ^{1}H NMR (400 MHz, DMSO-d_6): δ 9.73 (s, 1H), 8.55 (s, 1H), 8.51 (s, 1H), 8.37 (s, 1H), 8.23–8.20 (m, 4H), 8.00 (d, J = 8.40 Hz, 2H), 7.90 (d, J = 8.00 Hz, 2H), 3.51–3.46 (m, 2H), 3.00–2.99 (m, 2H), 1.93–1.90 (m, 2H). MS (ESI, *m/z*): 510.2 $[M + 1]^+$. ESI-HRMS (*m/z*): $[M + 1]^+$ calcd for $C_{26}H_{23}N_5O_3F_3$, 510.1753; found, 510.1754.

4′-Bromo-5-(4-(4-(trifluoromethyl)phenyl)-1H-1,2,3-triazol-1-yl)-[1,1′-biphenyl]-3-carboxylic Acid (15).—Method A. Yield: 77%. HPLC purity: 99% (R_t = 12.93 min). ^{1}H NMR (400 MHz, CD_3OD): δ 9.17 (s, 1H), 8.43 (s, 1H), 8.35 (s, 1H), 8.25 (s, 1H), 8.16 (d, J = 8.00 Hz, 2H), 7.79 (d, J = 8.00 Hz, 2H), 7.72 (d, J = 8.00 Hz, 2H), 7.66 (d, J = 8.40 Hz, 2H). MS (ESI, *m/z*): 488.0, 490.0 $[M + 1]^+$. ESI-HRMS (*m/z*): $[M + 1]^+$ calcd for $C_{22}H_{14}N_3O_2F_3Br$, 488.0221; found, 488.0218.

4′-(2-Amino-2-oxoethyl)-5-(4-(4-(trifluoromethyl)phenyl)-1H-1,2,3-triazol-1-yl)-[1,1′-biphenyl]-3-carboxylic Acid (16).—Method A. Yield: 64%. HPLC purity: 99% (R_t = 8.55 min). ^{1}H NMR (400 MHz, CD_3OD): δ 9.24 (s, 1H), 8.50 (s, 1H), 8.38 (s, 2H), 8.16 (d, J = 8.00 Hz, 2H), 7.79–7.74 (m, 4H), 7.48 (d, J = 7.60 Hz, 2H), 3.60 (s, 2H). MS (ESI, *m/z*): 467.1 $[M + 1]^+$. ESI-HRMS (*m/z*): $[M + 1]^+$ calcd for $C_{24}H_{18}N_4O_3F_3$, 467.1331; found, 467.1332.

4′-(2-Cyanoethyl)-5-(4-(4-(trifluoromethyl)phenyl)-1H-1,2,3-triazol-1-yl)-[1,1′-biphenyl]-3-carboxylic Acid (17).—The mixture of compound **38** (30 mg, 0.063 mmol), $Pd(PPh_3)_4$ (4 mg, 0.003 mmol), and 2 M K_2CO_3 aqueous solution (90 μL, 0.180 mmol) in *N,N*-dimethylformamide/water (1:1, 3 mL) was purged with nitrogen gas for 15 min, and then 3-(4-bromophenyl)propionitrile (16 mg, 0.076 mmol) was added to the mixture. The mixture was stirred at 90 °C for 12 h and then allowed to be cooled at room temperature. This mixture was partitioned between ethyl acetate (5 mL) and water (10 mL). The aqueous

layer was extracted with ethyl acetate (5 mL × 2), and then the combined organic layer was washed with brine (3 mL), dried ($MgSO_4$), filtered, and evaporated under reduced pressure. The residue was purified by silica gel column chromatography (chloroform/methanol = 10:1) to afford the compound **17** (18 mg, 61%) as a white solid. HPLC purity: 99% (R_t = 7.63 min). ^{1}H NMR (400 MHz, CD_3OD): δ 9.27 (s, 1H), 8.53 (s, 1H), 8.40 (m, 2H), 8.17 (d, J = 8.00 Hz, 2H), 7.80–7.77 (m, 4H), 7.48 (d, J = 8.00 Hz, 2H), 3.03 (t, J = 7.20 Hz, 2H), 2.81 (t, J = 7.20 Hz, 2H). MS (ESI, *m/z*): 463.1 $[M + 1]^+$. ESI-HRMS (*m/z*): $[M + 1]^+$ calcd for $C_{25}H_{18}N_4O_2F_3$, 463.1382; found, 463.1381.

4′-(3-Aminopropyl)-5-(4-(4-(trifluoromethyl)phenyl)-1H-1,2,3-triazol-1-yl)-[1,1′-biphenyl]-3-carboxylic Acid (18).—Method B. Yield: 98%. HPLC purity: 98% (R_t = 8.14 min). ^{1}H NMR (400 MHz, CD_3OD): δ 9.27 (s, 1H), 8.52 (s, 1H), 8.42 (s, 1H), 8.38 (s, 1H), 8.17 (d, J = 7.60 Hz, 2H), 7.80–7.75 (m, 4H), 7.43 (d, J = 8.00 Hz, 2H), 2.99 (t, J = 7.60 Hz, 2H), 2.82 (t, J = 7.60 Hz, 2H), 2.05–2.02 (m, 2H). MS (ESI, *m/z*): 467.2 $[M + 1]^+$. ESI-HRMS (*m/z*): $[M + 1]^+$ calcd for $C_{25}H_{22}N_4O_2F_3$, 467.1695; found, 467.1689.

4′-(3-Aminoprop-1-yn-1-yl)-5-(4-(4-(trifluoromethyl)phenyl)-1H-1,2,3-triazol-1-yl)-[1,1′-biphenyl]-3-carboxylic Acid (19).—Method B. Yield: 62%. HPLC purity: 97% (R_t = 10.49 min). ^{1}H NMR (400 MHz, DMSO-d_6): δ 9.67 (s, 1H), 8.42 (s, 1H), 8.26 (s, 1H), 8.21 (d, J = 8.00 Hz, 2H), 8.16 (s, 1H), 7.88 (d, J = 8.40 Hz, 2H), 7.79 (d, J = 8.00 Hz, 2H), 7.53 (d, J = 8.00 Hz, 2H), 3.53 (s, 2H). MS (ESI, *m/z*): 463.1 $[M + 1]^+$. ESI-HRMS (*m/z*): $[M + 1]^+$ calcd for $C_{25}H_{18}N_4O_2F_3$, 463.1382; found, 463.1380.

4′-(3-((tert-Butoxycarbonyl)amino)propyl)-5-(4-(4-(trifluoromethyl)phenyl)-1H-1,2,3-triazol-1-yl)-[1,1′-biphenyl]-3-carboxylic Acid (20).—Method A. Yield: 66%. HPLC purity: 99% (R_t = 10.56 min). ^{1}H NMR (400 MHz, CD_3OD): δ 9.24 (s, 1H), 8.49 (s, 1H), 8.38–8.36 (m, 2H), 8.16 (d, J = 8.00 Hz, 2H), 7.78 (d, J = 8.00 Hz, 2H), 7.70 (d, J = 8.40 Hz, 2H), 7.37 (d, J = 8.00 Hz, 2H), 3.10 (t, J = 7.20 Hz, 2H), 2.71 (t, J = 7.20 Hz, 2H), 1.87–1.78 (m, 2H), 1.45 (s, 9H). MS (ESI, *m/z*): 589.2 $[M + Na]^+$. ESI-HRMS (*m/z*): $[M + 1]^+$ calcd for $C_{30}H_{29}N_4O_4F_3Na$, 589.2039; found, 589.2043.

4′-(4-Hydroxybutyl)-5-(4-(4-(trifluoromethyl)phenyl)-1H-1,2,3-triazol-1-yl)-[1,1′-biphenyl]-3-carboxylic Acid (21).—Method A. Yield: 39%. HPLC purity: 99% (R_t = 7.40 min). ^{1}H NMR (400 MHz, CD_3OD): δ 9.25 (s, 1H), 8.50 (s, 1H), 8.38 (s, 2H), 8.16 (d, J = 8.00 Hz, 2H), 7.79 (d, J = 8.40 Hz, 2H), 7.70 (d, J = 8.00 Hz, 2H), 7.37 (d, J = 8.00 Hz, 2H), 3.59 (t, J = 6.40 Hz, 2H), 2.72 (t, J = 7.60 Hz, 2H), 1.78–1.71 (m, 2H), 1.64–1.57 (m, 2H). MS (ESI, *m/z*): 482.2 $[M + 1]^+$. ESI-HRMS (*m/z*): $[M + 1]^+$ calcd for $C_{26}H_{23}N_3O_3F_3$, 482.1692; found, 482.1694.

4′-(1-Aminocyclopropyl)-5-(4-(4-(trifluoromethyl)phenyl)-1H-1,2,3-triazol-1-yl)-[1,1′-biphenyl]-3-carboxylic Acid (22).—Method A. Yield: 69%. HPLC purity: 98% (R_t = 6.80 min). ^{1}H NMR (400 MHz, CD_3OD): δ 9.27 (s, 1H), 8.55–8.39 (m, 3H), 8.15 (broad s, 2H), 7.88 (broad s, 2H), 7.78 (broad s, 2H), 7.63 (broad s, 2H), 1.43–1.38 (m, 4H). MS (ESI, *m/z*): 465.2 $[M + 1]^+$. ESI-HRMS (*m/z*): $[M + 1]^+$ calcd for $C_{25}H_{20}N_4O_2F_3$, 465.1538; found, 465.1539.

4′-(1-(Aminomethyl)cyclopropyl)-5-(4-(4-(trifluoromethyl)-phenyl)-1H-1,2,3-triazol-1-yl)-[1,1′-biphenyl]-3-carboxylic Acid (23).—Method B. Yield: 52%. HPLC purity: 97% (R_t = 10.85 min). ^{1}H NMR (400 MHz, CD_3OD): δ 9.08 (s, 1H), 8.38 (s, 1H), 8.30 (s, 1H), 8.16 (s, 1H), 8.09 (d, J = 8.00 Hz, 2H), 7.77–7.73 (m, 4H), 7.55 (d, J = 8.00 Hz, 2H), 3.22 (s, 2H), 1.09–1.06 (m, 4H). MS (ESI, *m/z*): 479.2 $[M + 1]^+$. ESI-HRMS (*m/z*): $[M + 1]^+$ calcd for $C_{26}H_{22}N_4O_2F_3$, 479.1695; found, 479.1693.

4′-(1-(((tert-Butoxycarbonyl)amino)methyl)cyclopropyl)-5-(4-(4-(trifluoromethyl)phenyl)-1H-1,2,3-triazol-1-yl)-[1,1′-biphenyl]-3-carboxylic Acid (24).—Method A. Yield: 51%. HPLC purity: 99% (R_t = 21.57 min). ^{1}H NMR (400 MHz, CD_3OD): δ 9.26 (s, 1H), 8.51 (s, 1H), 8.40–8.38 (m, 2H), 8.17 (d, J = 8.00 Hz, 2H), 7.80 (d, J = 8.00 Hz, 2H), 7.73 (d, J = 8.00 Hz, 2H), 7.51 (d, J = 8.00 Hz, 2H), 3.34 (s, 2H), 1.39–1.28 (m, 9H), 0.94–0.86 (m, 4H). MS (ESI, *m/z*): 601.2 $[M + Na]^+$. ESI-HRMS (*m/z*): $[M + Na]^+$ calcd for $C_{31}H_{29}N_4O_4F_3Na$, 601.2039; found, 601.2040.

4′-(1-Aminocyclobutyl)-5-(4-(4-(trifluoromethyl)phenyl)-1H-1,2,3-triazol-1-yl)-[1,1′-biphenyl]-3-carboxylic Acid (25).—Method B. Yield: 65%. HPLC purity: 99% (R_t = 8.69 min). ^{1}H NMR (400 MHz, CD_3OD): δ 9.27 (s, 1H), 8.55 (s, 1H), 8.45 (s, 1H), 8.41 (s, 1H), 8.16 (d, J = 8.00 Hz, 2H), 7.93 (d, J = 8.40 Hz, 2H), 7.79 (d, J = 8.40 Hz, 2H), 7.69 (d, J = 8.40 Hz, 2H), 2.89–2.82 (m, 2H), 2.70–2.63 (m, 2H), 2.33–2.24 (m, 1H), 2.07–1.97 (m, 1H). MS (eSI, *m/z*): 479.3 $[M + 1]^+$. ESI-HRMS (*m/z*): $[M + 1]^+$ calcd for $C_{26}H_{22}N_4O_2F_3$, 479.1695; found, 479.1696.

4′-(1-((tert-Butoxycarbonyl)amino)cyclobutyl)-5-(4-(4-(trifluoromethyl)phenyl)-1H-1,2,3-triazol-1-yl)-[1,1′-biphenyl]-3-carboxylic Acid (26).—Method A. Yield: 47%. HPLC purity: 99% (R_t = 10.76 min). ^{1}H NMR (400 MHz, CD_3OD): δ 9.18 (s, 1H), 8.40–8.39 (m, 2H), 8.26 (s, 1H), 8.17 (d, J = 8.00 Hz, 2H), 7.80–7.76 (m, 4H), 7.59 (d, J = 8.40 Hz, 2H), 2.60–2.46 (m, 4H), 2.16–2.07 (m, 1H), 1.99–1.88 (m, 1H), 1.40–1.25 (m, 9H). MS (ESI, *m/z*): 579.2 $[M + 1]^+$. ESI-HRMS (*m/z*): $[M + 1]^+$ calcd for $C_{31}H_{30}N_4O_4F_3$, 579.2219; found, 579.2219.

4′-(3-(Hydroxymethyl)oxetan-3-yl)-5-(4-(4-(trifluoromethyl)-phenyl)-1H-1,2,3-triazol-1-yl)-[1,1′-biphenyl]-3-carboxylic Acid (27).—Method A. Yield: 47%. HPLC purity: 99% (R_t = 8.71 min). ^{1}H NMR (400 MHz, CD_3OD): δ 9.25 (s, 1H), 8.51 (s, 1H), 8.41 (s, 1H), 8.39 (s, 1H), 8.15 (d, J = 8.40 Hz, 2H), 7.80–7.77 (m, 4H), 7.32 (d, J = 8.00 Hz, 2H), 4.97 (d, J = 5.60 Hz, 2H), 4.89 (d, J = 6.00 Hz, 2H), 3.94 (s, 2H). MS (ESI, *m/z*): 496.2 $[M + 1]^+$. ESI-HRMS (*m/z*): $[M + 1]^+$ calcd for $C_{26}H_{21}N_3O_4F_3$, 496.1484; found, 496.1488.

4′-(Isoxazol-3-yl)-5-(4-(4-(trifluoromethyl)phenyl)-1H-1,2,3-triazol-1-yl)-[1,1′-biphenyl]-3-carboxylic Acid (28).—Method A. Yield: 74%. HPLC purity: 98% (R_t = 11.86 min). ^{1}H NMR (400 MHz, CD_3OD): δ 9.28 (s, 1H), 8.75 (s, 1H), 8.57 (s, 1H), 8.46 (s, 2H), 8.17 (d, J = 7.60 Hz, 2H), 8.05 (d, J = 8.00 Hz, 2H), 7.94 (d, J = 8.40 Hz, 2H), 7.79 (d, J = 8.00 Hz, 2H), 7.00 (s, 1H). MS (ESI, *m/z*): 477.1 $[M + 1]^+$. ESI-HRMS (*m/z*): $[M + 1]^+$ calcd for $C_{25}H_{16}N_4O_3F_3$, 477.1175; found, 477.1177.

4′-(5-(Hydroxymethyl)isoxazol-3-yl)-5-(4-(4-(trifluoromethyl)-phenyl)-1H-1,2,3-triazol-1-yl)-[1,1′-biphenyl]-3-carboxylic Acid (29).—Method A. Yield: 43%. HPLC purity: 98% (R_t = 20.10 min). ^{1}H NMR (400 MHz, DMSO-d_6): δ 9.77 (s, 1H), 8.57 (s, 1H), 8.54 (s, 1H), 8.36 (s, 1H), 8.20 (d, J = 8.00 Hz, 2H), 8.08–8.01 (m, 4H), 7.91 (d, J = 8.00 Hz, 2H), 7.05 (s, 1H), 5.75 (t, J = 6.00 Hz, 1H), 4.64 (d, J = 6.00 Hz, 2H). MS (ESI, *m/z*): 507.1 $[M + 1]^+$. ESI-HRMS (*m/z*): $[M + 1]^+$ calcd for $C_{26}H_{18}N_4O_4F_3$, 507.1280; found, 507.1271.

4′-(5-(2-Hydroxyethyl)isoxazol-3-yl)-5-(4-(4-(trifluoromethyl)-phenyl)-1H-1,2,3-triazol-1-yl)-[1,1′-biphenyl]-3-carboxylic Acid (30).—Method A. Yield: 55%. HPLC purity: 95% (R_t = 10.69 min). ^{1}H NMR (400 MHz, DMSO-d_6): δ 9.74 (s, 1H), 8.51 (s, 1H), 8.46 (s, 1H), 8.35 (s, 1H), 8.20 (d, J = 8.00 Hz, 2H), 8.03–7.98 (m, 4H), 7.90 (d, J = 8.00 Hz, 2H), 6.93 (s, 1H), 3.77 (t, J = 6.40 Hz, 2H), 2.97 (d, J = 6.40 Hz, 2H). MS (ESI, *m/z*): 521.1 $[M + 1]^+$. ESI-HRMS (*m/z*): $[M + 1]^+$ calcd for $C_{27}H_{20}N_4O_4F_3$, 521.1437; found, 521.1435.

4′-(1H-Tetrazol-5-yl)-5-(4-(4-(trifluoromethyl)phenyl)-1H-1,2,3-triazol-1-yl)-[1,1′-biphenyl]-3-carboxylic Acid (31).—Method A. Yield: 43%. HPLC purity: 98% (R_t = 15.95 min). ^{1}H NMR (400 MHz, CD_3OD): δ 9.24 (s, 1H), 8.49 (s, 1H), 8.45 (s, 1H), 8.35 (s, 1H), 8.22–8.17 (m, 4H), 7.92 (d, J = 8.40 Hz, 2H), 7.80 (d, J = 8.00 Hz, 2H). MS (ESI, *m/z*): 478.1 $[M + 1]^+$. ESI-HRMS (*m/z*): $[M + 1]^+$ calcd for $C_{23}H_{15}N_7O_2F_3$, 478.1239; found, 478.1242.

4-(4-(5-(Hydroxymethyl)isoxazol-3-yl)phenyl)-7-(4-(trifluoromethyl)phenyl)-2-naphthoic Acid (32).—Method A. Yield: 93%. HPLC purity: 98% (R_t = 12.07 min). ^{1}H NMR (400 MHz, DMSO-d_6): δ 8.79 (s, 1H), 8.68 (s, 1H), 8.09–8.05 (m, 5H), 8.01–7.98 (m, 1H), 7.95 (m, 1H), 7.91–7.89 (m, 2H), 7.70 (d, J = 8.40 Hz, 2H), 7.04 (s, 1H), 5.80–5.73 (m, 1H), 4.66–4.63 (m, 2H). MS (ESI, *m/z*): 490.1 $[M + 1]^+$. ESI-HRMS (*m/z*): $[M + 1]^+$ calcd for $C_{28}H_{19}NO_4F_3$, 490.1266; found, 490.1269.

4′-(5-(Hydroxymethyl)isoxazol-3-yl)-5-(4-(trifluoromethyl)-benzamido)-[1,1′-biphenyl]-3-carboxylic Acid (33).—Method A. Yield: 62%. HPLC purity: 99% (R_t = 10.29 min). ^{1}H NMR (400 MHz, CD_3OD): δ 8.35 (broad s, 2H), 8.17–8.13 (m, 3H), 7.97 (d, J = 8.40 Hz, 2H), 7.86–7.81 (m, 4H), 6.82 (s, 1H), 4.74 (s, 2H). MS (ESI, *m/z*): 483.1 $[M + 1]^+$. ESI-HRMS (*m/z*): $[M + 1]^+$ calcd for $C_{25}H_{18}N_2O_5F_3$, 483.1168; found, 483.1170.

4-(4-(Piperidin-4-yl)phenyl)-6-(4-(4-(trifluoromethyl)phenyl)-1H-1,2,3-triazol-1-yl)picolinic Acid (34).—Method B. Yield: 60%. HPLC purity: 99% (R_t = 7.87 min). ^{1}H NMR (400 MHz, DMSO-d_6): δ 9.55 (s, 1H), 8.31–8.26 (m, 4H), 7.91–7.85 (m, 4H), 7.47 (d, J = 8.00 Hz, 2H), 3.68–3.65 (m, 1H), 3.02–2.88 (m, 4H), 1.95–1.83 (m, 4H). MS (ESI, *m/z*): 494.2 $[M + 1]^+$. ESI-HRMS (*m/z*): $[M + 1]^+$ calcd for $C_{26}H_{23}N_5O_2F_3$, 494.1804; found, 494.1805.

2-(4-(Piperidin-4-yl)phenyl)-6-(4-(4-(trifluoromethyl)phenyl)-1H-1,2,3-triazol-1-yl)isonicotinic Acid (35).—Method B. Yield: 65%. HPLC purity: 95% (R_t = 10.72 min). ^{1}H NMR (400 MHz, DMSO-d_6): δ 9.79 (s, 1H), 8.42 (s, 2H), 8.34–8.33 (m, 4H), 7.89 (d, J = 8.00 Hz, 2H), 7.44 (d, J = 8.00 Hz, 2H), 3.62–3.59 (m, 1H), 3.07–2.92 (m, 4h), 2.03–1.89

(m, 4H). MS (ESI, *m/z*): 494.2 $[M + 1]^+$. ESI-HRMS (*m/z*): $[M + 1]^+$ calcd for $C_{26}H_{23}N_5O_2F_3$, 494.1804; found, 494.1805.

6-(4-(Piperidin-4-yl)phenyl)-4-(4-(4-(trifluoromethyl)phenyl)-1H-1,2,3-triazol-1-yl)picolinic Acid (36).—Method B. Yield: 65%. HPLC purity: 99% (R_t = 11.24 min). ^{1}H NMR (400 MHz, DMSO-d_6): δ 9.94 (s, 1H), 8.71 (s, 1H), 8.56 (s, 1H), 8.28 (d, J = 7.20 Hz, 2H), 8.19 (d, J = 7.60 Hz, 2H), 7.93 (d, J = 7.20 Hz, 2H), 7.46 (d, J = 7.20 Hz, 2H), 3.43–3.40 (m, 2H), 3.07–2.92 (m, 3h), 2.03–2.00 (m, 2H), 1.91–1.84 (m, 2H). MS (ESI, *m/z*): 494.2 $[M + 1]^+$. ESI-HRMS (*m/z*): $[M + 1]^+$ calcd for $C_{26}H_{23}N_5O_2F_3$, 494.1804; found, 494.1808.

2-(Dimethylamino)-2-oxoethyl 4′-(Piperidin-4-yl)-5-(4-(4-(trifluoromethyl)phenyl)-1H-1,2,3-triazol-1-yl)-[1,1′-biphenyl]-3-carboxylate (37a).—Method B. Yield: 78%. HPLC purity: 97% (R_t = 20.45 min). ^{1}H NMR (400 MHz, CD_3OD): δ 9.29 (s, 1H), 8.59 (s, 1H), 8.47 (s, 1H), 8.45 (s, 1H), 8.17 (d, J = 8.00 Hz, 2H), 7.82–7.79 (m, 4H), 7.47 (d, J = 8.00 Hz, 2H), 5.18 (s, 2H), 3.56–3.53 (m, 2H), 3.23–3.16 (s, 2H), 3.13 (s, 3H), 3.05–2.99 (m, 1H), 3.02 (s, 3H), 2.18–2.14 (m, 2H), 2.03–1.92 (m, 2H). MS (ESI, *m/z*): 578.3 $[M + 1]^+$. ESI-HRMS (*m/z*): $[M + 1]^+$ calcd for $C_{31}H_{31}N_5O_3F_3$, 578.2379; found, 578.2390.

2-(Dimethylamino)-2-oxoethyl 4-(4-(5-(Hydroxymethyl)isoxazol-3-yl)phenyl)-7-(4-(trifluoromethyl)phenyl)-2-naphthoate (37b).—To a solution of **32** (3.5 mg, 0.007 mmol) in DMF (1 mL) was added Cs_2CO_3 (3.0 mg, 0.010 mmol). 2-Chloro-*N,N*-dimethylacetamide (1.0 mg, 0.007 mmol) was added to the reaction mixture under a N_2 atmosphere, and the reaction mixture was stirred at 45 °C for 1 h under a N_2 atmosphere. The reaction mixture was partitioned between ethyl acetate (5 mL) and water (5 mL), and the aqueous phase was extracted with ethyl acetate (2 × 5 mL). The combined organic layers were dried over Na_2SO_4, filtered, and concentrated under pressure. The residue was purified by silica gel chromatography (chloroform/methanol = 30:1) to afford compound **37b** (2.7 mg, 68%) as a white solid. HPLC purity: 99% (R_t = 17.73 min). ^{1}H NMR (400 MHz, CD_3OD): δ 8.85–8.84 (m, 1H), 8.45–8.44 (m, 1H), 8.08–7.97 (m, 7H), 7.81 (d, J = 8.40 Hz, 2H), 7.66 (d, J = 8.00 Hz, 2H), 6.88 (s, 1H), 5.14 (s, 2H), 4.76 (s, 2H), 3.12 (s, 3H), 3.00 (s, 3h). MS (ESI, *m/z*): 575.2 $[M + 1]^+$. ESI-HRMS (*m/z*): $[M + 1]^+$ calcd for $C_{32}H_{26}N_2O_5F_3$, 575.1794; found, 575.1786.

2-(Dimethylamino)-2-oxoethyl 4-(4-(1-Acetylpiperidin-4-yl)-phenyl)-7-(4-(trifluoromethyl)phenyl)-2-naphthoate (37c).—Compound **1b** (24 mg, 0.046 mmol) was converted to compound **37c** (20 mg, 72%) as a white solid, using a similar procedure to that used in the preparation of compound **87**. HPLC purity: 99% (R_t = 16.43 min). ^{1}H NMR (400 MHz, CD_3OD): δ 8.80 (s, 1H), 8.42 (s, 1H), 8.03–7.98 (m, 4H), 7.93–7.91 (m, 1H), 7.80 (d, J = 7.60 Hz, 2H), 7.47–7.43 (m, 4H), 5.14 (s, 2H), 4.75–4.72 (m, 1H), 4.12–4.08 (m, 1H), 3.27–3.24 (m, 1H), 3.12 (s, 3H), 3.00 (s, 3H), 2.95–2.92 (m, 1H), 2.81–2.75 (m, 1H), 2.18 (s, 3H), 2.04–1.97 (m, 2H), 1.84–1.68 (m, 2H). MS (ESI, *m/z*): 603.2 $[M + 1]^+$. ESI-HRMS (*m/z*): $[M + 1]^+$ calcd for $C_{35}H_{34}N_2O_4F_3$, 603.2471; found, 603.2479.

Methyl 4′-((tert-Butoxycarbonyl)amino)-5-(4-(4-(trifluoromethyl)phenyl)-1H-1,2,3-triazol-1-yl)-[1,1′-biphenyl]-3-carboxylate (39).—Method C. Yield: 40%. ^{1}H NMR (400 MHz, $CDCl_3$): δ 8.40 (s, 1H), 8.33 (s, 1H), 8.29 (broad s, 2H), 8.06 (d, J = 8.00 Hz, 2H), 7.74 (d, J = 8.40 Hz, 2H), 7.64 (d, J = 8.40 Hz, 2H), 7.52 (d, J = 8.40 Hz, 2H), 4.01 (s, 3H), 1.54 (s, 9H). MS (ESI, *m/z*): 539.2 $[M + 1]^+$. ESI-HRMS (*m/z*): $[M + 1]^+$ calcd for $C_{28}H_{26}N_4O_4F_3$, 539.1906; found, 539.1916.

Methyl 4′-Amino-5-(4-(4-(trifluoromethyl)phenyl)-1H-1,2,3-triazol-1-yl)-[1,1′-biphenyl]-3-carboxylate (40).—Method B. Yield: 57%. ^{1}H NMR (400 MHz, $CDCl_3$): δ 8.38 (s, 1H), 8.32 (s, 1H), 8.26–8.24 (m, 2H), 8.06 (d, J = 8.00 Hz, 2H), 7.74 (d, J = 8.00 Hz, 2H), 7.54 (d, J = 8.40 Hz, 2H), 6.81 (d, J = 8.40 Hz, 2H), 4.00 (s, 3H). MS (ESI, *m/z*): 439.1 $[M + 1]^+$. ESI-HRMS (*m/z*): $[M + 1]^+$ calcd for $C_{23}H_{18}N_4O_2F_3$, 439.1382; found, 439.1378.

Methyl 4′-Acetamido-5-(4-(4-(trifluoromethyl)phenyl)-1H-1,2,3-triazol-1-yl)-[1,1′-biphenyl]-3-carboxylate (41).—40 (12 mg, 0.027 mmol) was dissolved in dichloromethane (1 mL) and degassed for 30 min with nitrogen gas. Acetic anhydride (3.2 μL, 0.033 mmol) was added to the reaction mixture and was stirred for 2 h at room temperature. The reaction mixture was partitioned between dichloromethane (10 mL) and saturated aqueous Na_2CO_3 solution (10 mL), and the aqueous phase was extracted with dichloromethane (10 mL × 2). The combined organic layers were dried over Na_2SO_4, filtered, and concentrated under pressure. The residue was purified by silica gel chromatography (hexane/ethyl acetate = 2:1) to afford compound **41** (10 mg, 76%) as a white solid. ^{1}H NMR (400 MHz, $CDCl_3$): δ 8.40 (s, 1H), 8.34 (s, 1H), 8.32–8.30 (m, 2H), 8.06 (d, J = 8.00 Hz, 2H), 7.74 (d, J = 8.40 Hz, 2H), 7.67 (s, 4H), 4.01 (s, 3H), 2.23 (s, 3H). MS (ESI, *m/z*): 481.2 $[M + 1]^+$. ESI-HRMS (*m/z*): $[M + 1]^+$ calcd for $C_{25}H_{20}N_4O_3F_3$, 481.1488; found, 481.1487.

Methyl 4′-Benzamido-5-(4-(4-(trifluoromethyl)phenyl)-1H-1,2,3-triazol-1-yl)-[1,1′-biphenyl]-3-carboxylate (42).—40 (12 mg, 0.027 mmol) was dissolved in dichloromethane (1 mL) at 0 °C. Triethylamine (4.2 μL, 0.030 mmol) and benzoyl chloride (3.2 μL, 0.027 mmol) were added, and the mixture was stirred for 18 h at room temperature. The reaction mixture was partitioned betweeen dichloromethane (10 mL) and water (10 mL), and the aqueous phase was extracted with dichloromethane (10 mL × 2). The combined organic layers were dried over Na_2SO_4, filtered, and concentrated under pressure. The residue was purified by silica gel chromatography (hexane/ethyl acetate = 3:1) to afford compound **42** (9 mg, 63%) as a white solid. ^{1}H NMR (400 MHz, $CDCl_3$): δ 8.41 (s, 1H), 8.37 (s, 1H), 8.33 (broad s, 2H), 8.10–8.05 (m, 2H), 7.94–7.90 (m, 3H), 7.82 (d, J = 8.40 Hz, 2H), 7.75–7.72 (m, 3H), 7.61–7.45 (m, 3H), 4.02 (s, 3H). MS (ESI, *m/z*): 543.2 $[M + 1]^+$. ESI-HRMS (*m/z*): $[M + 1]^+$ calcd for $C_{30}H_{21}N_4O_3F_3$, 543.1644; found, 543.1647.

tert-Butyl 4-((3′-(Methoxycarbonyl)-5′-(4-(4-(trifluoromethyl)-phenyl)-1H-1,2,3-triazol-1-yl)-[1,1′-biphenyl]-4-yl)carbamoyl)-piperidine-1-carboxylate (43).—To a solution of compound **40** (27 mg, 0.061 mmol) in *N,N*-dimethylformamide (2 mL) were added Boc-Inp-OH (15 mg, 0.067 mmol), HATU (25 mg, 0.067 mmol), and *N,N*-diisopropylethylamine (13 μL, 0.080 mmol), and then this reaction mixture was stirred at

room temperature for 2 h. The reaction mixture was partitioned between ethyl acetate (5 mL) and water (5 mL), and the aqueous layer was extracted with ethyl acetate (5 mL × 2). The combined organic layer was washed with brine (3 mL), dried over $MgSO_4$, filtered, and evaporated under reduced pressure. The residue was purified by silica gel column chromatography (hexane/ethyl acetate = 3:1) to afford compound **43** (37 mg, 94%) as a white solid. ^{1}H NMR (400 MHz, $CDCl_3$): δ 8.40 (s, 1H), 8.34–8.33 (m, 1H), 8.32–8.30 (m, 2H), 8.06 (d, J = 8.40 Hz, 2H), 7.74 (d, J = 8.00 Hz, 2H), 7.68 (s, 4H), 4.25–4.18 (m, 2H), 4.01 (s, 3H), 2.84–2.78 (m, 2H), 2.46–2.40 (m, 1H), 1.95–1.92 (m, 2H), 1.78–1.76 (m, 2H), 1.47 (s, 9H). MS (ESI, *m/z*): 672.2 $[M + Na]^+$. ESI-HRMS (*m/z*): $[M + Na]^+$ calcd for $C_{34}H_{34}N_5O_5F_3Na$, 672.2410; found, 672.2413.

3′-(Methoxycarbonyl)-5′-(4-(4-(trifluoromethyl)phenyl)-1H-1,2,3-triazol-1-yl)-[1,1′-biphenyl]-4-carboxylic Acid (44).—Method C. Yield: 45%. ^{1}H NMR (400 MHz, DMSO-d_6): δ 9.78 (s, 1H), 8.59–8.56 (m, 2H), 8.36 (s, 1H), 8.19 (d, J = 8.00 Hz, 2H), 8.10 (d, J = 8.40 Hz, 2H), 8.00 (d, J = 8.40 Hz, 2H), 7.91 (d, J = 8.40 Hz, 2H), 3.98 (s, 3H). MS (ESI, *m/z*): 468.1 $[M + 1]^+$. ESI-HRMS (*m/z*): $[M + 1]^+$ calcd for $C_{24}H_{17}N_3O_4F_3$, 468.1171; found, 468.1169.

Methyl 4′-((3-((tert-Butoxycarbonyl)amino)propyl)carbamoyl)-5-(4-(4-(trifluoromethyl)phenyl)-1H-1,2,3-triazol-1-yl)-[1,1′-biphenyl]-3-carboxylate (45).—Method C. Yield: 68%. ^{1}H NMR (400 MHz, CD_3OD): δ 9.15 (s, 1H), 8.41 (s, 1H), 8.32 (s, 1H), 8.25 (s, 1H), 8.04 (d, J = 8.00 Hz, 2H), 7.93 (d, J = 8.40 Hz, 2H), 7.78 (d, J = 8.40 Hz, 2H), 7.71 (d, J = 8.00 Hz, 2H), 3.95 (s, 3H), 3.44 (t, J = 6.80 Hz, 2H), 3.17–3.14 (m, 2H), 1.80–1.76 (m, 2H). MS (ESI, *m/z*): 646.2 $[M + Na]^+$. ESI-HRMS (*m/z*): $[M + Na]^+$ calcd for $C_{32}H_{32}N_5O_5F_3Na$, 646.2253; found, 646.2255.

4′-((3-((tert-Butoxycarbonyl)amino)propyl)carbamoyl)-5-(4-(4-(trifluoromethyl)phenyl)-1H-1,2,3-triazol-1-yl)-[1,1′-biphenyl]-3-carboxylic Acid (46).—Method A. Yield: 77%. ^{1}H NMR (400 MHz, CD_3OD): δ 9.27 (s, 1H), 8.57 (s, 1H), 8.46 (s, 1H), 8.41 (s, 1H), 8.15 (d, J = 8.00 Hz, 2H), 7.99 (d, J = 7.60 Hz, 2H), 7.89 (d, J = 8.00 Hz, 2H), 7.78 (d, J = 8.00 Hz, 2H), 3.47–3.43 (m, 2H), 3.17–3.14 (m, 2H), 1.80–1.77 (m, 2H). MS (ESI, *m/z*): 610.2 $[M + 1]^+$. ESI-HRMS (*m/z*): $[M + 1]^+$ calcd for $C_{31}H_{31}N_5O_5F_3$, 610.2277; found, 610.2270.

Methyl 4′-Bromo-5-(4-(4-(trifluoromethyl)phenyl)-1H-1,2,3-triazol-1-yl)-[1,1′-biphenyl]-3-carboxylate (47).—Method C. Yield: 53%. ^{1}H NMR (400 MHz, $CDCl_3$): δ 8.40 (s, 1H), 8.35–8.32 (m, 3H), 8.06 (d, J = 8.00 Hz, 2H), 7.74 (d, J = 8.40 Hz, 2H), 7.65 (d, J = 8.40 Hz, 2H), 7.57 (d, J = 8.40 Hz, 2H), 4.02 (s, 3H). MS (ESI, *m/z*): 502.0, 504.0 $[M + 1]^+$. ESI-HRMS (*m/z*): $[M + 1]^+$ calcd for $C_{23}H_{16}N_3O_2F_3Br$, 502.0378; found, 502.0382.

Methyl 4′-(2-Amino-2-oxoethyl)-5-(4-(4-(trifluoromethyl)-phenyl)-1H-1,2,3-triazol-1-yl)-[1,1′-biphenyl]-3-carboxylate (48).—Method D. Yield: 73%. ^{1}H NMR (400 MHz, $CDCl_3$): δ 8.41 (s, 1H), 8.36–8.33 (m, 3H), 8.06 (d, J = 8.00 Hz, 2H), 7.75–7.69 (m, 2H), 7.50–7.44 (m, 2H), 7.16 (d, J = 8.40 Hz, 2H), 4.02 (s, 3H), 3.67 (s, 2H). MS (ESI, *m/z*): 481.2 $[M + 1]^+$. ESI-HRMS (*m/z*): $[M + 1]^+$ calcd for $C_{25}H_{20}N_4O_3F_3$, 481.1488; found, 481.1492.

Methyl 4′-(3-((tert-Butoxycarbonyl)amino)propyl)-5-(4-(4-(trifluoromethyl)phenyl)-1H-1,2,3-triazol-1-yl)-[1,1′-biphenyl]-3-carboxylate (49).—Method E. Yield: 55%. ^{1}H NMR (400 MHz, $CDCl_3$): δ 8.40 (s, 1H), 8.35 (s, 1H), 8.33–8.31 (m, 2H), 8.06 (d, J = 8.00 Hz, 2H), 7.74 (d, J = 8.40 Hz, 2H), 7.62 (d, J = 8.40 Hz, 2H), 7.33 (d, J = 8.00 Hz, 2H), 4.01 (s, 3H), 3.20–3.18 (m, 2H), 2.72 (t, J = 7.60 Hz, 2H), 1.90–1.82 (m, 2H), 1.45 (s, 9H). MS (ESI, *m/z*): 525.2 [M + 1-*tert*-buty1]$^+$.

Methyl 4′-(3-((tert-Butoxycarbonyl)amino)prop-1-yn-1-yl)-5-(4-(4-(trifluoromethyl)phenyl)-1H-1,2,3-triazol-1-yl)-[1,1′-biphenyl]-3-carboxylate (50).—Method C. Yield: 35%. ^{1}H NMR (400 MHz, CD_3OD): δ 9.24 (s, 1H), 8.51 (s, 1H), 8.40 (s, 1H), 8.34 (s, 1H), 8.13 (d, J = 8.00 Hz, 2H), 7.78–7.74 (m, 4H), 7.56 (d, J = 8.40 Hz, 2H), 4.10–4.08 (m, 2H), 4.00 (s, 3H), 1.48 (s, 9H). MS (ESI, *m/z*): 577.2 [M + 1]$^+$. ESI-HRMS (*m/z*): [M + 1]$^+$ calcd for $C_{31}H_{28}N_4O_4F_3$, 577.2063; found, 577.2057.

Methyl 4′-(4-Hydroxybutyl)-5-(4-(4-(trifluoromethyl)phenyl)-1H-1,2,3-triazol-1-yl)-[1,1′-biphenyl]-3-carboxylate (51).—Method E. Yield: 27%. ^{1}H NMR (400 MHz, $CDCl_3$): δ 8.48 (s, 1H), 8.40 (s, 1H), 8.32 (s, 2H), 8.06 (d, J = 8.00 Hz, 2H), 7.74 (d, J = 8.00 Hz, 2H), 7.62 (d, J = 8.00 Hz, 2H), 7.33 (d, J = 8.00 Hz, 2H), 4.01 (s, 3h), 3.72–3.68 (m, 2H), 2.73 (t, J = 7.60 Hz, 2H), 1.80–1.72 (m, 2H), 1.68–1.58 (m, 2H). MS (ESI, *m/z*): 496.2 [M + 1]$^+$. ESI-HRMS (*m/z*): [M + 1]$^+$ calcd for $C_{27}H_{25}N_3O_3F_3$, 496.1848; found, 496.1855.

4′-(3-((tert-Butoxycarbonyl)amino)prop-1-yn-1-yl)-5-(4-(4-(trifluoromethyl)phenyl)-1H-1,2,3-triazol-1-yl)-[1,1′-biphenyl]-3-carboxylic Acid (52).—Method A. Yield: 88%. ^{1}H NMR (400 MHz, DMSO-d_6): δ 9.76 (s, 1H), 8.50 (d, J = 6.40 Hz, 2H), 8.30 (s, 1H), 8.19 (d, J = 8.00 Hz, 2H), 7.91–7.88 (m, 4H), 7.58 (d, J = 8.40 Hz, 2H), 4.02 (s, 2H), 1.41 (s, 9H). MS (ESI, *m/z*): 563.2 [M + 1]$^+$. ESI-HRMS (*m/z*): [M + 1]$^+$ calcd for $C_{30}H_{26}N_4O_4F_3$, 563.1906; found, 563.1897.

tert-Butyl (3-(4-Bromobenzamido)propyl)carbamate (54a).—4-Bromobenzoic acid **53a** (Scheme S2, Supporting Information, 100 mg, 0.497 mmol) was converted to compound **54a** (54 mg, 31%) as a white solid, using a similar procedure to that used in the preparation of compound **43**. ^{1}H NMR (400 MHz, $CDCl_3$): δ 7.73 (d, J = 8.00 Hz, 2H), 7.57 (d, J = 8.40 Hz, 2H), 3.51–3.46 (m, 2H), 3.26–3.22 (m, 2H), 1.71–1.68 (m, 2H), 1.44 (s, 9H).

tert-Butyl (3-(4-Bromophenyl)prop-2-yn-1-yl)carbamate (54b).—To a mixture of 1-bromo-4-iodobenzene **53b** (Scheme S2, Supporting Information, 300 mg, 1.06 mmol), $PdCl_2(PPh_3)_2$ (37 mg, 0.053 mmol), and copper iodide (20 mg, 0.106 mmol) in THF were added triethylamine (295 μL, 2.12 mmol) and *N*-Boc-propargylamine (247 mg, 1.59 mmol) at room temperature under a N_2 atmosphere, and then this reaction mixture was stirred at room temperature for 12 h under a N_2 atmosphere. The reaction mixture was partitioned with ethyl acetate (100 mL) and aqueous saturated NH_4Cl solution (50 mL), and then the aqueous layer was extracted with ethyl acetate (100 mL × 2). The combined organic layer was dried (Na_2SO_4), filtered, and evaporated under reduced pressure. The residue was purified by silica gel column chromatography (hexane/ethyl acetate = 5:1) to afford the

compound **54b** (310 mg, 94%) as a white solid. ^{1}H NMR (400 MHz, $CDCl_3$): δ 7.45 (d, J = 8.40 Hz, 2H), 7.28 (d, J = 8.40 Hz, 2H), 4.16–4.15 (m, 2H), 1.48 (s, 9H).

Methyl 4′-(1-((tert-Butoxycarbonyl)amino)cyclopropyl)-5-(4-(4-(trifluoromethyl)phenyl)-1H-1,2,3-triazol-1-yl)-[1,1′-biphenyl]-3-carboxylate (55).—Method E. Yield: 30%. ^{1}H NMR (400 MHz, $CDCl_3$): δ 8.39 (s, 1H), 8.35–8.30 (m, 3H), 8.06 (d, J = 8.00 Hz, 2H), 7.74 (d, J = 8.00 Hz, 2H), 7.63 (d, J = 8.40 Hz, 2H), 7.34 (d, J = 8.00 Hz, 2H), 4.01 (s, 3H), 1.46 (s, 9H), 1.35–1.30 (m, 4H). MS (ESI, *m/z*): 579.2 $[M + 1]^+$. ESI-HRMS (*m/z*): $[M + 1]^+$ calcd for $C_{31}H_{30}N_4O_4F_3$, 579.2219; found, 579.2220.

Methyl 4′-(1-Aminocyclopropyl)-5-(4-(4-(trifluoromethyl)-phenyl)-1H-1,2,3-triazol-1-yl)-[1,1′-biphenyl]-3-carboxylate (56).—Method B. Yield: 90%. ^{1}H NMR (400 MHz, CD_3OD): δ 9.29 (s, 1H), 8.56 (s, 1H), 8.49 (s, 1H), 8.41 (s, 1H), 8.17 (d, J = 8.00 Hz, 2H), 7.90 (d, J = 8.40 Hz, 2H), 7.80 (d, J = 8.00 Hz, 2H), 7.64 (d, J = 8.0 Hz, 2H), 4.02 (s, 3H), 1.43–1.40 (m, 4H). MS (ESI, *m/z*): 479.1 $[M + 1]^+$. ESI-HRMS (*m/z*): $[M + 1]^+$ calcd for $C_{26}H_{22}N_4O_2F_3$, 479.1695; found, 479.1699.

Methyl 4′-(1-(((tert-Butoxycarbonyl)amino)methyl)cyclopropyl)-5-(4-(4-(trifluoromethyl)phenyl)-1H-1,2,3-triazol-1-yl)-[1,1′-biphenyl]-3-carboxylate (57).—Method E. Yield: 30%. ^{1}H NMR (400 MHz, $CDCl_3$): δ 8.40 (s, 1H), 8.35–8.30 (m, 3H), 8.06 (d, J = 8.40 Hz, 2H), 7.74 (d, J = 8.40 Hz, 2H), 7.64 (d, J = 8.00 Hz, 2H), 7.44 (d, J = 8.00 Hz, 2H), 4.01 (s, 3H), 3.39–3.35 (m, 2H), 1.40 (s, 9H), 0.93–0.79 (m, 4H). MS (ESI, *m/z*): 615.2 $[M + Na]^+$. ESI-HRMS (*m/z*): $[M + Na]^+$ calcd for $C_{32}H_{31}N_4O_4F_3Na$, 615.2195; found, 615.2199.

Methyl 4′-(1-((tert-Butoxycarbonyl)amino)cyclobutyl)-5-(4-(4-(trifluoromethyl)phenyl)-1H-1,2,3-triazol-1-yl)-[1,1′-biphenyl]-3-carboxylate (58).—Method E. Yield: 70%. ^{1}H NMR (400 MHz, $CDCl_3$): δ 8.40 (s, 1H), 8.38 (s, 1H), 8.33 (s, 2H), 8.06 (d, J = 8.00 Hz, 2H), 7.74 (d, J = 8.00 Hz, 2H), 7.68 (d, J = 8.00 Hz, 2H), 7.57 (d, J = 7.60 Hz, 2H), 4.01 (s, 3H), 2.63–2.44 (m, 4H), 2.20–2.09 (m, 1H), 1.97–1.85 (m, 1H), 1.47–1.29 (m, 9H). MS (ESI, *m/z*): 593.3 $[M + 1]^+$. ESI-HRMS (*m/z*): $[M + 1]^+$ calcd for $C_{32}H_{32}N_4O_4F_3$, 593.2376; found, 593.2383.

Methyl 4′-(3-(Hydroxymethyl)oxetan-3-yl)-5-(4-(4-(trifluoromethyl)phenyl)-1H-1,2,3-triazol-1-yl)-[1,1′-biphenyl]-3-carboxylate (59).—Method E. Yield: 44%. ^{1}H NMR (400 MHz, $CDCl_3$): δ 8.41 (s, 1H), 8.36 (s, 1H), 8.34 (s, 2H), 8.06 (d, J = 8.00 Hz, 2H), 7.75–7.64 (m, 4H), 7.54 (d, J = 8.00 Hz, 2H), 5.01 (d, J = 5.60 Hz, 2H), 4.83 (d, J = 5.60 Hz, 2H), 4.11 (d, J = 5.60 Hz, 2H), 4.02 (s, 3H). MS (ESI, *m/z*): 510.2 $[M + 1]^+$. ESI-HRMS (*m/z*): $[M + 1]^+$ calcd for $C_{27}H_{23}N_3O_4F_3$, 510.1641; found, 510.1640.

Methyl 4′-(Isoxazol-3-yl)-5-(4-(4-(trifluoromethyl)phenyl)-1H-1,2,3-triazol-1-yl)-[1,1′-biphenyl]-3-carboxylate (60).—Method F. Yield: 91%. ^{1}H NMR (400 MHz, acetone-d_6): δ 9.48 (s, 1H), 8.88 (d, J = 1.60 Hz, 1H), 8.62–8.61 (m, 2H), 8.46–8.45 (m, 1H), 8.26 (d, J = 8.00 Hz, 2H), 8.14 (d, J = 8.40 Hz, 2H), 8.04 (d, J = 8.40 Hz, 2H), 7.88 (d,

J = 8.00 Hz, 2H), 7.13 (d, *J* = 1.60 Hz, 1H), 4.03 (s, 3h). MS (ESI, *m/z*): 491.1 $[M + 1]^+$. ESI-HRMS (*m/z*): $[M + 1]^+$ calcd for $C_{26}H_{18}N_4O_3F_3$, 491.1331; found, 491.1328.

Methyl 4′-(5-(Hydroxymethyl)isoxazol-3-yl)-5-(4-(4-(trifluoromethyl)phenyl)-1H-1,2,3-triazol-1-yl)-[1,1′-biphenyl]-3-carboxylate (61).—Method E. Yield: 46%. ^{1}H NMR (400 MHz, $CDCl_3$): δ 8.40 (s, 1H), 8.38 (s, 1H), 8.36–8.35 (m, 2H), 8.04 (d, *J* = 7.71 8.40 Hz, 2H), 7.93 (d, *J* = 8.00 Hz, 2H), 7.78 (d, *J* = 8.40 Hz, 2H), 7.71 (d, *J* = 8.00 Hz, 2H), 6.62 (s, 1H), 4.84 (s, 2H), 4.00 (s, 3H). MS (ESI, *m/z*): 521.2 $[M + 1]^+$. ESI-HRMS (*m/z*): $[M + 1]^+$ calcd for $C_{27}H_{20}N_4O_4F_3$, 521.1437; found, 521.1430.

Methyl 4′-(5-(2-Hydroxyethyl)isoxazol-3-yl)-5-(4-(4-(trifluoromethyl)phenyl)-1H-1,2,3-triazol-1-yl)-[1,1′-biphenyl]-3-carboxylate (62).—Method F. Yield: 80%. ^{1}H NMR (400 MHz, DMSO-d_6): δ 9.76 (s, 1H), 8.58 (s, 1H), 8.54 (s, 1H), 8.35 (s, 1H), 8.18 (d, *J* = 8.40 Hz, 2H), 8.04–8.00 (m, 4H), 7.90 (d, *J* = 8.40 Hz, 2H), 6.94 (s, 1H), 3.97 (s, 3H), 3.77 (q, *J* = 6.40 Hz, 2H), 2.97 (d, *J* = 6.40 Hz, 2H). MS (ESI, *m/z*): 535.2 $[M + 1]^+$. ESI-HRMS (*m/z*): $[M + 1]^+$ calcd for $C_{28}H_{22}N_4O_4F_3$, 535.1593; found, 535.1592.

Methyl 4′-(1H-Tetrazol-5-yl)-5-(4-(4-(trifluoromethyl)phenyl)-1H-1,2,3-triazol-1-yl)-[1,1′-biphenyl]-3-carboxylate (63).—Method C. Yield: 53%. ^{1}H NMR (400 MHz, CD_3OD): δ 9.26 (s, 1H), 8.52 (s, 1H), 8.44 (s, 1H), 8.39 (s, 1H), 8.18 (d, *J* = 8.40 Hz, 2H), 8.12 (d, *J* = 8.40 Hz, 2H), 7.90 (d, *J* = 8.40 Hz, 2H), 7.76 (d, *J* = 8.40 Hz, 2H), 4.00 (s, 3H). MS (ESI, *m/z*): 492.1 $[M + 1]^+$. ESI-HRMS (*m/z*): $[M + 1]^+$ calcd for $C_{24}H_{17}N_7O_2F_3$, 492.1396; found, 492.1399.

Ethyl 4-(4-(5-(Hydroxymethyl)isoxazol-3-yl)phenyl)-7-(4-(trifluoromethyl)phenyl)-2-naphthoate (65).—Method F. Yield: 50%. ^{1}H NMR (400 MHz, DMSO-d_6): δ 8.81 (s, 1H), 8.71 (s, 1H), 8.09–8.05 (m, 5H), 7.99–7.97 (m, 1H), 7.94–7.93 (m, 1H), 7.89 (d, *J* = 8.00 Hz, 2H), 7.68 (d, *J* = 8.00 Hz, 2H), 7.04 (s, 1H), 5.77 (t, *J* = 6.00 Hz, 1H), 4.66 (d, *J* = 6.00 Hz, 2H), 4.41 (q, *J* = 7.20 Hz, 2H), 1.38 (t, *J* = 7.20 Hz, 3H). MS (ESI, *m/z*): 518.2 $[M + 1]^+$. ESI-HRMS (*m/z*): $[M + 1]^+$ calcd for $C_{30}H_{23}NO_4F_3$, 518.1579; found, 518.1582.

Methyl 3-Amino-5-bromobenzoate (66).—3-Bromo-5-aminobenzoic acid (**65**, 1.01 g, 4.62 mmol) was stirred in methanol (15 mL) with ice cooling, and the yellow solution was treated with thionyl chloride (4.00 mL, 55.0 mmol) dropwise over 20 min. The resulting mixture was warmed up to room temperature and left stirring for 15 h. The reaction mixture was quenched with aqueous saturated $NaHCO_3$ solution at 0 °C. The solvent was then removed under vacuum, and the residue was suspended in ethyl acetate (200 mL). The organic phase was washed with brine (100 mL), dried (Na_2SO_4), and concentrated in vacuo to afford the title compound **66** (1.08 g, 98%) as a yellow solid. ^{1}H NMR (400 MHz, DMSO-d_6): δ 7.16 (dd, *J* = 1.48, 2.12 Hz, 1H), 7.13 (t, *J* = 1.64 Hz, 1H), 6.96 (t, *J* = 2.00 Hz, 1H), 5.74 (s, 2H), 3.81 (s, 3H). MS (ESI, *m/z*): 231 $[M + 1]^+$. ESI-HRMS (*m/z*): $[M + 1]^+$ calcd for $C_8H_8BrNO_2$, 229.9817; found, 229.9818.

Methyl 3-Bromo-5-(4-(trifluoromethyl)benzamido)benzoate (67).—To a solution of compound **66** (70 mg, 0.304 mmol) in *N,N*-dimethylformamide (6 mL) were added 4-(trifluoromethyl)benzoic acid (136 mg, 0.717 mmol), HATU (218 mg, 0.573 mmol), and *N,N*-diisopropylethylamine (250 μL, 1.43 mmol), and then this reaction mixture was stirred at room temperature for 5 h. The reaction mixture was partitioned between ethyl acetate (20 mL) and water (10 mL), and the aqueous layer was extracted with ethyl acetate (20 mL × 2). The combined organic layer was washed with brine (10 mL), dried over Na_2SO_4, filtered, and evaporated under reduced pressure. The residue was purified by silica gel column chromatography (hexane/ethyl acetate = 7:1) to afford compound **67** (86 mg, 70%) as a white solid. ^{1}H NMR (400 MHz, $CDCl_3$): δ 8.32–8.31 (m, 1H), 8.05–8.04 (m, 1H), 7.99–7.98 (m, 3H), 7.79 (d, J = 8.40 Hz, 2H), 3.93 (s, 3H). MS (ESI, *m/z*): 402.0 $[M + 1]^+$. ESI-HRMS (*m/z*): $[M + 1]^+$ calcd for $C_{16}H_{12}NO_3F_3Br$, 401.9953; found, 401.9948.

Methyl 3-(4,4,5,5-Tetramethyl-1,3,2-dioxaborolan-2-yl)-5-(4-(trifluoromethyl)benzamido)benzoate (68).—To a solution of compound **67** (40 mg, 0.099 mmol) in 1,4-dioxane (3 mL) were added bis(pinacolato)diboron (63 mg, 0.248 mmol), $PdCl_2$(dppf) (2.0 mg, 0.002 μmol), and potassium acetate (30 mg, 0.298 mmol), and then this reaction mixture was stirred at 70 °C for 6 h. The reaction mixture was partitioned between ethyl acetate (20 mL) and water (10 mL), and the aqueous layer was extracted with ethyl acetate (10 mL × 2). The combined organic layer was washed with brine (5 mL), dried over Na_2SO_4, filtered, and evaporated under reduced pressure. The residue was purified by silica gel column chromatography (hexane/ethyl acetate = 2:1) to afford compound **68** (29.0 mg, 65%) as a white solid. ^{1}H NMR (400 MHz, $CDCl_3$): δ 8.50 (s, 1H), 8.29 (s, 1H), 8.15 (s, 1H), 7.99 (d, J = 8.00 Hz, 2H), 7.78 (d, J = 8.40 Hz, 2H), 3.93 (s, 3H), 1.35 (s, 12H). MS (ESI, *m/z*): 450.2 $[M + 1]^+$. ESI-HRMS (*m/z*): $[M + 1]^+$ calcd for $C_{22}H_{24}NO_5F_3B$, 450.1700; found, 450.1701.

Methyl 4′-(5-(Hydroxymethyl)isoxazol-3-yl)-5-(4-(trifluoromethyl)benzamido)-[1,1′-biphenyl]-3-carboxylate (69).—Method C. Yield: 45%. ^{1}H NMR (400 MHz, CD_3OD): δ 8.44 (m, 1H), 8.36–8.35 (m, 1H), 8.17–8.13 (m, 3H), 7.98 (d, J = 8.40 Hz, 2H), 7.87–7.82 (m, 4H), 6.83 (s, 1H), 4.74 (s, 2H), 3.97 (s, 3H). MS (ESI, *m/z*): 497.1 $[M + 1]^+$. ESI-HRMS (*m/z*): $[M + 1]^+$ calcd for $C_{26}H_{20}N_2O_5F_3$, 497.1324; found, 497.1323.

Methyl 2-Amino-6-bromoisonicotinate (72).—Compound **69** (200 mg, 0.922 mmol) was converted to compound **72** (83 mg, 40%) as a white solid, using a similar procedure to that used in the preparation of compound **66**. ^{1}H NMR (400 MHz, CD_3OD): δ 7.13 (d, 1H), 7.00 (d, 1H), 3.89 (s, 3H). MS (ESI, *m/z*): 231.0 $[M + 1]^+$. ESI-HRMS (*m/z*): $[M + 1]^+$ calcd for $C_7H_8BrN_2O_2$, 230.9769; found, 230.9769.

Methyl 4-Amino-6-bromopicolinate (73).—Compound **70** (320 mg, 1.47 mmol) was converted to compound **73** (136 mg, 40%) as a white solid, using a similar procedure to that used in the preparation of compound **66**. ^{1}H NMR (400 MHz, DMSO-d_6): δ 7.23 (d, 1H), 6.79 (d, 1H), 3.81 (s, 3H). MS (ESI, *m/z*): 231.0 $[M + 1]^+$. ESI-HRMS (*m/z*): $[M + 1]^+$ calcd for $C_7H_8BrN_2O_2$, 230.9769; found, 230.9765.

Methyl 6-Azido-4-bromopicolinate (74).—Compound **71** (121 mg, 0.523 mmol) was dissolved in acetonitrile (4 mL) and cooled to 0 °C in an ice bath. *tert*-Butyl nitrite (124 μL, 1.047 mmol) was added to the reaction mixture and stirred at 0 °C for 30 min. After that, azidotrimethylsilane (206 μL, 1.57 mmol) was added to the reaction mixture at 0 °C dropwise. The resulting solution was stirred at room temperature for 12 h. The reaction mixture was concentrated under reduced pressure. The residue was purified by silica gel column chromatography (hexane/ethyl acetate = 3:1) to afford compound **74** (50 mg, 37%) as a white solid. ^{1}H NMR (400 MHz, $CDCl_3$): δ 7.98 (s, 1H), 7.26 (s, 1H), 3.99 (s, 3H).

Methyl 2-Azido-6-bromoisonicotinate (75).—Compound **72** (27 mg, 0.107 mmol) was converted to compound **75** (30 mg, 65%) as a white solid, using a similar procedure to that used in the preparation of compound **74**. ^{1}H NMR (400 MHz, $CDCl_3$): δ 7.76 (d, 1H), 7.29 (d, 1H), 3.94 (s, 3H).

Methyl 4-Azido-6-bromopicolinate (76).—Compound **73** (21 mg, 0.090 mmol) was converted to compound **76** (12 mg, 52%) as a white solid, using a similar procedure to that used in the preparation of compound **74**. ^{1}H NMR (400 MHz, $CDCl_3$): δ 7.75 (broad s, 1H), 7.31 (broad s, 1H), 4.02 (s, 3H).

Methyl 4-Bromo-6-(4-(4-(trifluoromethyl)phenyl)-1H-1,2,3-triazol-1-yl)picolinate (77).—To a solution of compound **74** (50 mg, 0.195 mmol) in *tert*-BuOH/water (5 mL, 1:1) were added 4-ethynyl-α,α,α-trifluorotoluene (50 μL, 0.292 mmol) and tris[(1-benzyl-1*H*-1,2,3-triazol-4-yl)methyl]amine (TBTA, 7 mg, 0.014 mmol). Subsequently, sodium ascorbate (58 mg, 0.292 mmol, freshly prepared 1 M aqueous solution) and $CuSO_4{\cdot}5H_2O$ (37 mg, 0.146 mmol, freshly prepared 7.5% aqueous solution) were added into the reaction mixture, and then this reaction mixture was stirred at room temperature for 1.5 h. The solvent of the reaction mixture was evaporated under reduced pressure. The residue was purified by silica gel column chromatography (hexane/ethyl acetate = 3:1) to afford compound **77** (30 mg, 36%) as a white solid. ^{1}H NMR (400 MHz, $CDCl_3$): δ 8.98 (s, 1H), 8.65 (d, 1H), 8.31 (d, 1H), 8.08 (d, J = 8.00 Hz, 2H), 7.74 (d, J = 8.00 Hz, 2H), 4.06 (s, 3H). MS (ESI, *m/z*): 427. 0 $[M + 1]^+$. ESI-HRMS (*m/z*): $[M + 1]^+$ calcd for $C_{16}H_{11}BrN_4O_2F_3$, 427.0017; found, 427.0013.

Methyl 2-Bromo-6-(4-(4-(trifluoromethyl)phenyl)-1H-1,2,3-triazol-1-yl)isonicotinate (78).—Compound **75** (27 mg, 0.107 mmol) was converted to compound **78** (30 mg, 65%) as a white solid, using a similar procedure to that used in the preparation of compound **77**. ^{1}H NMR (400 MHz, CD_3OD): δ 9.28 (s, 1H), 8.65 (d, 1H), 8.20–8.18 (m, 3H), 7.79 (d, J = 8.00 Hz, 2H), 4.03 (s, 3H). MS (ESI, *m/z*): 427.0 $[M + 1]^+$. ESI-HRMS (*m/z*): $[M + 1]^+$ calcd for $C_{16}H_{11}BrN_4O_2F_3$, 427.0017; found, 427.0018.

Methyl 6-Bromo-4-(4-(4-(trifluoromethyl)phenyl)-1H-1,2,3-triazol-1-yl)picolinate (79).—Compound **76** (7.0 mg, 0.027 mmol) was converted to compound **79** (8.0 mg, 69%) as a white solid, using a similar procedure to that used in the preparation of compound **77**. ^{1}H NMR (400 MHz, CD_3OD): δ 9.24 (s, 1H), 8.68 (s, 1H), 8.42 (s, 1H), 8.08 (d, J = 8.00

Hz, 2H), 7.73 (d, J = 8.00 Hz, 2H), 4.04 (s, 3H). MS (ESI, *m/z*): 427.0 $[M + 1]^+$. ESI-HRMS (*m/z*): $[M + 1]^+$ calcd for $C_{16}H_{11}BrN_4O_2F_3$, 427.0017; found, 427.0022.

Methyl 4-(4-(1-(tert-Butoxycarbonyl)piperidin-4-yl)phenyl)-6-(4-(4-(trifluoromethyl)phenyl)-1H-1,2,3-triazol-1-yl)picolinate (80).—Method C. Yield: 35%. ^{1}H NMR (400 MHz, $CDCl_3$): δ 9.05 (s, 1H), 8.67 (d, 1H), 8.41 (d, 1H), 8.10 (d, J = 8.00 Hz, 2H), 7.78–7.73 (m, 4H), 7.41 (d, J = 8.40 Hz, 2H), 4.35–4.21 (m, 2H), 2.90–2.79 (m, 3H), 1.93–1.89 (m, 2H), 1.75–1.63 (m, 2H), 1.49 (s, 9H). MS (ESI, *m/z*): 608.3 $[M + 1]^+$.

Methyl 2-(4-(1-(tert-Butoxycarbonyl)piperidin-4-yl)phenyl)-6-(4-(4-(trifluoromethyl)phenyl)-1H-1,2,3-triazol-1-yl)isonicotinate (81).—Method C. Yield: 63%. ^{1}H NMR (400 MHz, CD_3OD): δ 9.36 (s, 1H), 8.49 (s, 1H), 8.38 (s, 1H), 8.20–8.16 (m, 4H), 7.78 (d, J = 8.40 Hz, 2H), 7.41 (d, J = 8.40 Hz, 2H), 4.26–4.16 (m, 2H), 4.04 (s, 3H), 2.95–2.77 (m, 3H), 1.88–1.85 (m, 2H), 1.69–1.59 (m, 2H), 1.49 (s, 9H). MS (ESI, *m/z*): 608.3 $[M + 1]^+$. ESI-HRMS (*m/z*): $[M + 1]^+$ calcd for $C_{32}H_{33}N_5O_4F_3$, 608.2485; found, 608.2492.

Methyl 6-(4-(1-(tert-Butoxycarbonyl)piperidin-4-yl)phenyl)-4-(4-(4-(trifluoromethyl)phenyl)-1H-1,2,3-triazol-1-yl)picolinate (82).—Method C. Yield: 91%. ^{1}H NMR (400 MHz, CD_3OD): δ 9.44–9.36 (m, 1H), 8.57–8.46 (m, 2H), 8.15–8.10 (m, 4H), 7.81–7.76 (m, 2H), 7.40–7.35 (m, 2H), 4.24–4.21 (m, 2H), 4.04 (s, 3H), 2.88–2.77 (m, 3H), 1.86–1.84 (m, 2H), 1.65–1.62 (m, 2H), 1.49 (s, 9H). MS (ESI, *m/z*): 608.2 $[M + 1]^+$. ESI-HRMS (*m/z*): $[M + 1]^+$ calcd for $C_{32}H_{33}N_5O_4F_3$, 608.2485; found, 608.2474.

4-(4-(1-(tert-Butoxycarbonyl)piperidin-4-yl)phenyl)-6-(4-(4-(trifluoromethyl)phenyl)-1H-1,2,3-triazol-1-yl)picolinic Acid (83).—Method A. Yield: 68%. ^{1}H NMR (400 MHz, DMSO-d_6): δ 9.64 (s, 1H), 8.57 (s, 1H), 8.41 (s, 1H), 8.30 (d, J = 8.00 Hz, 2H), 7.94 (d, J = 8.40 Hz, 2H), 7.87 (d, J = 8.00 Hz, 2H), 7.48 (d, J = 8.40 Hz, 2H), 4.11–4.05 (m, 2H), 2.90–2.73 (m, 3H), 1.82–1.79 (m, 2H), 1.60–1.50 (m, 2H), 1.42 (s, 9H). MS (ESI, *m/z*): 594.2 $[M + 1]^+$. ESI-HRMS (*m/z*): $[M + 1]^+$ calcd for $C_{31}H_{31}N_5O_4F_3$, 594.2328; found, 594.2320.

2-(4-(1-(tert-Butoxycarbonyl)piperidin-4-yl)phenyl)-6-(4-(4-(trifluoromethyl)phenyl)-1H-1,2,3-triazol-1-yl)isonicotinic Acid (84).—Method A. Yield: 91%. ^{1}H NMR (400 MHz, CD_3OD): δ 9.38 (s, 1H), 8.53 (s, 1H), 8.42 (s, 1H), 8.19 (t, J = 8.40 Hz, 4H), 7.79 (d, J = 8.40 Hz, 2H), 7.42 (d, J = 8.00 Hz, 2H), 4.26–4.15 (m, 2H), 2.96–2.73 (m, 3H), 1.89–1.76 (m, 2H), 1.70–1.55 (m, 2H), 1.49 (s, 9H). MS (ESI, *m/z*): 616.3 $[M + Na]^+$. ESI-HRMS (*m/z*): $[M + Na]^+$ calcd for $C_{31}H_{30}N_5O_4F_3Na$, 616.2148; found, 616.2158.

6-(4-(1-(tert-Butoxycarbonyl)piperidin-4-yl)phenyl)-4-(4-(4-(trifluoromethyl)phenyl)-1H-1,2,3-triazol-1-yl)picolinic Acid (85).—Method A. Yield: 77%. ^{1}H NMR (400 MHz, CD_3OD): δ 9.27 (s, 1H), 8.58–8.52 (m, 2H), 8.10 (m, 4H), 7.74 (d, J = 7.60 Hz, 2H), 7.39 (broad s, 2H), 4.24–4.21 (m, 2H), 2.89–2.73 (m, 3H), 1.89–

1.86 (m, 2H), 1.70–1.60 (m, 2H), 1.47 (s, 9H). MS (ESI, *m/z*): 594.2 $[M + 1]^+$. ESI-HRMS (*m/z*): $[M + 1]^+$ calcd for $C_{31}H_{31}N_5O_4F_3$, 594.2328; found, 594.2318.

tert-Butyl 4-(3′-((2-(Dimethylamino)-2-oxoethoxy)carbonyl)-5′-(4-(4-(trifluoromethyl)phenyl)-1H-1,2,3-triazol-1-yl)-[1,1′-biphenyl]-4-yl)piperidine-1-carboxylate (87).—To a solution of **86** (166 mg, 0.280 mmol), which was synthesized according to literature procedures reported,[1] in DMF (10 mL) was added K_2CO_3 (116 mg, 0.840 mmol). 2-Chloro-*N,N*-dimethylacetamide (68 mg, 0.560 mmol) was added to the reaction mixture under a N_2 atmosphere, and the reaction mixture was stirred at 45 °C for 1 h under a N_2 atmosphere. The reaction mixture was partitioned between ethyl acetate (10 mL) and water (10 mL), and the aqueous phase was extracted with ethyl acetate (2 × 10 mL). The combined organic layers were dried over Na_2SO_4, filtered, and concentrated under pressure. The residue was purified by silica gel chromatography (hexane/ethyl acetate = 3:1) to afford compound **87** (205 mg, 70%) as a white solid. ^{1}H NMR (400 MHz, $CDCl_3$): δ 8.43–8.41 (m, 2H), 8.38–8.36 (m, 2H), 8.05 (d, J = 8.00 Hz, 2H), 7.73 (d, J = 8.40 Hz, 2H), 7.65 (d, J = 8.40 Hz, 2H), 7.34 (d, J = 8.40 Hz, 2H), 5.05 (s, 2H), 3.76–3.72 (m, 2H), 3.07 (s, 3H), 3.02 (s, 3H), 2.87–2.77 (m, 2H), 2.76–2.67 (m, 1H), 1.89–1.83 (m, 2H), 1.72–1.62 (m, 2H), 1.49 (s, 9H). MS (ESI, *m/z*): 622.2 [M + 1-*tert*-butyl]$^+$.

tert-Butyl 4-(3′-(Hydroxymethyl)-5′-(4-(4-(trifluoromethyl)-phenyl)-1H-1,2,3-triazol-1-yl)-[1,1′-biphenyl]-4-yl)piperidine-1-carboxylate (89).—To a solution of **88** (35 mg, 0.058 mmol), which was synthesized according to literature procedures reported,[1] in THF at 0 °C, 2 M lithium aluminum hydride solution in THF (2.6 mg, 0.070 mmol) was added dropwise over a period of 0.5 h under a N_2 atmosphere. After the addition was complete, the reaction mixture was stirred at 0 °C under a N_2 atmosphere for 1 h. The unreacted LAH was quenched with saturated aqueous NH_4Cl, and the reaction mixture was extracted with dichloromethane three times. The combined organic extracts were dried with anhydrous Na_2SO_4, and the mixture was filtered through a Celite pad. The filtered mixture was concentrated in vacuum and chromatographed on silica gel with hexanes/ethyl acetate = 3:1 to afford **89** (15 mg, 45%) as a white solid. ^{1}H NMR (400 MHz, CD_3OD): δ 9.16 (s, 1H), 8.15 (d, J = 8.00 Hz, 2H), 8.05 (s, 1H), 7.90 (s, 1H), 7.80–7.76 (m, 3H), 7.70 (d, J = 8.40 Hz, 2H), 7.38 (d, J = 8.40 Hz, 2H), 4.80 (s, 2H), 4.25–4.22 (m, 2H), 2.96–2.77 (m, 3H), 1.88–1.85 (m, 2H), 1.68–1.59 (m, 2H), 1.49 (s, 9H). MS (ESI, *m/z*): 579.2 $[M + 1]^+$. ESI-HRMS (*m/z*): $[M + 1]^+$ calcd for $C_{32}H_{34}N_4O_3F_3$, 579.2583; found, 579.2588.

tert-Butyl 4-(3′-(((Di-tert-butoxyphosphoryl)oxy)methyl)-5′-(4-(4-(trifluoromethyl)phenyl)-1H-1,2,3-triazol-1-yl)-[1,1′-biphenyl]-4-yl)piperidine-1-carboxylate (90).—A stirred solution of **89** (12 mg, 0.020 mmol) in dry THF (1.0 mL) was treated successively with tetrazole (17 mg, 0.242 mmol) and di-*tert*-butyl *N,N*-diethylphosphoramidite (115 μL, 0.414 mmol) at room temperature under a N_2 atmosphere. The resulting solution was stirred at room temperature for 1 h under a N_2 atmosphere, and the reaction mixture was cooled to −78 °C. 3-Chloroperbenzoic acid (MCPBA, contains 50%, 78 mg) was added, and the reaction mixture was warmed to 0 °C and stirred for 0.5 h. The reaction mixture was partitioned between ethyl acetate (10 mL) and aqueous saturated $NaHCO_3$ solution (10 mL), and the aqueous phase was extracted with ethyl acetate (2 × 10

mL). The combined organic layers were dried over Na_2SO_4, filtered, and concentrated under pressure. The residue was purified by silica gel chromatography (chloroform/methanol = 30:1) to afford compound **90** (13 mg, 84%) as a white solid. ^{1}H NMR (400 MHz, CD_3OD): δ 9.22 (s, 1H), 8.18–8.16 (m, 3H), 8.01 (s, 1H), 7.83–7.79 (m, 3H), 7.71 (d, J = 8.40 Hz, 2H), 7.41 (d, J = 8.40 Hz, 2H), 5.23–5.22 (m, 2H), 4.27–4.23 (m, 2H), 2.96–2.77 (m, 3H), 1.91–1.87 (m, 2H), 1.71–1.59 (m, 2H), 1.52–1.50 (m, 27H). MS (ESI, *m/z*): 793.3 $[M + Na]^+$. ESI-HRMS (*m/z*): $[M + Na]^+$ calcd for $C_{40}H_{50}N_4O_6F_3PNa$, 793.3318; found, 793.3303.

Solubility and Lipophilicity Measurements.

Solubility was measured using a modified pION method.[2,25,26] Lipophilicity was determined based on the HPLC retention time as preported.[2,27]

Competitive Binding Assay Using CHO Cells Expressing hP2Y$_{14}$R (CHO-hP2Y$_{14}$R).

The fluorescence assay procedures used are similar to previous reports.[2,7] Twenty-four hours prior to the assay, CHO-hP2Y$_{14}$R cells were plated in a flat bottom 96-well plate at a density of 1×10^4 cells well^{-1} and grown at 37 °C and 5% CO_2(g) in Gibco Dulbecco's modified Eagle's medium/nutrient mixture F-12 (DMEM/F12, 1:1) supplemented with 10% fetal bovine serum, 100 units mL^{-1} penicillin, 100 μg mL^{-1} streptomycin, and 0.500 mg mL^{-1} selective antibiotic G418 sulfate. Cells were used for binding assays when confluency reached 80–90%. Unlabeled P2Y$_{14}$R antagonists (test compounds) were stored frozen as 5 mM stock solutions in DMSO. A 10-fold serial dilution of each ligand was prepared in the appropriate complete cell medium to generate solutions of unlabeled ligands with concentrations ranging from 100 μM to 100 pM. CHO-hP2Y$_{14}$R cells were first incubated with unlabeled ligand solutions for 30 min in an incubator at 37 °C and 5% CO_2(g) without shaking followed by another 30 min of incubation with 20 nM fluorescent antagonist **2** under the same condition. After the incubation periods, the cell medium was removed, and the cells were washed three times with sterile 1× Dulbecco's phosphate-buffered saline (DPBS) minus Ca^{2+}/Mg^{2+}. Cells were then detached from the plate using Corning Cellstripper and resuspended in sterile 1× DPBS minus Ca^{2+}+/Mg^{2+} for flow cytometry analysis. All competitive binding assays were performed on a BD FACSCalibur flow cytometer in conjunction with the software programs BD Bioscience PlateManager and CellQuest. The gathered data were analyzed to obtain IC_{50} values using GraphPad Prism 8.0 (GraphPad, San Diego, CA).

Competitive Binding Assay Using HEK293 Cells Expressing mP2Y$_{14}$R (HEK293-mP2Y$_{14}$R).

HEK293-mP2Y$_{14}$R cells were plated in a flat bottom 96-well plate at a density of 2×10^4 cells well^{-1} 48 h prior to the assay and were grown at 37 °C and 5% CO_2(g) in Eagle's minimum essential medium (EMEM) supplemented with 10% fetal bovine serum, 100 units mL^{-1} penicillin, 100 μg mL^{-1} streptomycin, and 0.555 mg mL^{-1} G418 sulfate. Cells were used for binding assays when confluency reached 80–90%. A 10-fold serial dilution of each test compounds (5 mM stock solution, DMSO) was prepared in the appropriate complete cell medium to generate solutions of unlabeled ligands with concentrations ranging from 100 μM to 1 nM. HEK293-mP2Y$_{14}$R cells were first incubated with unlabeled ligand solutions for 30 min in an incubator at 37 °C and 5% CO_2(g) without shaking followed by

another 30 min incubation with 20 nM fluorescent antagonist **2** under the same condition. After the incubation periods, the cell medium was removed, and the cells were washed three times with sterile 1× DPBS minus Ca^{2+}/Mg^{2+}. Cells were then detached from the plate using Corning Cellstripper and resuspended in sterile 1× DPBS minus Ca^{2+}/Mg^{2+} for flow cytometry analysis. All competitive binding assays were performed on a BD FACSCalibur flow cytometer in conjunction with the software programs BD Bioscience PlateManager and CellQuest. The gathered data were analyzed to obtain IC_{50} values using GraphPad Prism 8.0.

Esterase Cleavage of Prodrugs 37a–37c.

HPLC Analysis.—The retention times of compounds were determined by Agilent 1100 series HPLC equipped with an Agilent Eclipse 5 μm XDB-C18 analytical column (250 × 4.6 mm, Agilent Technologies Inc., Palo Alto, CA). Separations were achieved with a flow rate of 1 mL min^{-1} and the following mobile phase: (1) Method A for **37a:** linear gradient solvent system, CH_3CN/0.1% formic acid and 5% methanol in water from 30:70 to 55:45 in 20 min, and then to 100% CH_3CN for 5 min and (2) Method B for **37b** and **37c:** linear gradient solvent system, CH_3CN/0.1% formic acid in water from 50:50 to 95:5 in 20 min, and then to 100% CH_3CN for 5 min. Peaks were detected by UV absorption with a diode array detector at 210, 254, and 280 nm.

Analysis of the Enzymatic Hydrolysis.—A solution of prodrug was prepared in HEPES buffer (50 mM, pH 7.3) with 10% DMSO and 10% Kolliphor EL at a concentration of 1.5 mM. Three aliquots (200 μL) from the 1.5 mM stock solution were each treated with a 100 μL solution of porcine liver esterase (PLE, 40 U in 400 μL HEPES buffer, 50 mM, pH 7.3). The samples were incubated (**37a** for 5, 35, 65, and 120 min at 37 °C or **37b** and **37c** for 0, 2, 6, 24, 48, and 72 h at 37 °C) with a mixing speed of 400 rpm in an Eppendorf (Enfield, CT) ThermoMixer prior to analysis. The samples were analyzed by HPLC at each internal of time.

Hydrolytic Stabilities of the Prodrugs in Aqueous Medium.—Solutions (1.0 mM) of the prodrugs (**37a– 37c**) in HEPES buffer (50 mM, pH 7.3) with 10% DMSO and 10% Kolliphor EL were examined immediately and after 24 h at 37 °C using identical HPLC conditions.

ADMET Measurements: In Vitro.

The procedures for the ADMET testing of compound **32** were reported in ref 2. hERG inhibition was determined by a patch clamp method (Supporting Information) and a fluorescence polarization assay (Predictor hERG fluorescence polarization assay system by Thermo Fisher, performed by Jai Research Foundation (JRF), Department of Toxicology, Valvada - 396 105, Dist. Valsad, Gujarat, India) and with a patch clamp electrophysiological assay (performed by Charles River Laboratories, Cleveland, OH).[29,30]

ADMET Measurements: In Vivo.

In vivo pharmacokinetic study is summarized in Table 5. The vehicle was prepared as follows.

Compound **32** was dissolved as a stock solution in pure DMSO. For intravenous administration through the tail vein of each male Wistar rat (body weight, 211–257 g), the stock solution was diluted with an aqueous solution of 20% 2-hydroxypropyl-beta-cyclodextrin (HPBCD) to make final volume ratio of 10:90 of DMSO/HPBCD. For intraperitoneal administration, the stock solution was added to an equal volume of Kolliphor EL (polyoxyl castor oil) followed by PBS. The final volume ratio of DMSO/Kolliphor EL/PBS was 15:15:70. A sample of dose formulation from each dose group was taken and stored at −70 °C.

The full procedures were approved by the Institutional Animal Ethics Committee (IAEC) of JRF, according to Association for Assessment and Accreditation of Laboratory Animal Care (AAALAC) standards. For the intravenous group, blood was collected through a jugular vein catheter at 0.083, 0.25, 0.5, 1, 2, 4, 8, 12, and 24 h post-dosing. For the intraperitoneal groups, blood was collected similarly at 0.25, 0.5, 1, 2, 4, 8, 12, and 24 h post-dosing. Blood samples of ~200 μL were collected from the jugular vein of each rat and collected in microcentrifuge tubes with heparin (20 IU mL^{-1} blood) added as an anticoagulant. Following inversion four to five times, blood samples were cooled on wet ice and centrifuged at 9000 rpm at 4 °C for 10 min. Plasma was collected and frozen immediately at −70 ± 10 °C.

The frozen plasma samples were analyzed using the following validated bioanalytical method. The plasma samples were thawed at room temperature and centrifuged at 6000 rpm at 4 °C for 5 min. Each plasma sample (25 μL) was combined in an Eppendorf tube with 25 μL of 25 ng mL^{-1} flufenamic acid as an internal standard and 50 μL of 5 mM ammonium acetate (pH 8). After vortexing, 1 mL of *tert*-butyl methyl ether was added as a liquid–liquid extraction solvent. Each sample was vortexed for 5 min and centrifuged at 10,000 rpm at 4 °C for 10 min. Aliquots of 0.9 mL were removed from the supernatant portion, and each was dried using a Caliper TurboVap LV evaporator (Biotage) under a N_2 stream at 40 °C. The residue was reconstituted with 500 μL of mobile phase, vortexed, and transferred to the HPLC (ExionLC, SCIEX) autosampler for injection (10 μL), with MS/MS (QTRAP 5500, SCIEX) analysis. The mobile phase consisted of acetonitrile/5 mM ammonium acetate, pH 8.0 (85:15, v/v), with a Waters XTerra MS C18 column (3.5 μm, 4.6 × 150 mm) at a flow rate of 0.400 mL min^{-1}. A 12-point calibration curve for the analyte area as a function of concentration injected had an $r = 0.9947$. Pharmacokinetic analysis of the plasma concentration–time data was performed using the noncompartmental model of WinNonlin software (version 8.2). No mortality or morbidity was observed in any of the groups, and all animals had normal clinical signs throughout the experimental period.

In Vivo Efficacy Studies.

All in vivo efficacy studies received prior institutional approval. Several potent antagonists (**1a, 1b, 3a,** and **32**) and three prodrug derivatives (**37a–37c**) were tested in the protease mouse model of allergic asthma (sensitization with ovalbumin/*Aspergillus*) at NIEHS as described.[2,6,33] The timeline used for ASP/OVA sensitization, $P2Y_{14}R$ antagonist treatment, and OVA challenge is shown in the study of Jung et al.[2]

Compound **32** was tested in a chronic constriction injury mouse model of neuropathic pain, using a protocol that was approved by the IACUC at St. Louis University.[7] The antagonist was administered 7 days post-chronic constriction injury of the sciatic nerve in adult male mice, at the time of peak pain, as reported for various $P2Y_{14}R$ antagonists.[2,7]

Supplementary Material

Refer to Web version on PubMed Central for supplementary material.

ACKNOWLEDGMENTS

We thank the Intramural Research Program of the NIH, NIDDK (ZIA DK31116), and NIEHS (ZIAES102025) and Kantum Diagnostics (Boston, MA) for support through NIDDK CRADA 17-0824. We thank Bryan L. Roth, National Institute of Mental Health's Psychoactive Drug Screening Program (Univ. North Carolina at Chapel Hill, contract #HHSN-271-2008-00025-C), for screening data. This work utilized the computational resources of the NIH HPC Biowulf cluster (http://hpc.nih.gov).

ABBREVIATIONS

ADME	absorption, distribution, metabolism, excretion, and toxicology
CHO	Chinese hamster ovary
DCM	dichloromethane
DIPEA	diisopropylethylamine
DMEM	Dulbecco's modified Eagle's medium
DMF	*N,N*-dimethylformamide
EL	extracellular loop
HATU	1-[bis(dimethylamino)methylene]-1*H*-1,2,3-triazolo[4,5-*b*]pyridinium 3-oxide hexafluorophosphate
IE	interaction energy
LAH	lithium aluminum hydride
MD	molecular dynamics
PDSP	Psychoactive Drug Screening Program
RMSD	root-mean-square deviation
SAR	structure–activity relationship
UDPG	uridine-5′-diphosphoglucose
TBAF	tetrabutylammonium fluoride
TEA	triethylamine
TFA	trifluoroacetic acid

THF	tetrahydrofuran
TM	transmembrane helix
TMS	trimethylsilyl

REFERENCES

(1). Yu J; Ciancetta A; Dudas S; Duca S; Lottermoser J; Jacobson KA Structure-guided modification of heterocyclic antagonists of the $P2Y_{14}$ receptor. J. Med. Chem 2018, 61, 4860–4882. [PubMed: 29767967]

(2). Jung Y-H; Yu J; Wen Z; Salmaso V; Karcz TP; Phung NB; Chen Z; Duca S; Bennett JM; Dudas S; Salvemini D; Gao Z-G; Cook DN; Jacobson KA Exploration of alternative scaffolds for $P2Y_{14}$ receptor antagonists containing a biaryl core. J. Med. Chem 2020, 63, 9563–9589. [PubMed: 32787142]

(3). Battistone MA; Mendelsohn AC; Spallanzani RG; Allegretti AS; Liberman RN; Sesma J; Kalim S; Wall SM; Bonventre JV; Lazarowski ER; Brown D; Breton S Pro-inflammatory $P2Y_{14}$ receptor inhibition protects against ischemic acute kidney injury in mice. J. Clin. Invest 2020, 130, 3734–3749. [PubMed: 32287042]

(4). Xu J; Morinaga H; Oh D; Li P; Chen A; Talukdar S; Mamane Y; Macini JA; Nawrocki AR; Lazarowski E; Olefsky JM; Kim JJ GPR105 ablation prevents inflammation and improves insulin sensitivity in mice with diet-induced obesity. J. Immunol 2012, 189, 1992–1999. [PubMed: 22778393]

(5). Jain S; Jacobson KA Adipocyte specific ablation of $P2Y_{14}R$ improves glucose metabolism in mice with diet-induced obesity. American Diabetes Assoc., 80th Scientific Session, Abstract; 2020.

(6). Karcz TP; Whitehead GS; Nakano K; Nakano H; Grimm SA; Williams JG; Deterding LJ; Jacobson KA; Cook DN UDP-glucose and $P2Y_{14}$ receptor amplify allergen-induced airway eosinophilia. J. Clin. Invest 2021, 131, e140709.

(7). Mufti F; Jung YH; Giancotti LA; Yu J; Chen Z; Phung NB; Jacobson KA; Salvemini D $P2Y_{14}$ receptor antagonists reverse chronic neuropathic pain in a mouse model. ACS Med. Chem. Lett 2020, 11, 1281–1286.

(8). Lin J; Liu F; Zhang Y.-y.; Song N; Liu M.-k.; Fang X.-y.; Liao D.-q.; Zhou C; Wang H; Shen J.-f. $P2Y_{14}$ receptor is functionally expressed in satellite glial cells and mediates interleukin-1β and chemokine CCL2 secretion. J. Cell. Physiol 2019, 234, 21199–21210. [PubMed: 31032956]

(9). Jacobson KA; Delicado EG; Gachet C; Kennedy C; von Kügelgen I; Li B; Miras-Portugal T; Novak I; Schöneberg T; Perez-Sen R; Thor D; Wu B; Yang Z; Müller CE Update of P2Y receptor pharmacology: IUPHAR review “27”. Br. J. Pharmacol 2020, 177, 2413–2433. [PubMed: 32037507]

(10). Kinoshita M; Nasu-Tada K; Fujishita K; Sato K; Koizumi S Secretion of matrix metalloproteinase-9 from astrocytes by inhibition of tonic $P2Y_{14}$-receptor-mediated signal(s). Cell. Mol. Neurobiol 2013, 33, 47–58. [PubMed: 22872320]

(11). Zhang Z; Hao K; Li H; Lu R; Liu C; Zhou M; Li B; Meng Z; Hu Q; Jiang C Design, synthesis and anti-inflammatory evaluation of 3-amide benzoic acid derivatives as novel $P2Y_{14}$ receptor antagonists. Eur. J. Med. Chem 2019, 181, 111564. [PubMed: 31376563]

(12). Hamel M; Henault M; Hyjazie H; Morin N; Bayly C; Skorey K; Therien AG; Mancini J; Brideau C; Kargman S Discovery of novel $P2Y_{14}$ agonist and antagonist using conventional and nonconventional methods. J. Biomol Screening 2011, 16, 1098–1105.

(13). Wang W; Liu C; Li H; Tian S; Liu Y; Wang N; Yan D; Li H; Hu Q Discovery of novel and potent $P2Y_{14}R$ antagonists via structure-based virtual screening for the treatment of acute gouty arthritis. J. Adv. Res 2020, 23, 133–142. [PubMed: 32123586]

(14). Junker A; Balasubramanian R; Ciancetta A; Uliassi E; Kiselev E; Martiriggiano C; Trujillo K; Mtchedlidze G; Birdwell L; Brown KA; Harden TK; Jacobson KA Structure-based design of 3-(4-aryl-1H-1,2,3-triazol-1-yl)-biphenyl derivatives as $P2Y_{14}$ receptor antagonists. J. Med. Chem 2016, 59, 6149–6168. [PubMed: 27331270]

(15). Zhang J; Zhang K; Gao Z-G; Paoletta S; Zhang D; Han GW; Li T; Ma L; Zhang W; Muller CE; Yang H; Jiang H; Cherezov V; Katritch V; Jacobson KA; Stevens RC; Wu B; Zhao Q Agonist-bound structure of the human $P2Y_{12}$ receptor. Nature 2014, 509, 119–122. [PubMed: 24784220]

(16). Kiselev E; Barrett MO; Katritch V; Paoletta S; Weitzer CD; Hammes E; Yin AL; Zhao Q; Stevens RC; Harden TK; Jacobson KA Exploring a 2-naphthoic acid template for the structure-based design of $P2Y_{14}$ receptor antagonist molecular probes. ACS Chem. Biol 2014, 9, 2833–2842. [PubMed: 25299434]

(17). Barrett MO; Sesma JI; Ball CB; Jayasekara PS; Jacobson KA; Lazarowski ER; Harden TK A selective high affinity antagonist of the $P2Y_{14}$ receptor inhibits UDP-glucose-stimulated chemotaxis of human neutrophils. Mol. Pharmacol 2013, 84, 41–49. [PubMed: 23592514]

(18). Robichaud J; Fournier J-F; Gagné S; Gauthier JY; Hamel M; Han Y; Hénault M; Kargman S; Levesque J-F; Mamane Y; Mancini J; Morin N; Mulrooney E; Wu J; Black WC Applying the pro-drug approach to afford highly bioavailable antagonists of $P2Y_{14}$. Bioorg. Med. Chem. Lett 2011, 21, 4366–4368. [PubMed: 21689930]

(19). Mazák K; Noszál B Physicochemical properties of zwitterionic drugs in therapy. ChemMedChem 2020, 15, 1102–1110. [PubMed: 32432820]

(20). Sabbadin D; Ciancetta A; Moro S Bridging molecular docking to membrane molecular dynamics to investigate GPCR-ligand recognition: The human A_{2A} adenosine receptor as a key study. J. Chem. Inf. Model 2014, 54, 169–183. [PubMed: 24359090]

(21). Strupczewski JT; Allen RC; Gardner BA; Schmid BL; Stache U; Glamkowski EJ; Jones MC; Ellis DB; Huger FP; Dunn RW Synthesis and neuroleptic activity of 3-(1-substituted-4-piperidinyl)-1,2-benzisoxazoles. J. Med. Chem 1985, 28, 761–769. [PubMed: 2861286]

(22). Ballesteros JA; Weinstein H [19] Integrated methods for the construction of three-dimensional models and computational probing of structure-function relations in G protein-coupled receptors. Methods Neurosci 1995, 25, 366–428.

(23). Pennington LD; Moustakas DT The necessary nitrogen atom: A versatile high-impact design element for multiparameter optimization. J. Med. Chem 2017, 60, 3552–3579. [PubMed: 28177632]

(24). Gardell SJ; Hopf M; Khan A; Dispagna M; Hampton Sessions E; Falter R; Kapoor N; Brooks J; Culver J; Petucci C; Ma CT; Cohen SE; Tanaka J; Burgos ES; Hirschi JS; Smith SR; Sergienko E; Pinkerton AB; Boosting NAD^+ with a small molecule that activates NAMPT. Nat. Commun 2019, 10, 3241. [PubMed: 31324777]

(25). Kiselyuk AS HNF4 alpha bioactive ligands discovered by a high-throughput screen for modulators of the human insulin promoter (Doctoral dissertation, pp. 65). University of California: San Diego, 2011. (https://escholarship.org/content/qt64k4q3gr/qt64k4q3gr.pdf)

(26). Yan Z; Caldwell G Optimization in Drug Discovery: In Vitro Methods (pp. 58); Humana Press.

(27). Valkó K Application of high-performance liquid chromatography based measurements of lipophilicity to model biological distribution. J. Chromatogr. A 2004, 1037, 299–310. [PubMed: 15214672]

(28). Besnard J; Ruda GF; Setola V; Abecassis K; Rodriguiz RM; Huang X-P; Norval S; Sassano MF; Shin AI; Webster LA; Simeons FRC; Stojanovski L; Prat A; Seidah NG; Constam DB; Bickerton GR; Read KD; Wetsel WC; Gilbert IH; Roth BL; Hopkins AL Automated design of ligands to polypharmacological profiles. Nature 2012, 492, 215–220. [PubMed: 23235874]

(29). Wible BA; Hawryluk P; Ficker E; Kuryshev YA; Kirsch G; Brown AM HERG-Lite®: a novel comprehensive high-throughput screen for drug-induced hERG risk. J. Pharmacol. Toxicol. Methods 2005, 52, 136–145. [PubMed: 15950494]

(30). Piper DR; Duff SR; Eliason HC; Frazee WJ; Frey EA; Fuerstenau-Sharp M; Jachec C; Marks BD; Pollok BA; Shekhani MS; Thompson DV; Whitney P; Vogel KW; Hess SD Development of the predictor HERG fluorescence polarization assay using a membrane protein enrichment approach. Assay Drug Dev. Technol 2008, 6, 213–223. [PubMed: 18471075]

(31). Perez C; Daniel KB; Cohen SM Evaluating prodrug strategies for esterase-triggered release of alcohols. ChemMedChem 2013, 8, 1662–1667. [PubMed: 23929690]

(32). Bennett GJ; Xie YK A peripheral mononeuropathy in rat that produces disorders of pain sensation like those seen in man. Pain 1988, 33, 87–107. [PubMed: 2837713]

(33). Whitehead GS; Thomas SY; Shalaby KH; Nakano K; Moran TP; Ward JM; Flake GP; Nakano H; Cook DN TNF is required for TLR ligand–mediated but not protease-mediated allergic airway inflammation. J. Clin. Invest 2017, 127, 3313–3326. [PubMed: 28758900]

(34). Mignani S; Rodrigues J; Tomas H; Jalal R; Singh PP; Majoral J-P; Vishwakarma RA Present drug-likeness filters in medicinal chemistry during the hit and lead optimization process: how far can they be simplified? Drug Discovery Today 2018, 23, 605–615. [PubMed: 29330127]

(35). Dalvie DK; Kalgutkar AS; Khojasteh-Bakht SC; Obach RS; O'Donnell JP Biotransformation reactions of five-membered aromatic heterocyclic rings. Chem. Res. Toxicol 2002, 15, 269–299. [PubMed: 11896674]

(36). Zhu J; Mo J; Lin H.-z.; Chen Y; Sun H.-p. The recent progress of isoxazole in medicinal chemistry. Bioorg. Med. Chem 2018, 26, 3065–3075. [PubMed: 29853341]

(37). Sun H; Shi M; Zhang W; Zheng Y-M; Xu Y-Z; Shi J-J; Liu T; Gunosewoyo H; Pang T; Gao ZB; Yang F; Tang J; Yu L-F Development of novel alkoxyisoxazoles as sigma-1 receptor antagonists with antinociceptive efficacy. J. Med. Chem 2016, 59, 6329–6343. [PubMed: 27309376]

(38). Ratnatilaka Na Bhuket P; Jithavech P; Ongpipattanakul B; Rojsitthisak P Interspecies differences in stability kinetics and plasma esterases involved in hydrolytic activation of curcumin diethyl disuccinate, a prodrug of curcumin. RSC Adv. 2019, 9, 4626–4634.

(39). Schrödinger Release 2019–3: Maestro, Schrödinger, LLC: New York, NY, 2019.

(40). Sastry GM; Adzhigirey M; Day T; Annabhimoju R; Sherman W Protein and ligand preparation: Parameters, protocols, and influence on virtual screening enrichments. J. Comput.-Aided Mol. Des 2013, 27, 221–234. [PubMed: 23579614]

(41). Harder E; Damm W; Maple J; Wu C; Reboul M; Xiang JY; Wang L; Lupyan D; Dahlgren MK; Knight JL; Kaus JW; Cerutti DS; Krilov G; Jorgensen WL; Abel R; Friesner RA OPLS3: A force field providing broad coverage of drug-like small molecules and proteins. J. Chem. Theory Comput 2016, 12, 281–296. [PubMed: 26584231]

(42). Friesner RA; Banks JL; Murphy RB; Halgren TA; Klicic JJ; Mainz DT; Repasky MP; Knoll EH; Shelley M; Perry JK; Shaw DE; Francis P; Shenkin PS Glide: A new approach for rapid, accurate docking and scoring. 1. Method and assessment of docking accuracy. J. Med. Chem 2004, 47, 1739–1749. [PubMed: 15027865]

(43). Doerr S; Harvey MJ; Noé F; De Fabritiis G HTMD: High-throughput molecular dynamics for molecular discovery. J. Chem. Theory Comput 2016, 12, 1845–1852. [PubMed: 26949976]

(44). Humphrey W; Dalke A; Schulten K VMD: Visual molecular dynamics. J. Mol. Graph 1996, 14, 33–38 27. [PubMed: 8744570]

(45). Lomize MA; Pogozheva ID; Joo H; Mosberg HI; Lomize AL OPM Database and PPM web server: Resources for positioning of proteins in membranes. Nucleic Acids Res. 2012, 40, D370–D376. [PubMed: 21890895]

(46). Jorgensen WL; Chandrasekhar J; Madura JD; Impey RW; Klein ML Comparison of simple potential functions for simulating liquid water. J. Chem. Phys 1983, 79, 926.

(47). Harvey MJ; Giupponi G; Fabritiis GD ACEMD: Accelerating biomolecular dynamics in the microsecond time scale. J. Chem. Theory Comput 2009, 5, 1632–1639. [PubMed: 26609855]

(48). Best RB; Zhu X; Shim J; Lopes PEM; Mittal J; Feig M; Mackerell AD Jr. Optimization of the additive CHARMM all-atom protein force field targeting improved sampling of the backbone φ, ψ and side-chain χ_1 and χ_2 dihedral angles. J. Chem. Theory Comput 2012, 8, 3257–3273. [PubMed: 23341755]

(49). Klauda JB; Venable RM; Freites JA; O'Connor JW; Tobias DJ; Mondragon-Ramirez C; Vorobyov I; MacKerell AD Jr.; Pastor RW Update of the CHARMM all-atom additive force field for lipids: Validation on six lipid types. J. Phys. Chem. B 2010, 114, 7830–7843. [PubMed: 20496934]

(50). Vanommeslaeghe K; MacKerell AD Jr. Automation of the CHARMM general force field (CGenFF) I: Bond perception and atom typing. J. Chem. Inf. Model 2012, 52, 3144–3154. [PubMed: 23146088]

(51). Vanommeslaeghe K; Raman EP; MacKerell AD Jr. Automation of the CHARMM general force field (CGenFF) II: Assignment of bonded parameters and partial atomic charges. J. Chem. Inf. Model 2012, 52, 3155–3168. [PubMed: 23145473]

(52). CHARMM General Force Field (CGenFF) program, http://cgenff.umaryland.edu/

(53). Kräutler V; van Gunsteren WF; Hünenberger PH A fast SHAKE algorithm to solve distance constraint equations for small molecules in molecular dynamics simulations. J. Comput. Chem 2001, 22, 501–508.

(54). Essmann U; Perera L; Berkowitz ML; Darden T; Lee H; Pedersen LG A smooth particle mesh Ewald method. J. Chem. Phys 1995, 103, 8577.

(55). Phillips JC; Braun R; Wang W; Gumbart J; Tajkhorshid E; Villa E; Chipot C; Skeel RD; Kalé L; Schulten K Scalable molecular dynamics with NAMD. J. Comput. Chem 2005, 26, 1781–1802. [PubMed: 16222654]

(56). Williams T; Kelley C Gnuplot 5.0.[Sl]; http://www.gnuplot.info.

(57). Tetko IV; Tanchuk VY Application of associative neural networks for prediction of lipophilicity in ALOGPS 2.1 program. J. Chem. Inf. Comput. Sci 2002, 42, 1136–1145. [PubMed: 12377001]

(58). Belley M; Deschenes D; Fortin R; Fournier J-F; Gagne S; Gareau Y; Gauthier JY; Li L; Robichaud J; Therien M; Tranmer GK; Wang Z et al. WO2009070873 A1, 6 11, 2009.

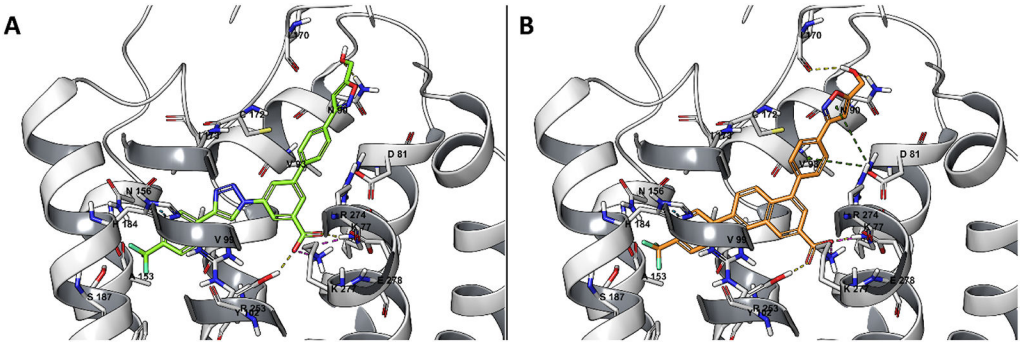

Figure 1.

Docking pose of compound **29** (A), in green, and compound **32** (B), in orange, at the $P2Y_{14}R$ structure (gray), obtained by MD-refined homology modeling using an agonist-bound $P2Y_{12}R$ structure (PDB ID: 4PXZ[34]) as the template.

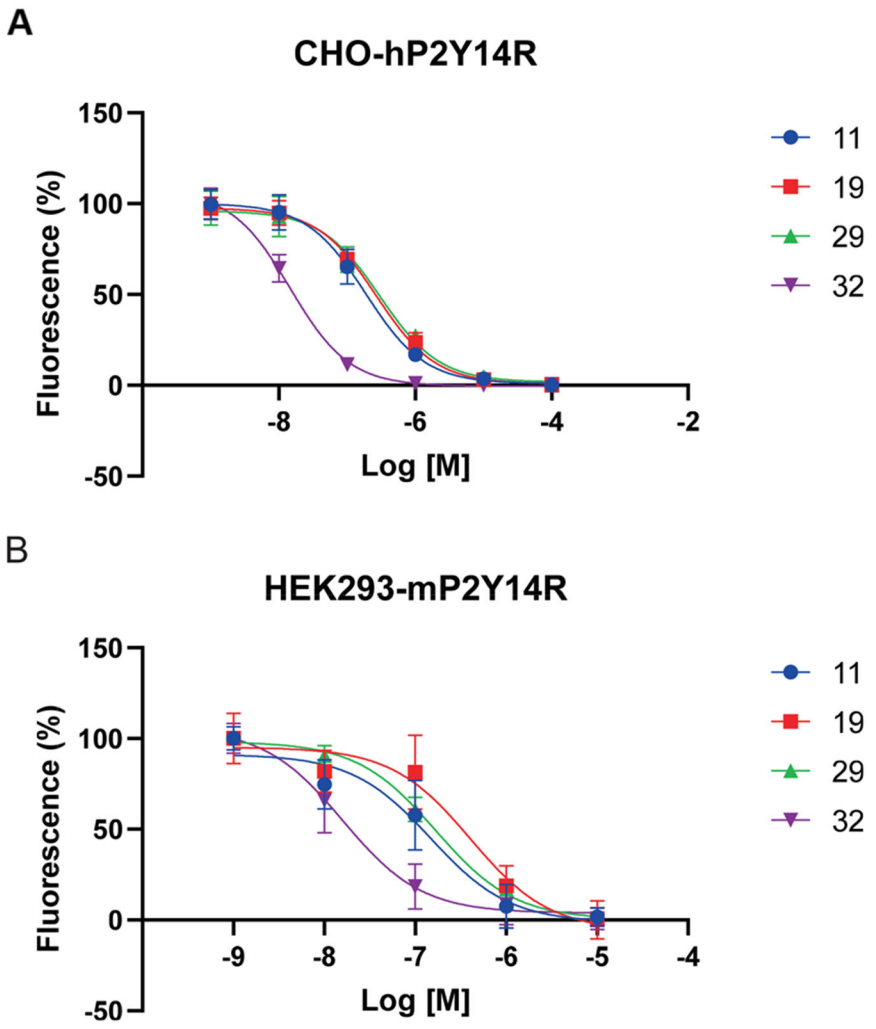

Figure 2.

Inhibition of binding of fluorescent antagonist **2** at hP2Y$_{14}$R (A) and at mP2Y$_{14}$R (B) by four novel P2Y$_{14}$R antagonist analogues (mean ± SD, n = 3–4 independent determinations, performed in triplicate).

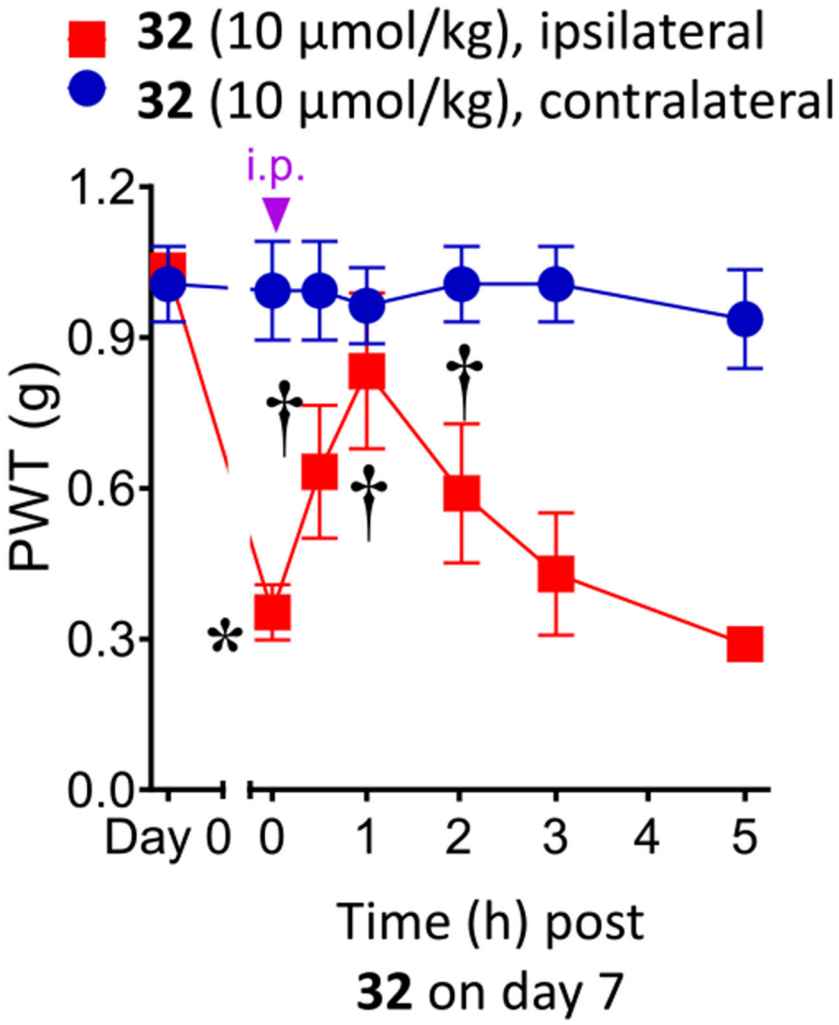

Figure 3.

Reversal of CCI-induced mechano-allodynia in the mouse induced by compound **32** (10 μmol kg^{-1}, i.p.). Mean ± SD is shown, $n = 3$; ANOVA, $^{*}P < 0.05$ vs day 0 and $^{\dagger}P < 0.05$ vs day 7 post-injury. **32** was dissolved in 5% DMSO in water as a vehicle, and a volume of 0.2 mL was injected.

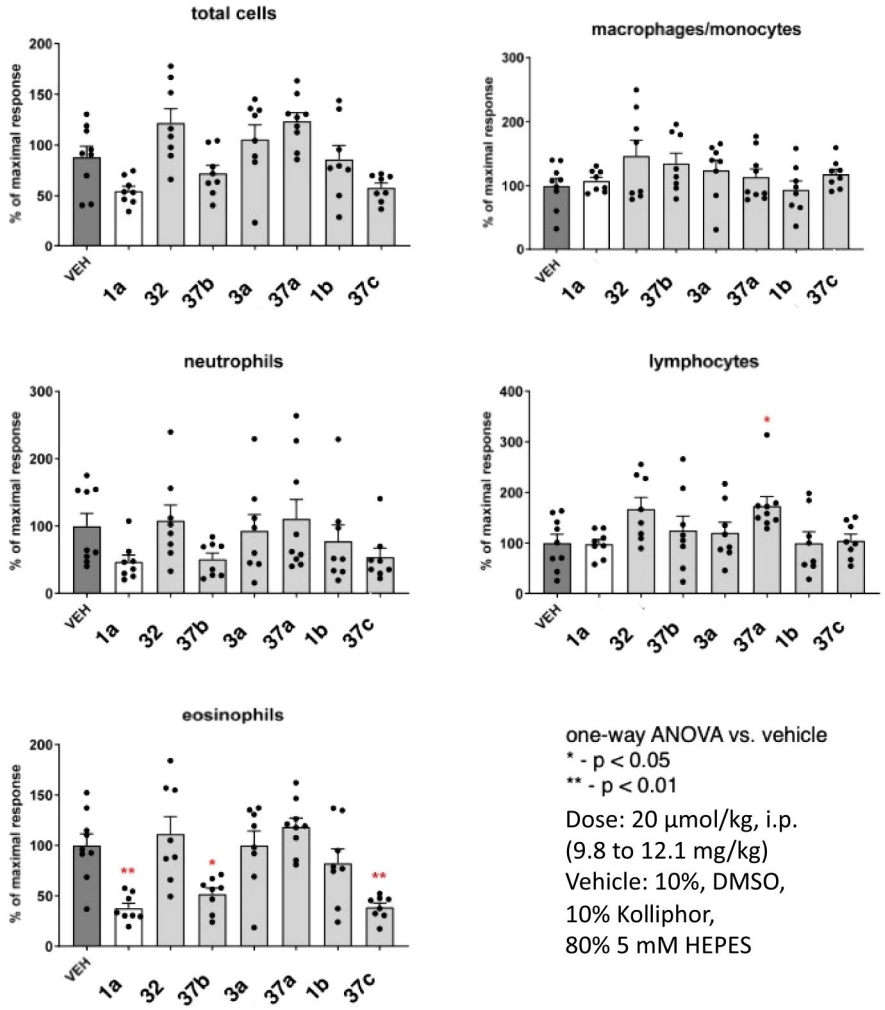

Figure 4.

Effects of $P2Y_{14}R$ antagonists and their prodrugs, compared to reference antagonist **1a**, during allergen challenge reduce eosinophilic airway inflammation in the protease model of asthma. Effect on BALF leukocytes of i.p. injection of the $P2Y_{14}R$ antagonists 2 days post-challenge of ASP/OVA-sensitized mice. $^{*}P < 0.05$, $^{**}P < 0.01$, $^{***}P < 0.001$, and $^{****}P < 0.0001$ vs vehicle by one-way ANOVA followed by Dunnett's test.

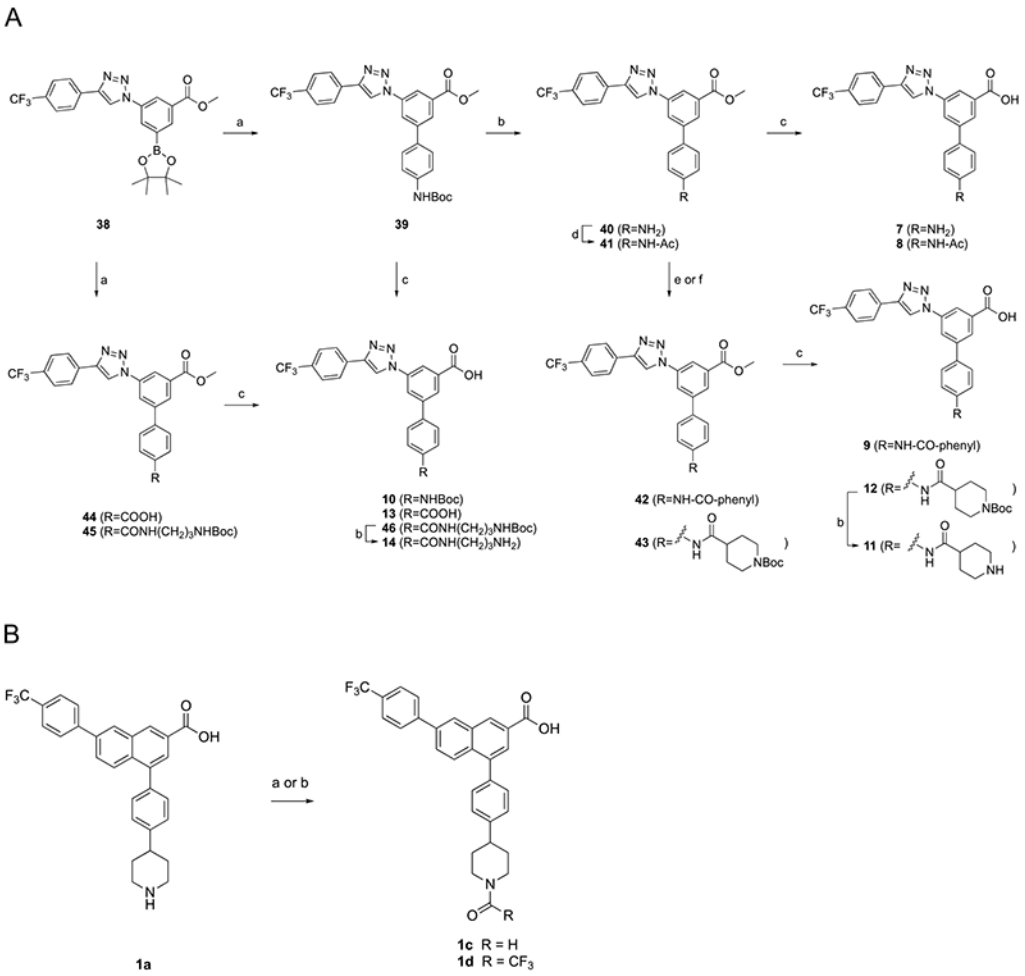

Scheme 1. (A) Synthesis of Triazole-Containing Derivatives with Acyl or Acylamino Replacement of the Piperidine Ring of 3a[a]

[a]Reagents and conditions: (a) *tert*-butyl (4-bromophenyl)carbamate, $Pd(PPh_3)_4$, K_2CO_3, DMF, 85 °C, 5 h, and 40–68%; (b) TFA/THF = 2:1, rt, 0.5 h, and 57–87%; (c) KOH, $MeOH/H_2O$ = 2:1, 50 °C, and 50–82%; (d) acetic anhydride, DCM, rt, 2 h, and 76%; (e) benzoyl chloride, TEA, DCM, rt, 18 h, and 63%; and (f) boc-isonipecotic acid (Boc-Inp-OH), HATU, DIPEA, DMF, rt, 2 h, and 94%. (B) Synthesis of *N*-acyl naphthalene-containing derivatives. reagents and conditions: **1c**: (a) Acetic formic anhydride (from Ac_2O/formic acid = 2:1, v/v), 0 °C for 3 h → room temperature for 12 h, and 71%. **1d**: (b) Trifluoroacetic Anhydride and 92%.

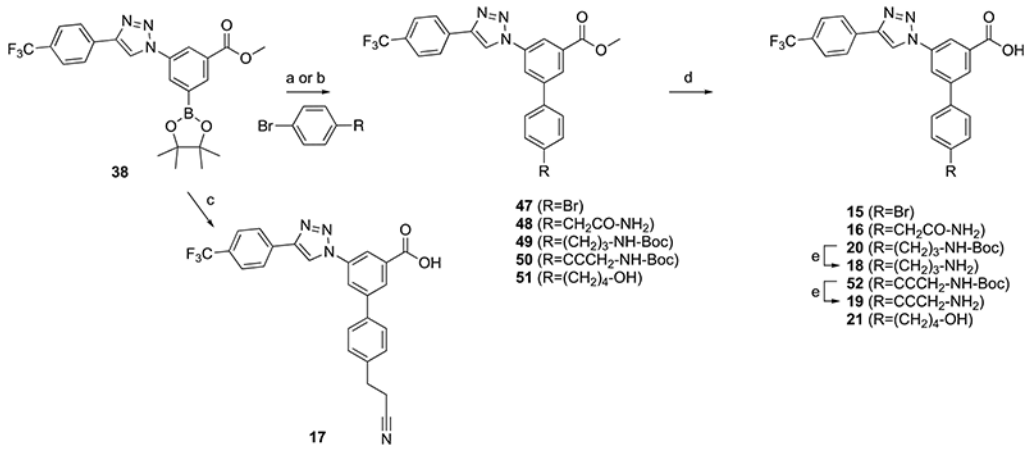

Scheme 2. Synthesis of Triazole-Containing Derivatives with Acyclic Replacement of the Piperidine Ring of 3a[a]

[a]Synthesis of intermediate **54** is in Scheme S1 (Supporting Information). Reagents and conditions: (a) $Pd(PPh_3)_4$, K_2CO_3, DMF, 85 °C, 5 h, and 27–55%; (b) $PdCl_2$(dppf), dimethoxyethane/Na_2CO_3 (aq, 2 M) = 10:1, 60 °C, 4 h, and 73%; (c) 3-(4-bromophenyl)propanenitrile, $Pd(PPh_3)_4$, K_2CO_3, DMF/H_2O = 1:1, 90 °C, 12 h, and 64%; (d) KOH, MeOH/H_2O = 2:1, 50 °C, and 39–88%; and (e) TFA/THF = 2:1, rt, 0.5 h, and 62–98%.

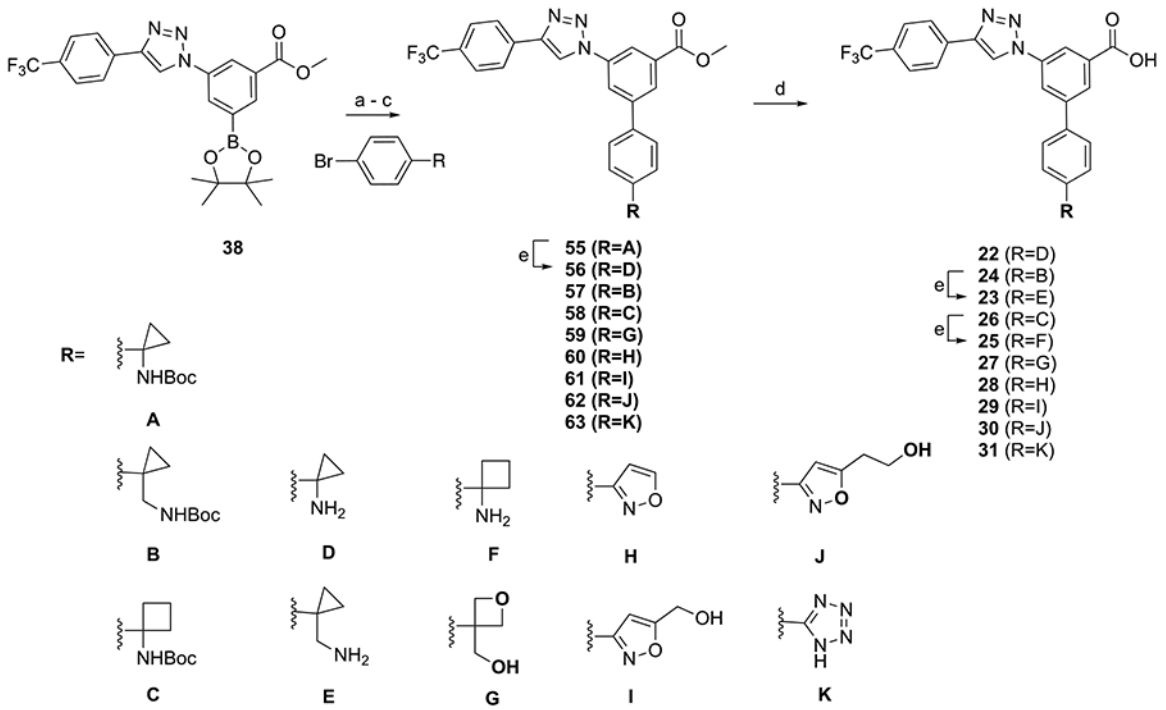

Scheme 3. Synthesis of Triazole-Containing Derivatives with Cyclic Replacement of the Piperidine Ring of 3a[a]

[a]Reagents and conditions: (a) $Pd(PPh_3)_4$, K_2CO_3, DMF, 85 °C, 5 h, and 46–91%; (b) $Pd(PPh_3)_4$, K_2CO_3, DMF, μW, 100 °C, 0.5 h, and 80–91%; (c) $Pd(PPh_3)_4$, K_2CO_3, DMF/H_2O = 1:1, 90 °C, 12 h, and 30–70%; (d) KOH, $MeOH/H_2O$ = 2:1, 50 °C, and 43–74%; and (e) TFA/THF = 2:1, rt, 0.5 h, and 52–90%.

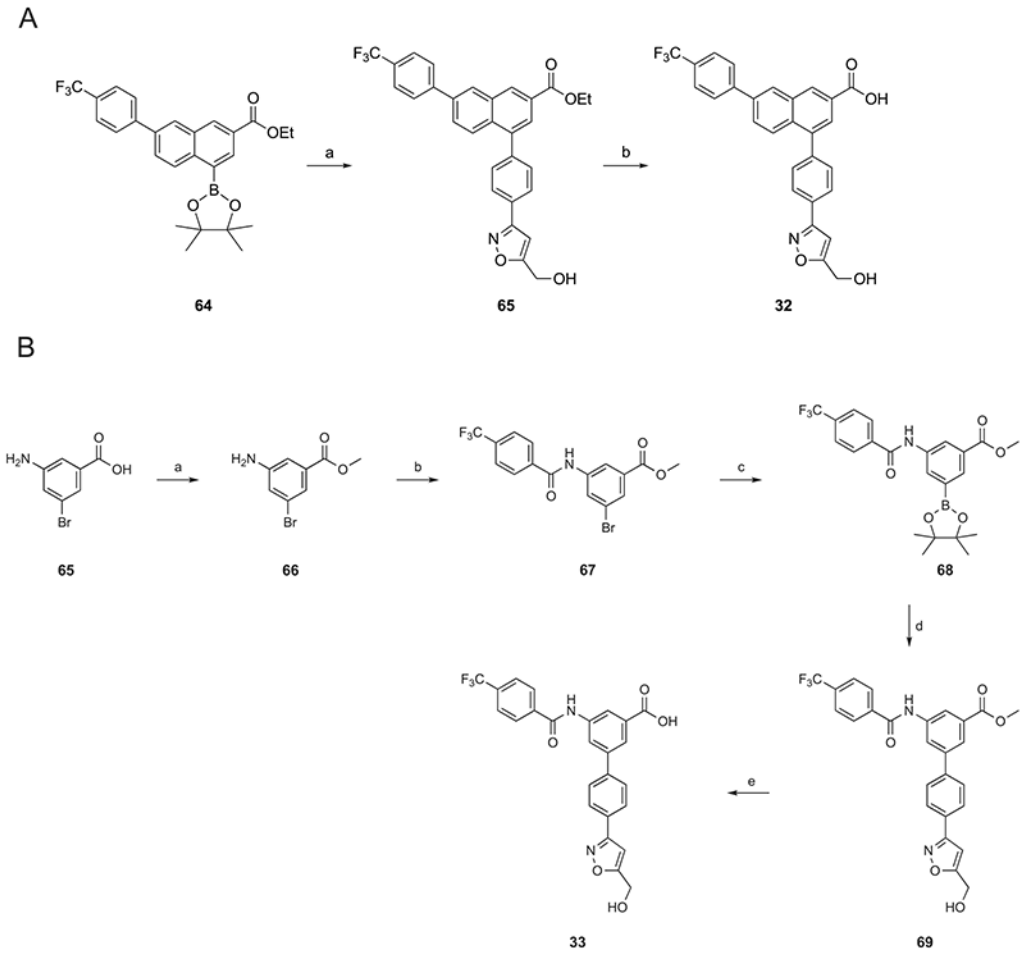

Scheme 4. (A) Synthesis of Naphthalene-Containing Isoxazole Derivative 32[a]

[a]Reagents and conditions: (a) (3-(4-bromophenyl)isoxazol-5-yl)methanol, $Pd(PPh_3)_4$, K_2CO_3, DMF, μW, 100 °C, 1.5 h, and 50% and (b) KOH, MeOH/H_2O = 2:1, 50 °C, and 98%. (B) Synthesis of amide-containing isoxazole derivative **33**. Reagents and conditions: (a) $SOCl_2$, MeOH, rt, 15 h, and 98%; (b) 4-(trifluoromethyl)benzoic acid, HATU, DIPEA, DMF, rt, 5 h, and 70%; (c) B_2pin_2, $PdCl_2$(dppf), KOAc, dioxane, 70 °C, 6 h, and 65%; (d) (3-(4-bromophenyl)isoxazol-5-yl)methanol, $Pd(PPh_3)_4$, K_2CO_3, DMF, 85 °C, 5 h, and 45%; and (e) KOH, MeOH, H_2O, 50 °C, 3 h, and 62%.

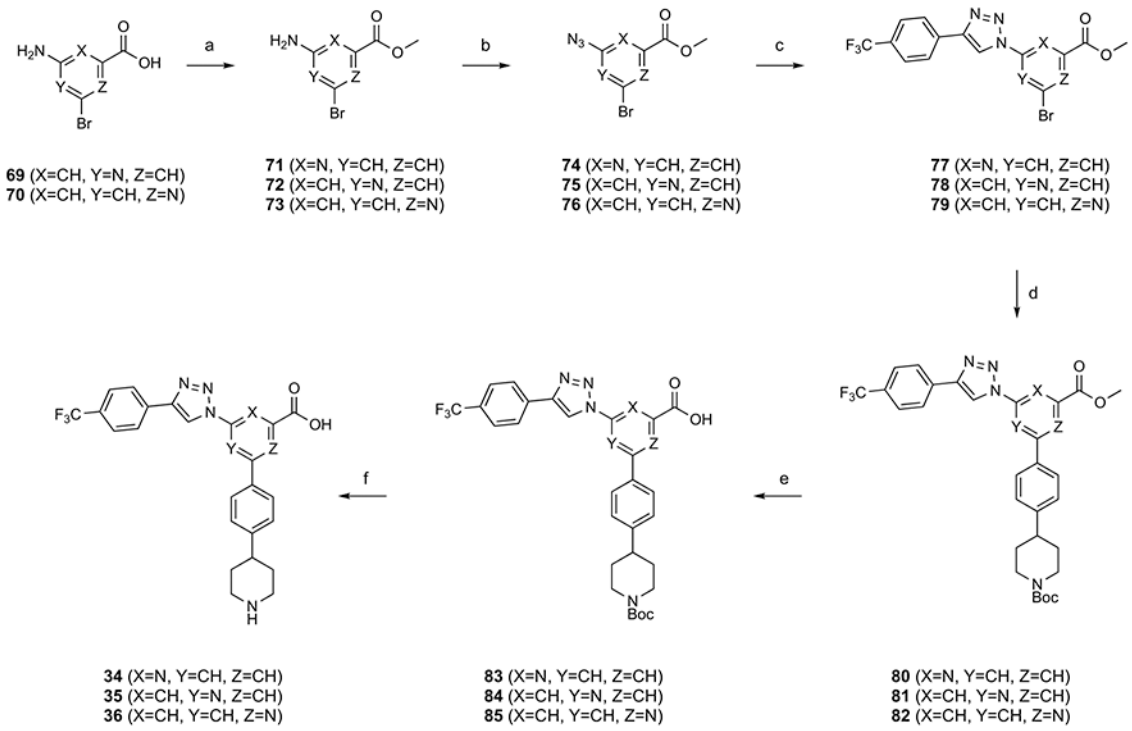

Scheme 5. Synthesis of Triazole-Containing Derivatives 34–36 for the Aza-Scan of the Central Phenyl Ring[a]

[a]Reagents and Conditions: (a) $SOCl_2$, MeOH, rt, 15 h, and 40%; (b) *tert*-butyl nitrite, azidotrimethylsilane, acetonitrile, rt, 1 h, and 37–65%; (c) 4-ethynyl-α,α,α-trifluorotoluene, $CuSO_4 \cdot 5H_2O$, Na ascorbate, TBTA, *tert*-BuOH/H_2O = 1:1, rt, 45 min, and 36–69%; (d) *tert*-butyl 4-(4-(4,4,5,5-tetramethyl-1,3,2-dioxaborolan-2-yl)phenyl)piperidine-1-carboxylate, $Pd(PPh_3)_4$, K_2CO_3, DMF, 85 °C, 4 h, and 35–91%; (e) KOH, MeOH/H_2O = 2:1, 50 °C, 5 h, and 68–91%; and (f) TFA/THF = 2:1, rt, 0.5 h, and 60–65%.

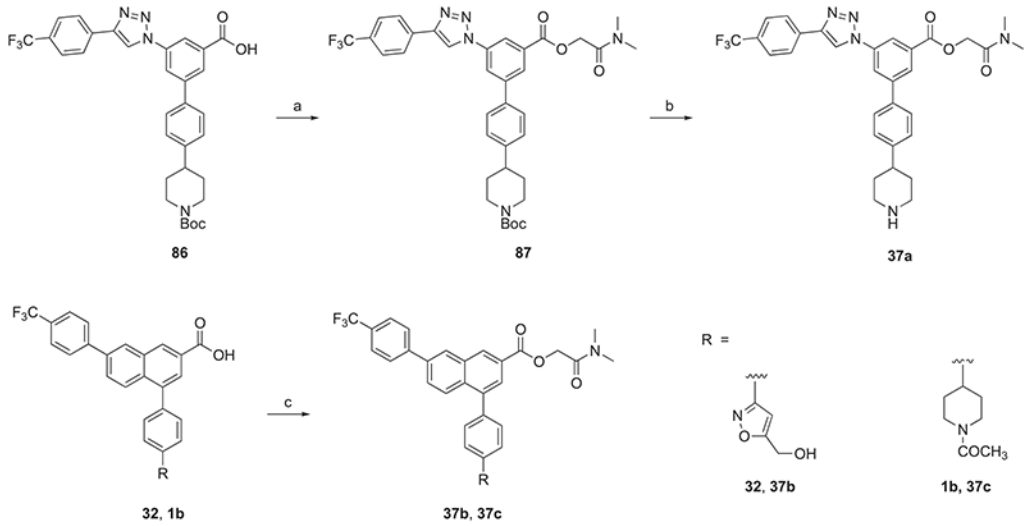

Scheme 6. Synthesis of Prodrug Derivatives 37a–37c[a]

[a]Reagents and conditions: (a) 2-chloro-*N,N*-dimethylacetamide, K_2CO_3, DMF, 45 °C, 1 h, and 70–72%; (b) TFA/THF = 2:1, rt, 0.5 h, and 78%; and (c) 2-chloro-*N,N*-dimethylacetamide, Cs_2CO_3, DMF, 45 °C, 1 h, and 68–72%.

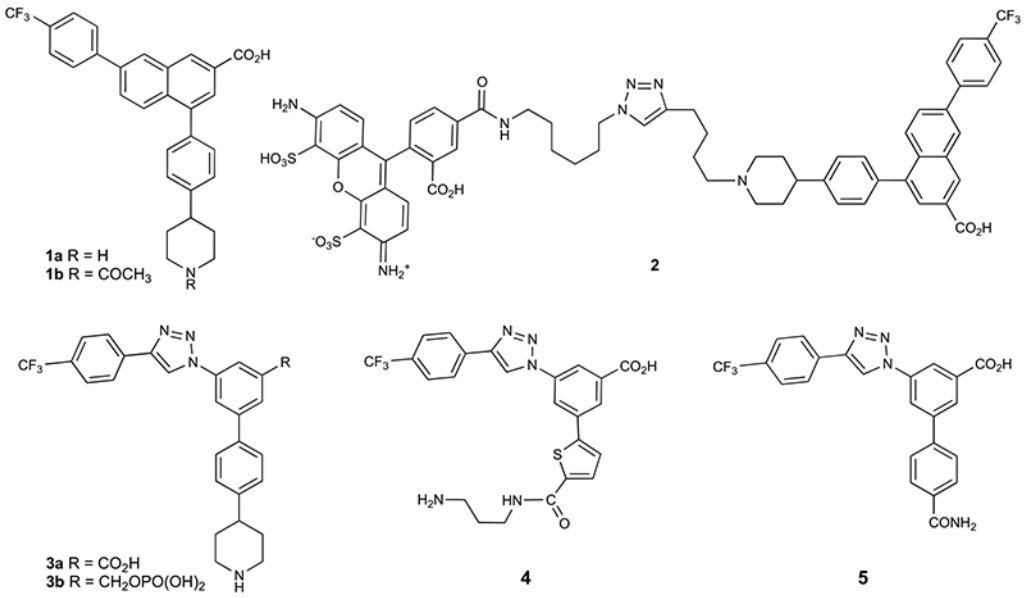

Chart 1. Structure of Reported P2Y$_{14}$R Antagonist Ligands, Including High Affinity Fluorescent Conjugate 2 Used to Determine Receptor Affinity in a Whole Cell Flow Cytometry Assay[a]

[a]One of the compounds shown, **3b**, was synthesized and characterized in the present study.

Table 1.

Inhibition of Fluorescent Antagonist (2) Binding in hP2Y$_{14}$R-Expressing CHO Cells (X, Y, and Z = CH, Unless Noted)

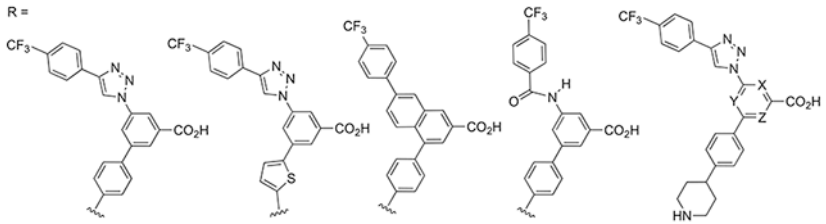

3a, 5 – 31 **4** **1, 32** **33** **34 – 36**

Compound	Structure[a] =	IC$_{50}$, hP2Y$_{14}$R (nM, mean±SEM)	cLogP[c]
	Archival compounds and close analogues		
1a[b]		7.96±3.5	6.18
1b[b]	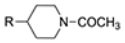	27.6±4.3	6.47
1c	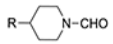	36.6±10.9	5.99
1d	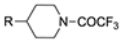	240±21	6.70
3a[b]		31.7±8.0	4.64
3b		60,500±6900	3.89
4[b]	R-CONH(CH$_2$)$_3$NH$_2$	169±42	0.84
5[b]	R-CONH$_2$	269±121	3.63
6[b]		233±26	3.95
	Phenyl-CO or NH		

R =

Compound	Structure [a] =	IC_{50}, hP2Y$_{14}$R (nM, mean±SEM)	cLogP [c]
3a, 5 – 31			
4			
1, 32			
33			
34 – 36			
7	R-NH_2	1480±160	4.03
8	R-NH-Ac	811±95	4.07
9	R-NH-CO-phenyl	1860±540	5.19
10	R-NH-Boc	3160±310	4.98
11		197±29	3.85
12		22,500±3700	4.85
13	R-COOH	632±23	3.88
14	R-CONH$(CH_2)_3NH_2$	588±43	0.92
	Phenyl-halo or acyclic		
15	R-Br	>10,000	4.71
16	R-CH_2CONH_2	1290±320	3.65
17	R-$(CH_2)_2$-CN	17,800±2900	4.74
18	R-$(CH_2)_3$-NH_2	292±67	1.60
19	R-C≡CCH_2-NH_2	308±63	1.47
20	R-$(CH_2)_3$-NH-Boc	42,500±27,000	5.37
21	R-$(CH_2)_4$-OH	9220±1220	4.84
	Phenyl-cyclic		

R =

Compound	Structure[a] =	IC_{50}, hP2Y$_{14}$R (nM, mean±SEM)	cLogP[c]
3a, 5 – 31			
4			
1, 32			
33			
34 – 36			
22		14,100±900	1.36
23		8910±750	1.57
24		18,800±2000	5.41
25		2000±180	1.70
26		>10,000	5.41
27		2860±440	4.73
28		2230±380	4.98
29		296±13	4.44
30		389±42	4.59

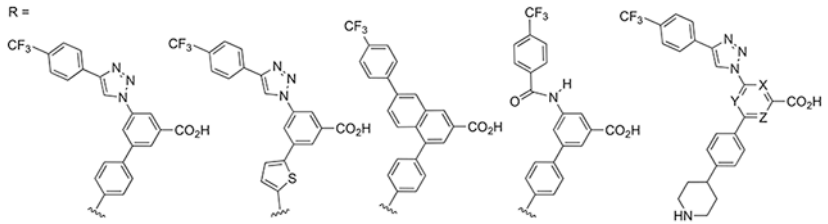

3a, 5 – 31 4 1, 32 33 34 – 36

Compound	Structure[a] =	IC_{50}, $hP2Y_{14}R$ (nM, mean±SEM)	cLogP[c]
31		895±122	3.65
	Alternative scaffolds		
32	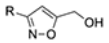	15.0±144	5.77
33	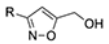	7400±1050	4.36
	*Aza-scan of **3a***		
34	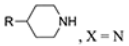	1690±280	4.16
35	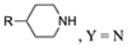	4900±540	4.10
36	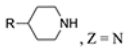	2920±310	4.01

[a] *p*-Phenyl substituted, unless noted. The structure of **3b** is shown in Chart 1. IC_{50} values are mean ± SEM for three to four separate determinations, unless noted.

[b] Reported by Yu et al.,[1] Jung et al.,[2] and Mufti et al.[7]

[c] cLogP calculated using the ALOGPS 2.1 program (www.vcclab.org/lab/alogps/).[57]

Table 2.

Species Dependence of Binding of Various $P2Y_{14}R$ Antagonists, as Determined in a Fluorescent Antagonist Binding Assay in Whole Cells ($n = 3–4$)[c]

compound	mP2Y$_{14}$R, IC$_{50}$ (nM)[a]	hP2Y$_{14}$R, IC$_{50}$ (nM)[a]
1b[b]	29.7 ± 9.3	27.6 ± 4.3
3a[b]	142 ± 58	31.7 ± 8.0
4[b]	384 ± 88	169 ± 42
5[b]	902 ± 344	269 ± 121
6[b]	499 ± 57	233 ± 26
11	155 ± 79	197 ± 29
19	375 ± 175	308 ± 63
29	184 ± 24	296 ± 13
32	18.6 ± 8.4	15.0 ± 4.4

[a]Fluorescence binding assays using **2** (20 nM, for a 45 min incubation) as a tracer. The hP2Y$_{14}$R was stably expressed in CHO cells, and the mP2Y$_{14}$R was stably expressed in HEK293 cells.

[b]Data from Jung et al.[2] and Mufti et al.[7]

[c]See Table 1 for structures.

Table 3.

Properties of Amidomethyl Ester Prodrugs 37a–37c[a]

compound (molecular charge, pH 7)	MW, TPSA (Å^2)	cLogP[b]	parent drug	$t_{1/2}$ (min, mean ± SEM) for esterase cleavage[c]
37a (+1)	577.2, 86.6	4.59	**3a**	20.2 ± 1.9
37b (uncharged)	574.6, 88.4	5.65	**32**	>72 (32.6 ± 0.9%)[d]
37c (uncharged)	602.7, 66.9	6.27	**1b**	>72 (27.2 ± 0.3%)[d]

[a] Structures are shown in Scheme 6.

[b] cLogP calculated using the ALOGPS 2.1 program (www.vcclab.org/lab/alogps/).[57]

[c] At pH 7.3 in the aqueous medium in the presence of PLE. See Experimental Procedures and Supporting Information (Figures S7-S9) for conditions and graphical representation of results. The prodrugs are stable under the same incubation conditions for 24 h in the absence of PLE.

[d] Percent cleavage at 72 h in parentheses.

Table 4.

In Vitro and In Vivo ADMET Data for Compound 32 Compared to Known $P2Y_{14}R$ Antagonist 5[a]

test	5[b]	32
simulated intestinal fluid ($t_{1/2}$, min)	>240	>240
simulated gastric fluid ($t_{1/2}$, min)	>240	161
CYP1A2 (IC_{50}, μM)	>30	>30
CYP2C9 (IC_{50}, μM)	>30	10.4
CYP2C19 (IC_{50}, μM)	>30	>30
CYP2D6 (IC_{50}, μM)	>30	>30
CYP3A4 (IC_{50}, μM)	>30	>30
plasma stability (species)[c] ($t_{1/2}$, min)	>240 (h), >240 (r), >240 (m)	>240 (r), >240 (m)
microsomal stability ($t_{1/2}$, min)	145 (m), 108 (r), 145 (h)	>240 (h), 47.7 (r), >240 (m)
hERG, IC_{50} (μM)[d]	0.166 (fluorescent)	>30 (patch clamp)
HepG2 cell toxicity, IC_{50} μM)	>30	8.47
$t_{1/2}$ (r)[e]	0.20 (0.5 mg kg^{-1}, i.v.)	7.23 (1.0 mg kg^{-1}, i.p.)
aqueous solubility[f] (pH 7.4, μg mL^{-1})	138 ± 4	7.63 ± 1.93
aqueous solubility[f] (pH 4.0, μg mL^{-1})	ND[g]	0.14 ± 0.02

[a]Procedures are in the Supporting Information and in Yu et al.[1] Dosing formulation: for i.v., DMSO/20% 2-hydroxypropyl-β-cyclodetrin (Sigma-Aldrich, 10:90); for i.p., DMSO/Kolliphor EL (Sigma-Aldrich)/PBS (15:15:70).

[b]Data determined by Yu et al.[1]

[c]Species tested for plasma stability were human, rat, and mouse; species as indicated for microsomal stability.

[d]Method noted in parentheses.

[e]By administration in rat (plasma half-life, h). See Table 5 for complete results for **32**.

[f]Mean ± SD, pION method.

[g]ND, not determined.

Table 5.

Pharmacokinetic Parameters[a] for Compound 32 Administered by Intravenous and Intraperitoneal Routes

dose (mg kg^{-1})	C_{max} (ng mL^{-1})	T_{max} (h)	$AUC_{0\text{-}last}$ (h ng mL^{-1})	$AUC_{0\text{-}\infty}$ (h ng mL^{-1})	$t_{1/2}$ (h)	MRT_{last} (h)	V_d (mL kg^{-1})	K_{el} (1 h^{-1})	F (%)	Cl (mL h^{-1} kg^{-1})
0.5, i.v.	359	0.083	234	238	0.689	0.703	2090	1.01	100	2110
1.0, i.p.	88.4	2.0	650	700	7.23	6.24	14,900	0.096	139	1430
3.0, i.p.	315	2.0	2060	2120	4.68	5.68	9570	0.148	147	1420
10, i.p.	786	4.0	4900	4920	2.98	5.02	8730	0.233	105	2030

[a] In healthy adult male Wistar rats; with 3 per group. Dosing formulation: for i.v., DMSO/20% 2-hydroxypropyl-β-cyclodetrin (Sigma-Aldrich, 10:90); for i.p., DMSO/Kolliphor EL (Sigma-Aldrich)/PBS (15:15:70). Abbreviations: C_{max}, maximal concentration; T_{max}, time at which maximal concentration observed; $AUC_{0\text{-}last}$, area under the plasma drug concentration–time curve up to the last quantifiable time point; $AUC_{0\text{-}\infty}$, area under the plasma drug concentration–time curve to infinite time; $T_{1/2}$, terminal half-life; MRT_{last}, mean residence time; Vd, volume of distribution; Kel, elimination rate constant; F, biovailability; and Cl, total body clearance.